R-9655

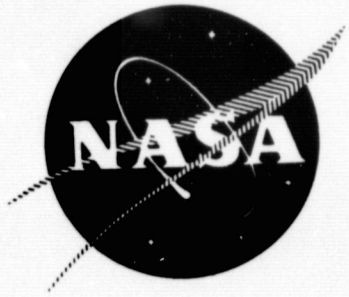

LOW-SPEED INDUCERS FOR CRYOGENIC UPPER-STAGE ENGINES

W. R. Bissell, D. S. Jenkins,
J. A. King, and E. D. Jackson

Rocketdyne, Division of Rockwell International
Canoga Park, California 91304

Prepared for

NATIONAL AERONAUTICS AND SPACE ADMINISTRATION
George C. Marshall Space Flight Center
Huntsville, Alabama 35812

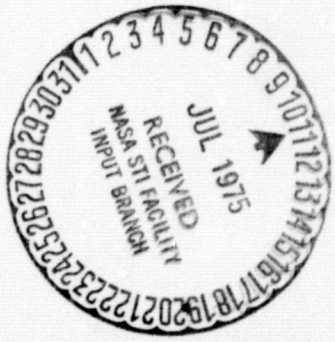

LOW-SPEED INDUCERS FOR CRYOGENIC UPPER-STAGE ENGINES

(Final Report)

W. R. Bissell, D. S. Jenkins,
J. A. King, and E. D. Jackson

May 1975

(NAS8-29189)

Rocketdyne, Division of Rockwell International
Canoga Park, California 91304

Prepared for

NATIONAL AERONAUTICS AND SPACE ADMINISTRATION
George C. Marshall Space Flight Center
Huntsville, Alabama 35812

FOREWORD

Rocketdyne, a division of Rockwell International Corporation, has prepared this final report which documents the work performed in fulfillment of the contract, "Low Speed Inducers for Cryogenic Upper-Stage Engines," during the period from November 1972 to February 1975. This program was sponsored by the National Aeronautics and Space Administration, Marshall Space Flight Center, Huntsville, Alabama, under Contract NAS8-29189. Mr. Charles Miller, NASA-MSFC, was the Technical Project Manager for the program. This report has been designated Rocketdyne Report Number R-9655.

ABSTRACT

Two-phase, low-speed hydrogen and oxygen inducers driven by electric motors and applicable to the Tug engine were designed and constructed. The oxygen inducer was tested in liquid and two-phase oxygen. Its head and flow performance were approximately as designed, and it was able to accelerate to full speed in 3 seconds and produce its design flow and head. The two-phase data were difficult to analyze, but the analysis indicated that the inducer was able to pump with vapor volume fractions in excess of 60 percent. The pump met all of its requirements (duration of runs and number of starts) to demonstrate its mechanical integrity.

CONTENTS

ILLUSTRATIONS

TABLES

SUMMARY AND CONCLUSION

Oxygen and hydrogen pumps were designed, fabricated and tested (oxygen only) in two-phase flow. Both pumps consisted of an inducer designed specifically to achieve two-phase flow operational capability followed by two rows of stator vanes designed to efficiently convert the tangential component of velocity into static pressure. Due to the low speeds and power of these pumps, electric motor drives integral with the pump housing were used as the drive system. The hydrogen motors were immersed in the hydrogen and the oxygen motors were sealed to prevent contact with the liquid oxygen.

The two-phase oxygen pump was tested for a total duration of 2893 seconds consisting of 98 starts. The pump was in perfect condition at the end of the test series showing no indications of mechanical degradation. The electric motor performance was good providing repeatable and well regulated speed transients. However, there was some question concerning the actual efficiency of the motor in operation. The pumps head-flow characteristic agreed well with the analytically predicted performance, some of the tests even indicating higher head than designed. The pump was capable of starting with speed ramp times of 3 and 7 seconds and with low inlet pressures (1 to 2 psi). There were even indications that the pump could start with some vapor present in the inlet lines.

The test facility problems encountered prevented obtaining as much suction performance data as desired nor were the data ideal from the standpoint of verifying the technological capabilities under investigation. However, the test data did indicate that the pump was capable of pumping two-phase oxygen with a vapor volume content in excess of 60 percent.

The two-phase hydrogen inducer was not tested. Testing was attempted, but the unit reached only part speed at a very high amperage. It was determined that the electric motor had been incorrectly designed and was therefore not properly wound. Analysis of the high current problem by the manufacturer showed that the probable

cause was that the "throw" of the stator windings was inevitable for a 2-pole machine. The error was attributed to taking notes from a drawing for a 4-pole machine and using them for a 2-pole design. At that point the stators were removed from the pumps and returned to the manufacturer for rewinding and the hydrogen tests were eliminated from the program.

INTRODUCTION

Studies of cryogenic upper-stage engine systems such as the Space Tug have shown low net positive suction pressures to trade favorably with vehicle payload. In fact, operation on saturated propellants in the tanks is highly desirable because it would eliminate stage prepressurization and reduce venting requirements.

Reference 1 describes the design, fabrication, and testing of an inducer in two-phase hydrogen. A mathematical model and a digital computer program were developed for the design and evaluation of inducers for pumping two-phase hydrogen. An inducer was designed according to the developed theory and tested in liquid hydrogen. It accepted 30 percent vapor by volume with no loss in main pump head.

In Ref. 2, a mathematical model and a digital computer program were developed for the design and evaluation of inducers for pumping two-phase oxygen. The model indicated that any design would have to be run at relatively low speeds to pump the mixture and that the Rocketdyne J-2S oxygen inducer was close to optimum and should perform the task. A J-2S pump was built up and tested in two-phase oxygen at speeds indicated by the mathematical model. The pump was able to handle two-phase oxygen over a wide range of inducer incidence angles and up to a vapor content of 37 percent by volume with very little loss in head. The pump was still able to produce some head at vapor fractions approaching 60 percent. It was concluded that low speed inducers appeared capable of operating in saturated hydrogen and oxygen over a wide operating range and deserved further investigation as prime candidate approaches to achieving an efficient and lightweight vehicle.

The purpose of this program was to design and construct two-phase, low-speed hydrogen and oxygen inducers and their drive systems applicable to the Tug engine. These were to be tested in saturated hydrogen and oxygen to demonstrate that the design technology to operate this hardware was available. The mechanical integrity of the inducers and their drive systems was also to be demonstrated. Upon satisfactory completion of the test program, the hardware was to be refurbished and delivered to MSFC along with two sets of final drawings.

The program was conducted in five phases:

Phase I	General Analysis
Phase II	Detailed Analysis and Design
Phase III	Fabrication
Phase IV	Testing
Phase V	Hardware Refurbishment

PHASE I--GENERAL ANALYSIS

PRELIMINARY ANALYSIS

Although it had been demonstrated in Ref. 1 and 2 that low-speed inducers could successfully operate in saturated hydrogen and oxygen, there were still many problems to resolve before it could be proven that operation with saturated propellants in the tanks was possible on a Space Tug type engine. Such questions as the following were asked:

1. What about the transient conditions imposed by a rapid start: Will the inertia of a long line prevent a rapid start?
2. How should the inducers be driven?
3. How much head should the inducers generate?
4. Will backflow deflectors help?
5. How can tests be run to simulate zero-gravity conditions?
6. Can the inducers pump from a sealed tank while the liquid produces its own ullage by boiling?

It was apparent that some of these questions could be answered by theoretical methods, and this was accomplished during Phase I of this program.

PRELIMINARY DESIGN POINT AND VAPOR FRACTION

Oxygen Inducer

The oxygen inducer was first sized to supply the main oxygen turbopump for a 15K thrust cryogenic upper-stage engine (NAS8-27794), the pump for the 20K thrust Space Tug study (NAS3-16751), and the RL-10 pump. It was assumed that the same inducer would meet the three requirements by simply changing speed. From the affinity laws we get:

$$\dot{w} = K_1 N$$

$$H = K_2 N^2$$

$$H = K_3 \dot{w}^2$$

where

$\dot{w}$ = flow in lb/sec

N = inducer rpm

H = inducer head rise, feet

The resultant inducer design points for the three engine thrust levels were:

	$\dot{w}$	H
15K	27.35	95.00
20K	36.78	171.80
RL-10	30.89	121.18

The Rocketdyne computer program for the expansion of saturated oxygen at 14.7 psia (T = 162.22 R, ρ = 71.212) was used because the contract specified a pressure range from 14.7 to 30 psia, and the lowest pressure is always the worst case for pumping two-phase fluids. In the program it was calculated that the entrance loss from the tank to the duct was 0.04 velocity head, the loss through a wide-open ball valve was 0.36 velocity head, and the friction loss in a 36-inch long duct was 0.12 velocity head. The following values were selected from the printout for the design of the 15K inducer:

Vapor fraction = 25.19 percent

$\dot{w}/A$ = 232.5 lb/sec/sq ft

C_m = 4.356 ft/sec

where

C_m = axial velocity entering the inducer annulus in ft/sec

A = inducer inlet annular area, sq ft

It was assumed that

$$\xi = 0.3 \text{ and } \phi = 0.07$$

where

D_h = inducer entrance hub diameter, inch

D_w = inducer entrance wall diameter, inch

D_i = inducer rotor entrance tip diameter, inch

U_i = inducer rotor entrance tip speed, ft/sec

$\xi = D_h/D_w$

ϕ (flow coefficient) $= C_m/U_i$

$$A = \frac{\dot{w}}{\dot{w}/A} = 0.117629 \text{ sq ft} = 16.938626 \text{ sq in.} = \frac{\pi D_w^2}{4}\left[1 - \xi^2\right]$$

From the above D_w = 4.868 inches and D_h = 1.460 inches. The inducer diametral clearance was set at 0.019 inch which is consistent with other Rocketdyne inducers, so that

D_i = 4.849 inches

U_i = 62.231 ft/sec

N = 2941 rpm

It was determined that the inducer tip speed was insufficient to provide the design head rise of 95 feet, so a centrifugal pump was necessary. For this it was assumed that ψ = 0.45.

where

g = acceleration of gravity taken as 32.174

D_t = tip diameter of the centrifugal pump rotor, inch

U = tip speed of the centrifugal pump rotor, ft/sec

ψ, the head coefficient, $\psi = \frac{g\Delta H}{U^2}$

From this, $U = 82.415$ ft/sec and $D_t = 6.422$ inches

The pump specific speed is based on the pump discharge flow in gal/min. As the vapor collapses in the pump, the pump discharge density will be 71.2 lb/cu ft (as compared to 53.3 at the inlet). Thus, the discharge flowrate and pump specific speed are

$$Q = \frac{\dot{w}}{71.2} = 0.384064 \text{ cfs} = 172.38 \text{ gpm}$$

$$N_s = \frac{2941.3\ \sqrt{172.38}}{(95)^{0.75}} = 1269$$

From Rocketdyne parametric studies of specific speed and pump size, the pump efficiency was determined as 77 percent.

The inducer horsepower for the three engine thrust levels was:

	N	hp
15K	2941	6.13
20K	3955	14.92
RL-10	3322	8.83

When the inducer is used in front of the RL-10 pump, it has a higher flow, higher axial velocity and, therefore, a higher vapor fraction than that of the 15K engine. (Rocketdyne understood that the tanks of the 20K engine are pressurized at design speed.) The inducer incidence angle must, therefore, be fixed by RL-10 conditions.

$$\text{RL-10} \quad \dot{w}/A = \frac{30.89}{0.117629} = 262.60 \text{ lb/sec/sq ft}$$

For this flow, the computer program gives a vapor fraction of 33.52 percent and an axial velocity of 5.524 ft/sec. The conditions and angles at the tip of the three inducers at the entrance are summarized in the following tabulation:

	C_m	U_i	$\phi = \tan\beta_f$	β_f	β_b	i	i/β_b
15K	4.35	62.23	0.07	4.00	8.17	4.17	0.5099
20K	4.39	83.68	0.05247	3.00	8.17	5.17	0.6324
RL-10	5.52	70.28	0.07859	4.49	8.17	3.68	0.45

where

β_f = fluid angle with the tangent at the inducer tip

β_b = blade angle with the tangent at the inducer tip

i = incidence angle; $i = \beta_b - \beta_f$

The table was constructed by setting $i/\beta_b = 0.45$ for the RL-10. Figure 1 (reproduced from Fig. 56 of Ref. 2) shows this to be about the minimum value for the pumping of two-phase oxygen. Note from the same figure that the values of 0.51 for the 15K and 0.63 for the 20K are quite acceptable.

Hydrogen Inducer

The inducer design points for the three engine thrust levels (based on the affinity laws) were:

	$\dot{w}$	H
15K	4.56	1268.68
20K	5.66	1954.59
RL-10	5.15	1618.22

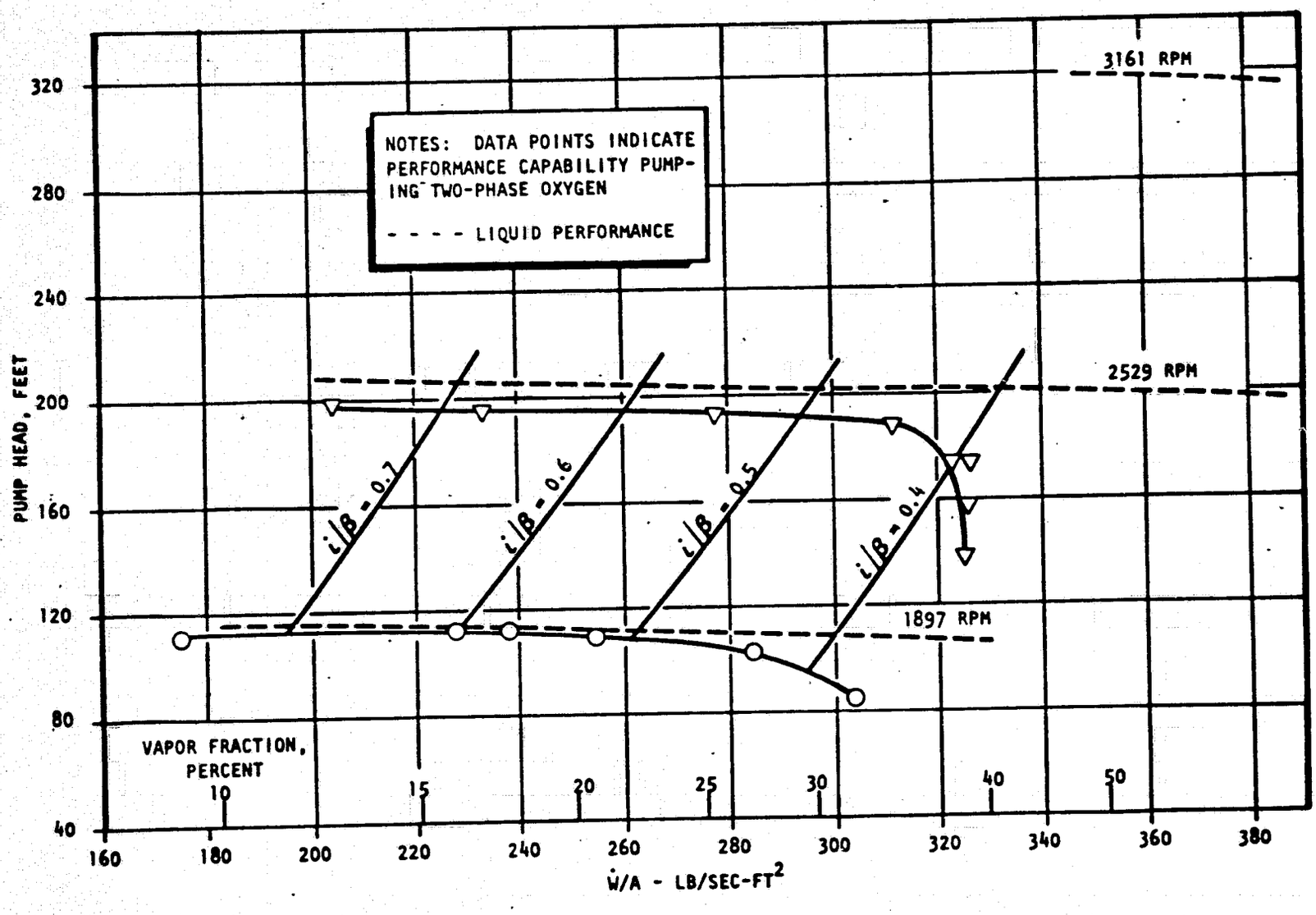

Figure 1. Performance Map of Pump Tested in Two-Phase Oxygen

The computer program for the expansion of saturated hydrogen at 14.7 psia (T = 36.48 R, ρ = 4.42036) was used. It was calculated that the entrance loss from the tank to the duct was 0.04 velocity head, the loss through a wide-open ball valve was 0.36 velocity head, and the friction loss in a 278-inch long duct was 1.071 velocity heads. These losses were used in the program and the following values were selected from the printout for the design of the 15K inducer:

Vapor fraction = 21.04% $\dot{w}/A$ = 96.230 lb/sec/sq ft C_m = 27.34 ft/sec

Several preliminary designs were made of the hydrogen inducers, and it was found that if a relatively high tip speed were used, the head could be generated with a constant tip diameter inducer containing only four full blades (no splitter blades or secondary stages such as is used in the Mark 25 hydrogen inducer). The Mark 25 inducer has a high head coefficient of 0.5 and an optimum flow coefficient. Then

$$A = \frac{\dot{w}}{\dot{w}/A} = 0.0473 \text{ sq ft} = 6.82 \text{ sq in.} = \frac{D_w^2}{4}\left[1 - \xi^2\right]$$

and from which

D_w = 3.090 inches

D_i = 3.078 inches

D_h = 0.927 inches

$\phi = \frac{27.343}{U_i} = 0.07$

U_i = 390.618 ft/sec

N = 29,084 rpm

$\psi = \frac{g\,H}{U_i^2} = 0.2675$

The flowrate leaving the inducer is

$$Q = \frac{\dot{w}}{4.420} = 1.031 \text{ cfs} = 463 \text{ gpm}$$

$$N_s = \frac{29,085 \sqrt{463}}{(1268.68)^{0.75}} = 2944$$

with a corresponding pump efficiency of 64 percent.

The following values were then determined for the three hydrogen incuders.

	N	hp
15K	29,085	16.43
20K	36,101	31.42
RL = 10	32,848	23.67

Similar to the oxygen inducer, the hydrogen inducer design was sized for the RL-10, thus

$$\dot{w}/A = \frac{5.15}{0.0473} = 108.681 \text{ lb/sec/sq ft}$$

From the computer program for expansion, the vapor fraction is 29.45 percent and the axial velocity is 34.43 ft/sec.

	C_m	U_i	$\phi=\tan\beta_f$	β_f	β_b	i	i/β_b
15K	27.343	390.618	0.07	4.00	8.11	4.11	0.50653
20K	27.021	484.846	0.05573	3.19	8.11	4.92	0.60685
RL-10	34.430	441.158	0.07804	4.46	8.11	3.65	0.45

This table was also constructed by setting $i/\beta_b = 0.45$ for the RL-10 design. Figure 2 (reproduced from Fig. 47 of Ref. 2) had also indicated this value as a lower limit for cold two-phase hydrogen. No data were available for upper limits in two-phase hydrogen, but it is probable that these limits are similar to those in oxygen.

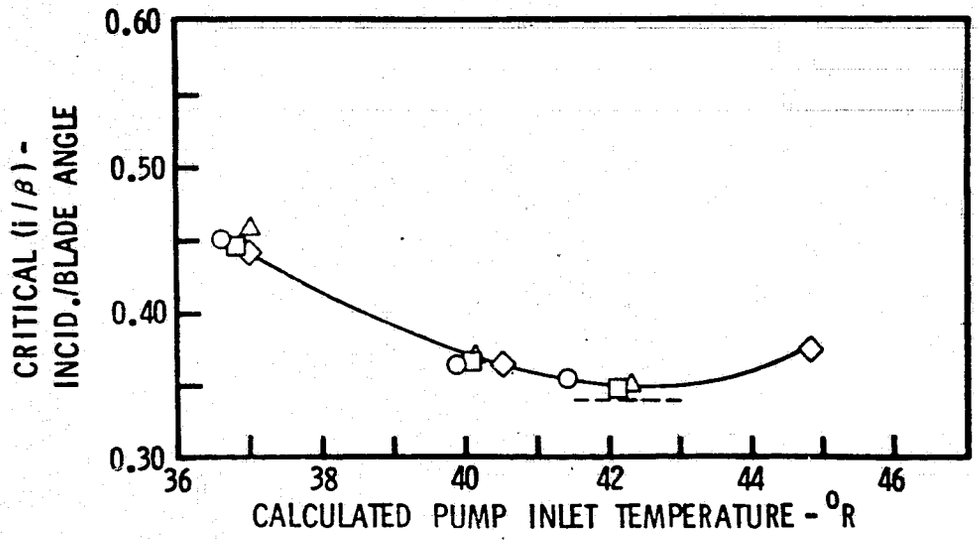

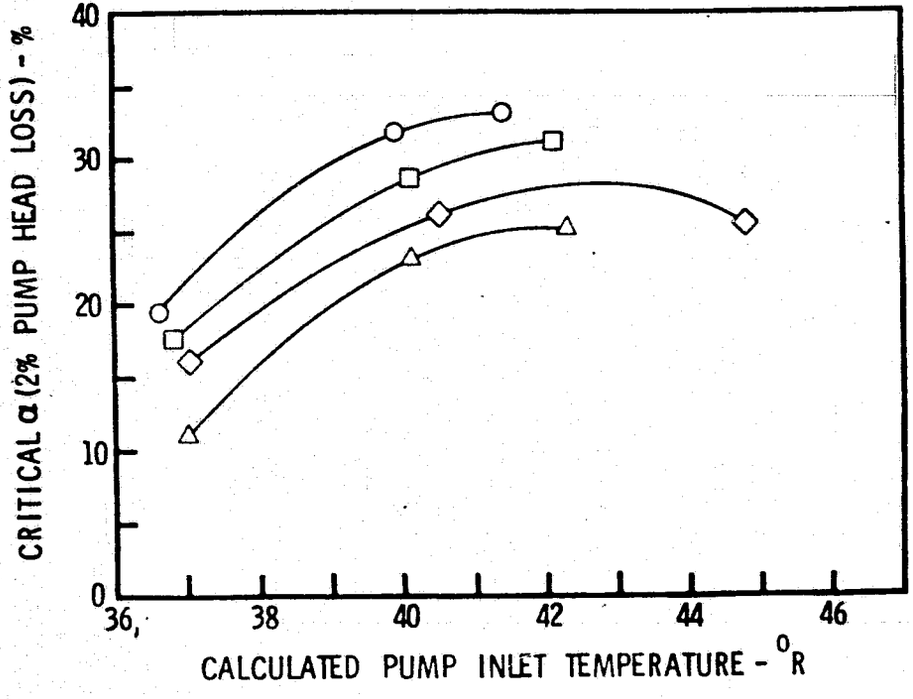

	ϕ_L	% Q/N
○	.0539	93.0
□	.0558	96.5
◇	.0576	100.0
△	.0600	103.5

329-972

Figure 2. Performance Summary of Two-Phase Flow Inducer (P/N XEOR 936071) N = 28,000 rpm

EFFECT OF LINE LENGTH ON A RAPID START

During a start transient, the stationary fluid in the line must be accelerated up to design speed. The inertia of the fluid can cause excess vapor at the pump inlet because a rapidly accelerating pump can "pull a hole" in the fluid. Oxygen, because it has a much higher inertia than hydrogen, presents the greater acceleration problem.

During Phase I, the line dynamics of both the oxygen and hydrogen pumps were modeled using the multielement lumped parameter method. This considers the effects of:

1. Propellant density as a function of stored weight.
2. Variable effective resistance proportional to 1/density.
3. Fluid inertia equal to line element length/(line area x g)

The basic flow equation is:

$$\Delta p = R/\rho \dot{w}^2 + L \frac{d\dot{w}}{dt}$$

where

Δp = line pressure drop

R = resistance

ρ = density

$\dot{w}$ = flowrate

L = inertia

The oxygen system was modeled first with the oxidizer tank forward and a long inlet line. The design conditions were:

Duct Length, inches	368
Saturated Expansion	
Pressure, psia	14.7
Entrance Loss, velocity head	0.04

Valve Loss, velocity head	0.36
Line Loss, velocity heads	1.23
Vapor Fraction, percent	25.97

Figure 3 shows the plotted results of the computer program printout. With either a 5- or a 10-second ramp (speed is increased linearly from 0 to design speed), the weight flow did not reach its maximum value until about 19 seconds. Therefore, a rapid start with a long line is not possible in saturated oxygen. (Vehicle acceleration forces were not considered and would make a difference.)

For the second trial on the oxygen system, the line length was reduced to 36 inches, the line loss to 0.12 velocity head, and the vapor fraction was 25.20 percent. The results are shown in Fig. 4. With a short line and a 5-second ramp, the weight flow reached its maximum value in about 5 seconds.

The hydrogen system was then modeled with the fuel tank forward and a long inlet line. The design conditions were:

Duct Length, inches	278
Saturated Expansion	
Pressure, psia	14.7
Entrance Loss, velocity head	0.04
Valve Loss, velocity head	0.36
Line Loss, velocity heads	1.71
Vapor Fraction, percent	21.04

The results are shown on Fig. 5. With the long line and a 5-second ramp, the weight flow of the hydrogen pump reached its maximum value in approximately 5 seconds.

Figure 6 shows the limit of the ramp rate of the hydrogen system with the long line. In this model it was assumed that the pump reached its design speed instantaneously.

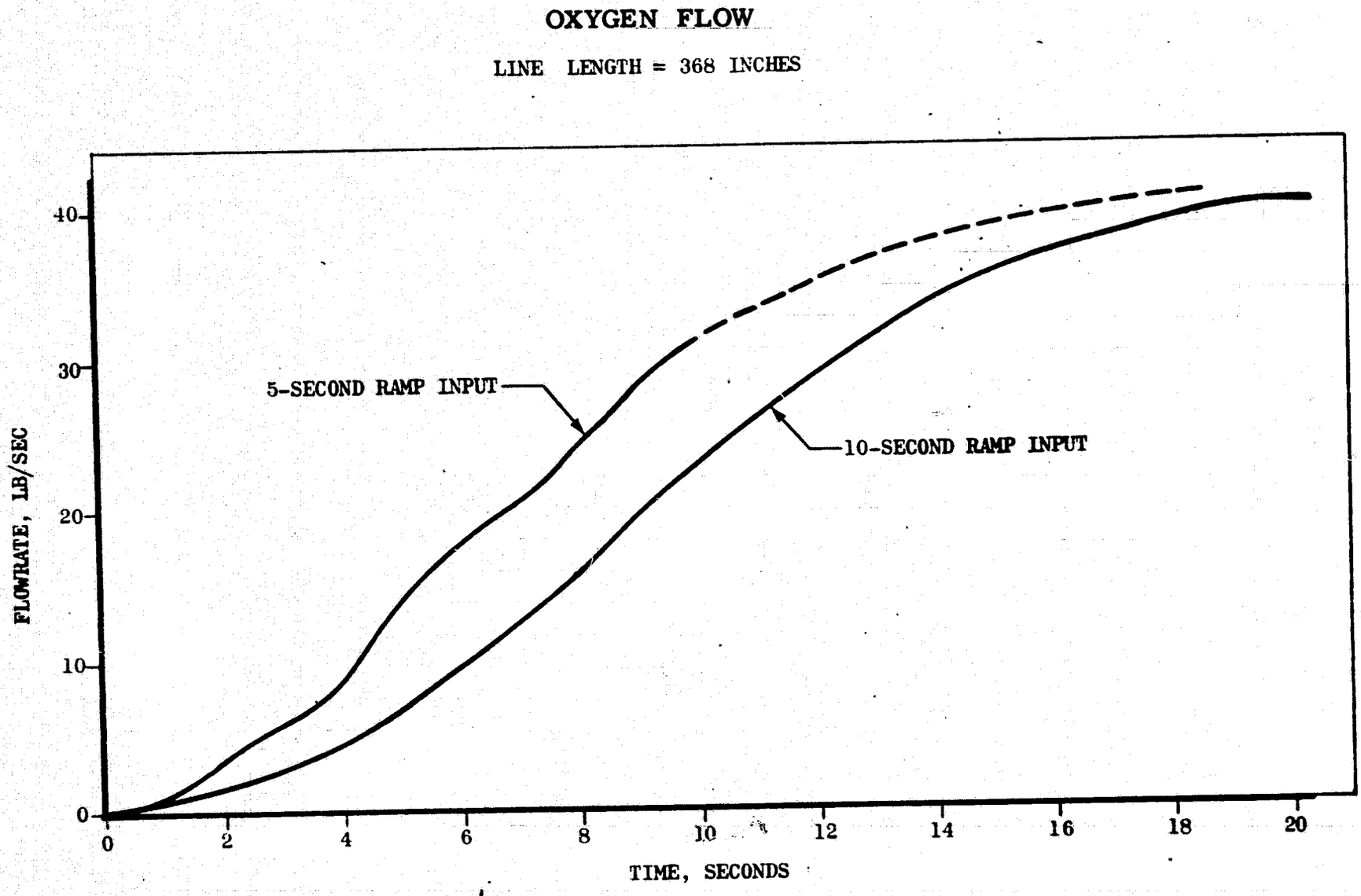

Figure 3. Oxygen Pump Ramp Rate With a Long Inlet Line

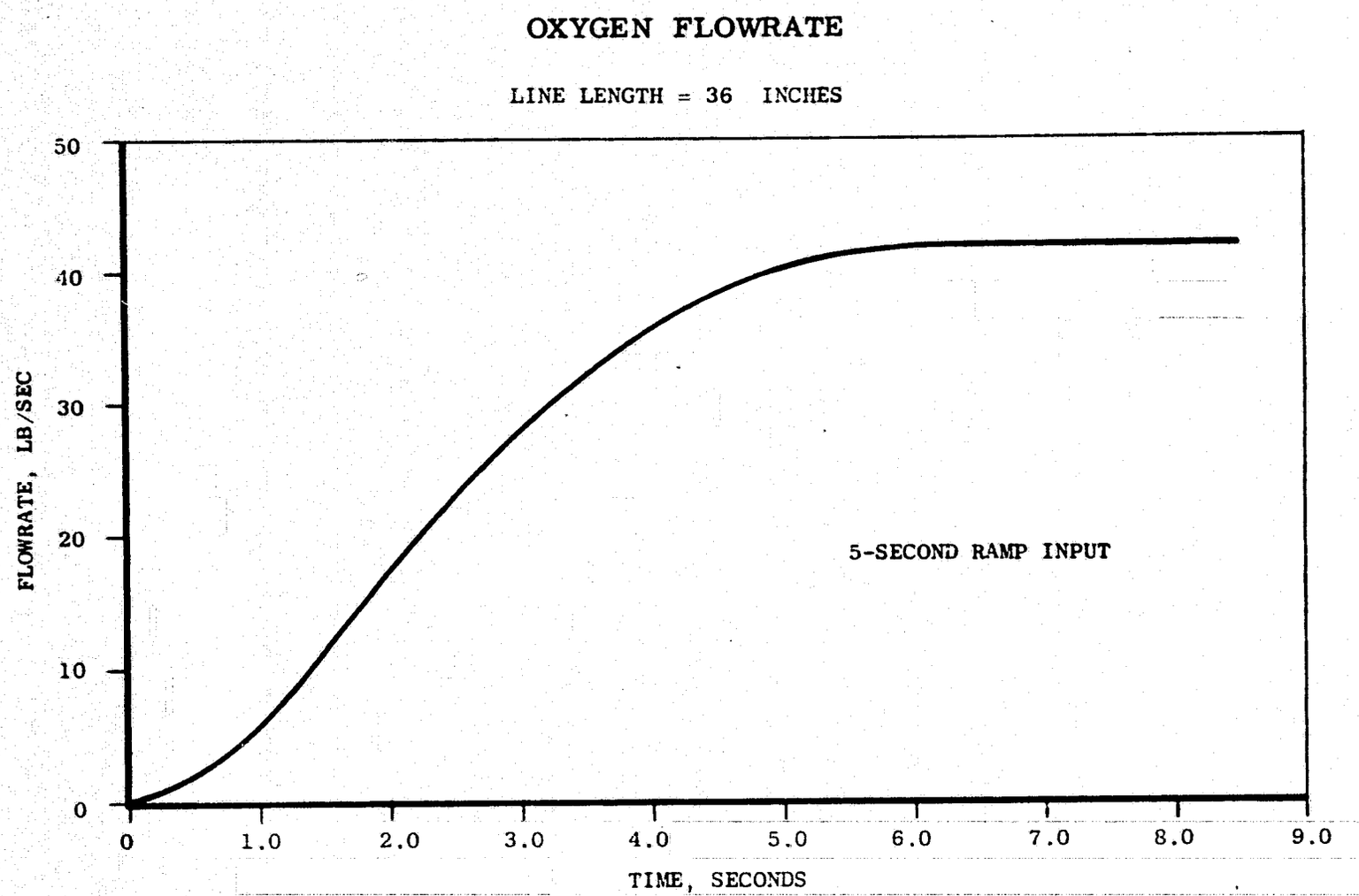

Figure 4. Oxygen Pump Ramp Rate With a Short Inlet Line

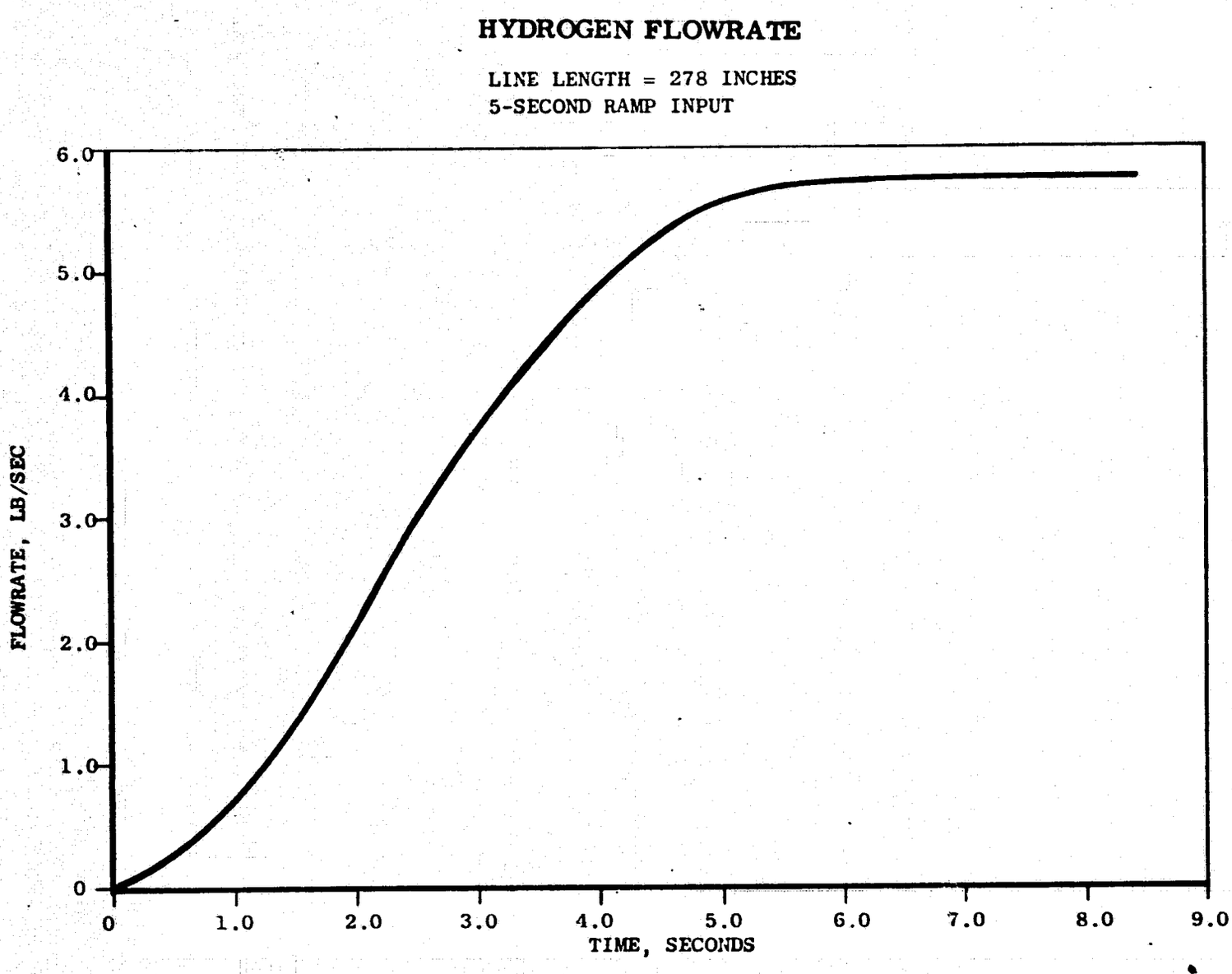

Figure 5. Hydrogen Pump Ramp Rate With a Long Inlet Line

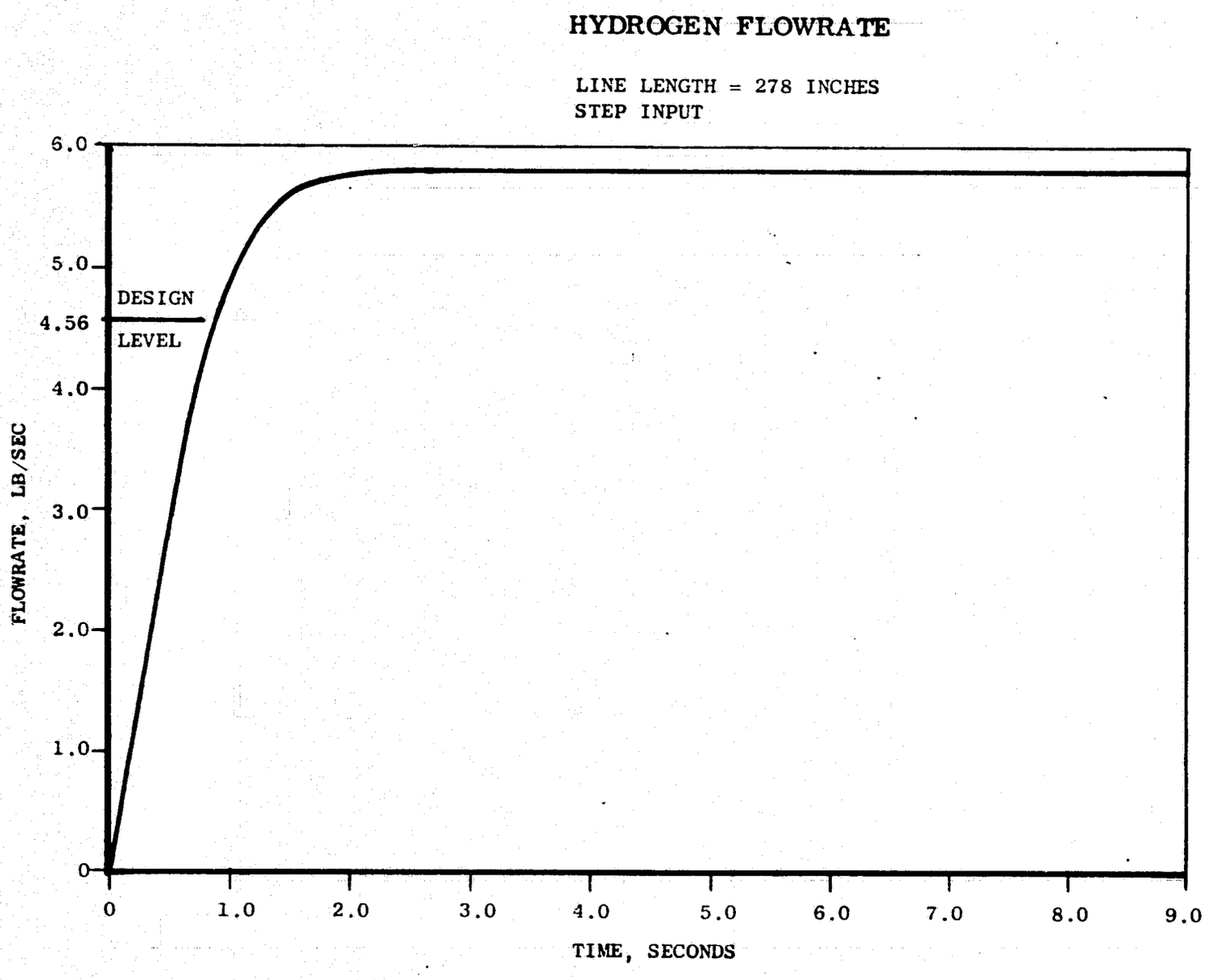

Figure 6. Maximum Ramp Rate of Hydrogen Pump With a Long Line

LOW-SPEED INDUCER DRIVE SELECTION

The low-speed inducer drive methods considered during the analysis period were gears, hydraulic turbines (both full and partial flow), hydrogen gas turbines, and finally, electric motors. The latter were not considered during the initial analysis because of the horsepower involved.

Gears

As is shown in Fig. 7, the low-speed oxygen inducer would be gear driven directly from the main LO_2 pump shaft. The gears would be dry-film lubricated and hydrogen cooled. This arrangement would necessitate the dynamic seal package shown on the drawing. The gear-driven low-speed hydrogen inducer shown on Fig. 8 would have both the bearings and the gearbox cooled by liquid hydrogen. The advantages of gear-driven inducers would be a positive drive and simplicity of design. The disadvantages would be gear life which has been demonstrated as 5.56 hours maximum at 16,000 fpm pitch line velocity, the gearbox coolant requirements, and the purged seal package required by the oxygen inducer.

Hydraulic Turbines

The full-flow hydraulic-turbine-driven inducer is located in line with its respective main pump as can be seen from Fig. 9 and 10. In this arrangement, the turbine is located between the main pump inducer and the impeller. The turbine derives its power from the discharge of the main pump inducer. The advantages of this arrangement are integrated packaging, no nonpropulsive propellant loss, and good life capability. The disadvantages are mechanical complexity, limited horsepower and head, and the fact that the inducer starts with (or even lags) the main pump so the start may be slow and there can be no chilldown benefit. A layout of a partial-flow hydraulic turbine drive is shown in Fig. 11. It utilizes a small portion of the main pump discharge flow to drive the turbine, after which the flow is returned to the inlet of the main pump. The development of the hydraulic-turbine-driven inducer

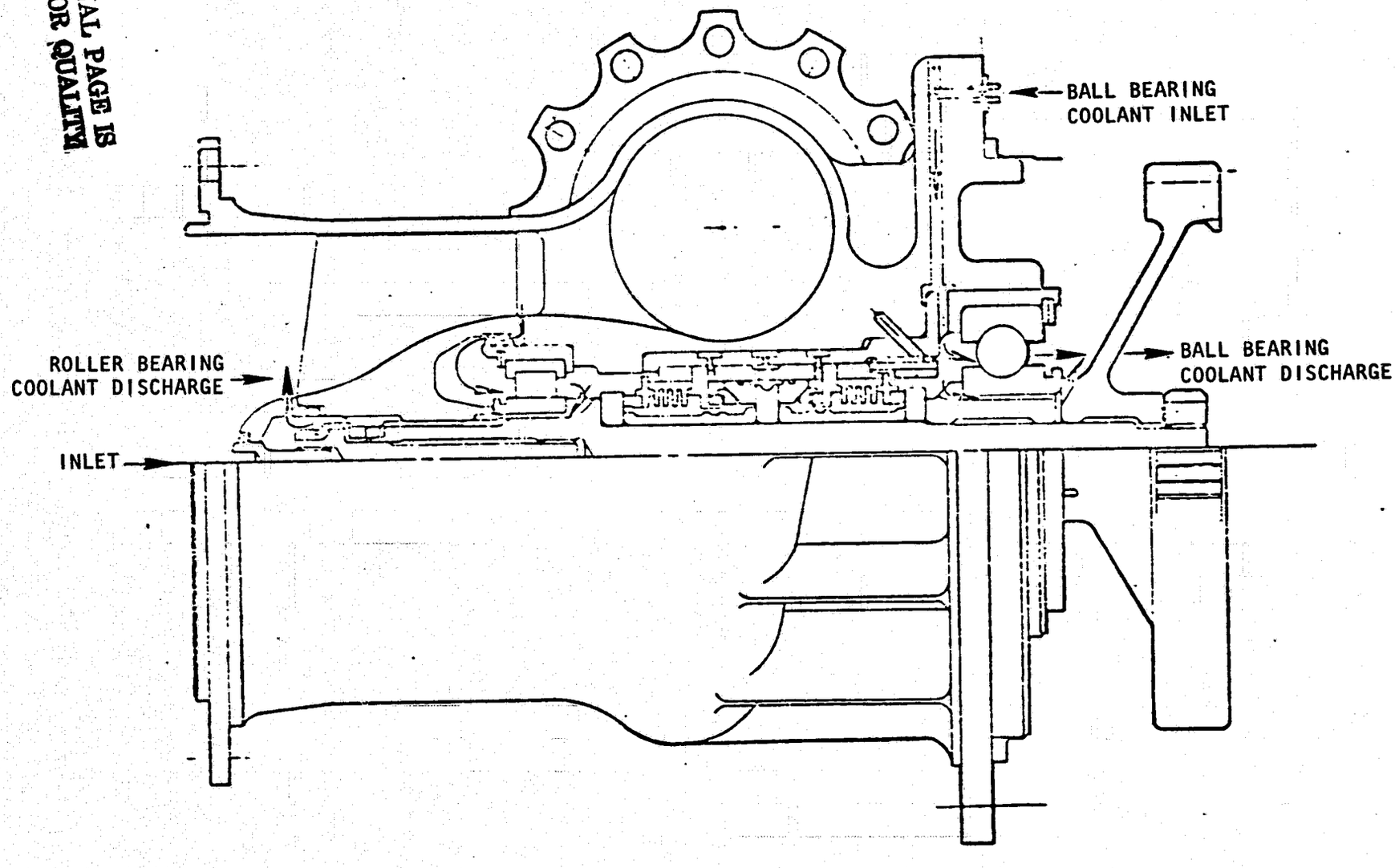

Figure 7. Gear Driven LO_2 Boost Pump Design

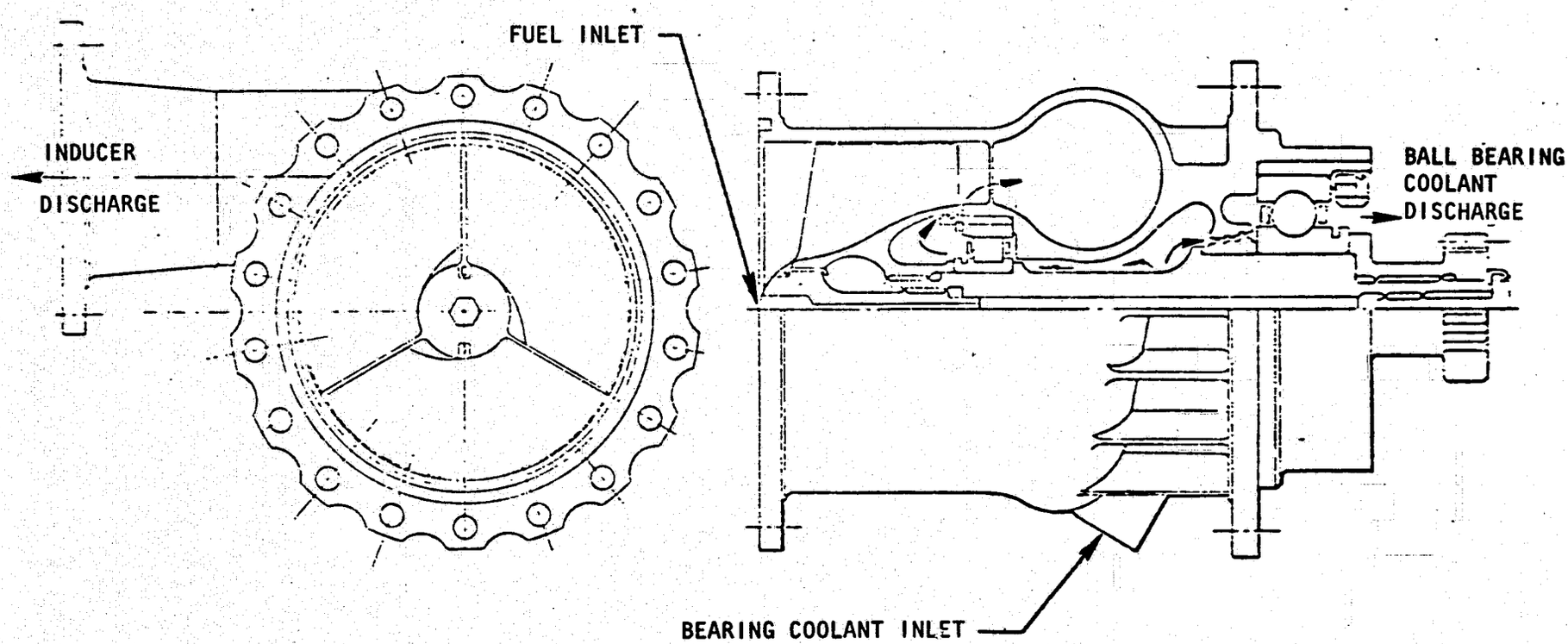

Figure 8. Gear Driven LH_2 Boost Pump Design

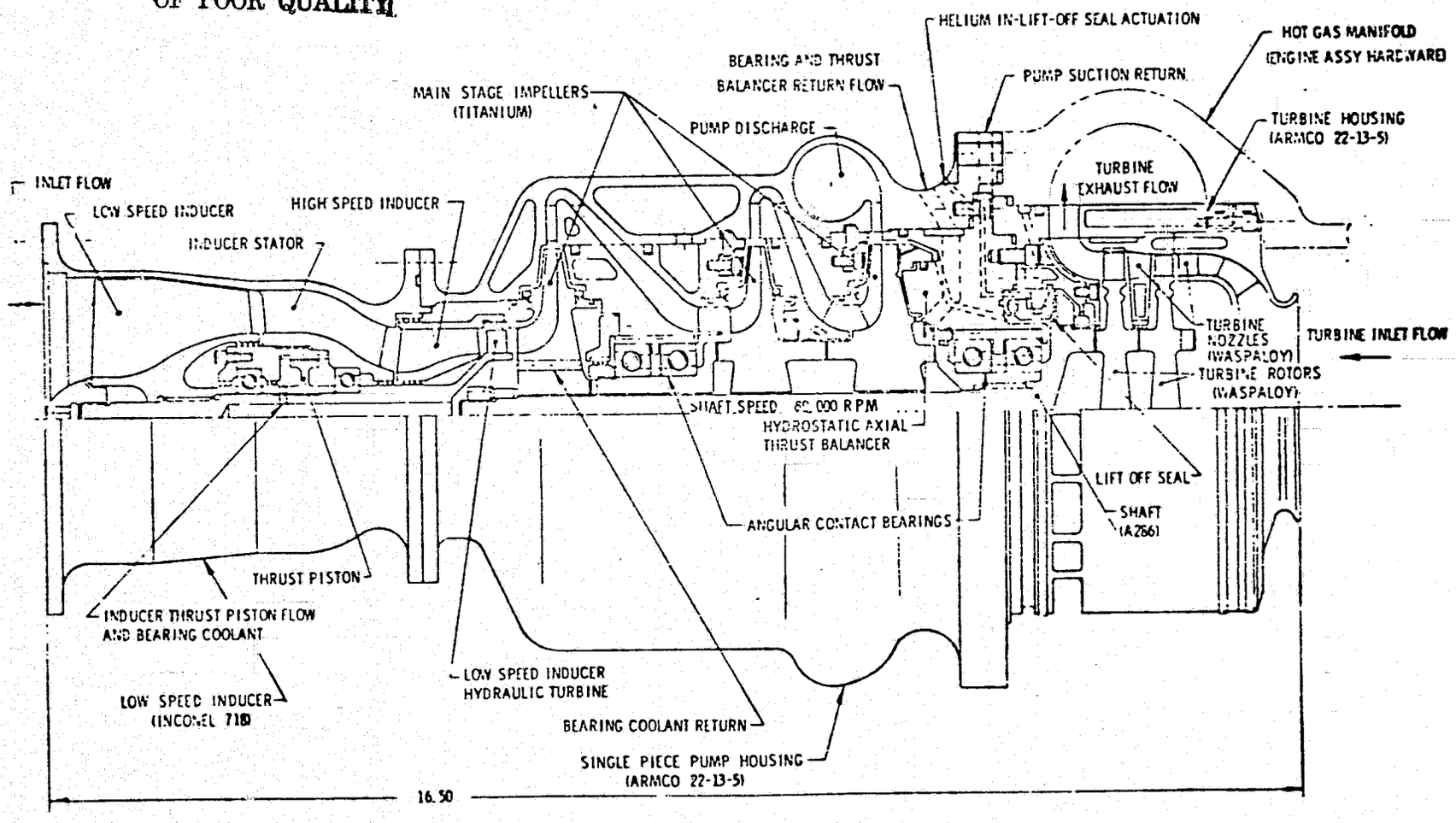

Figure 9. Fuel Turbopump Concept (Full Flow Hydraulic Boost Pump Drive)

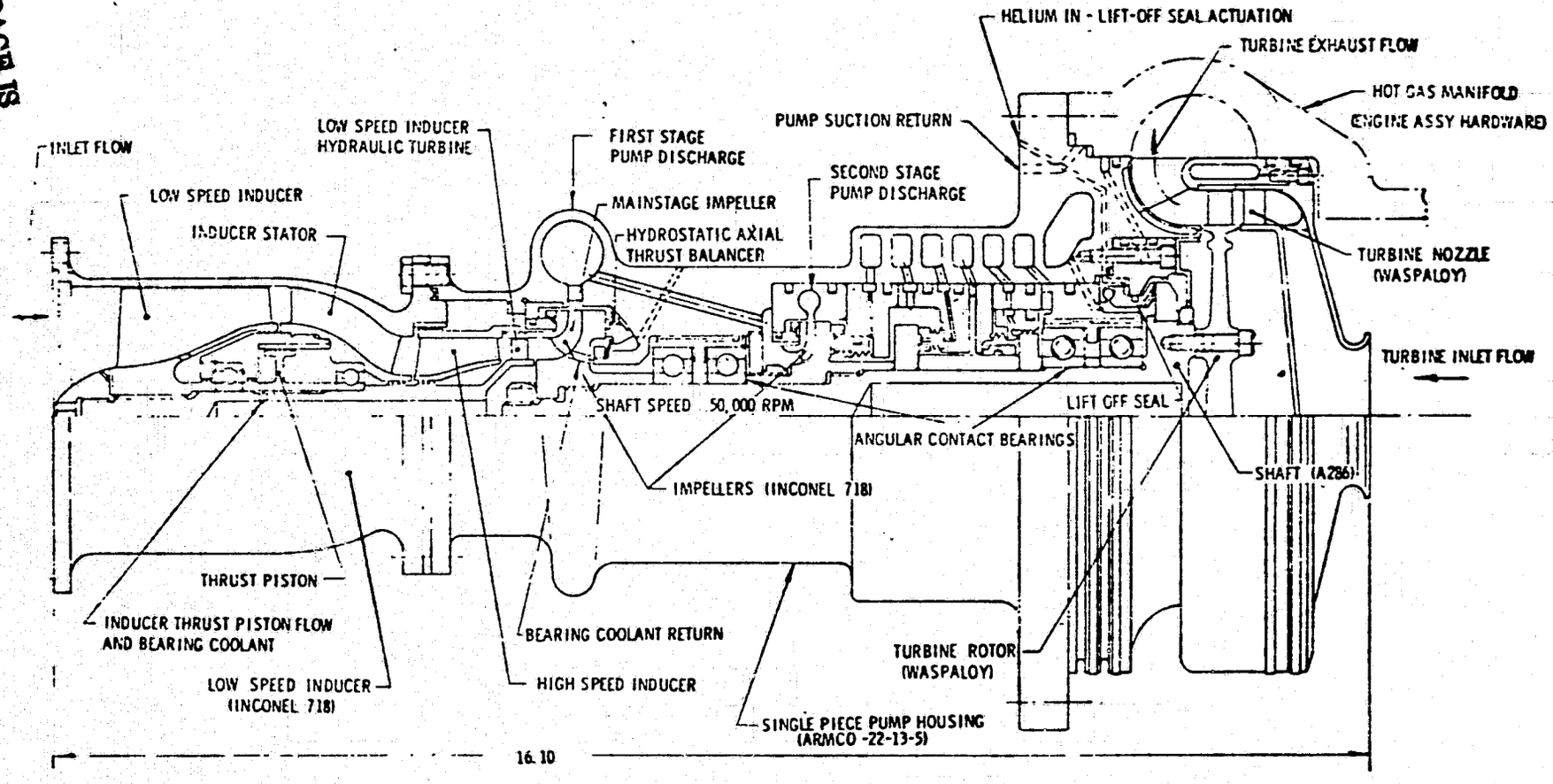

Figure 10. Oxidizer Turbopump Concept (Full Flow Hydraulic Boost Pump Drive)

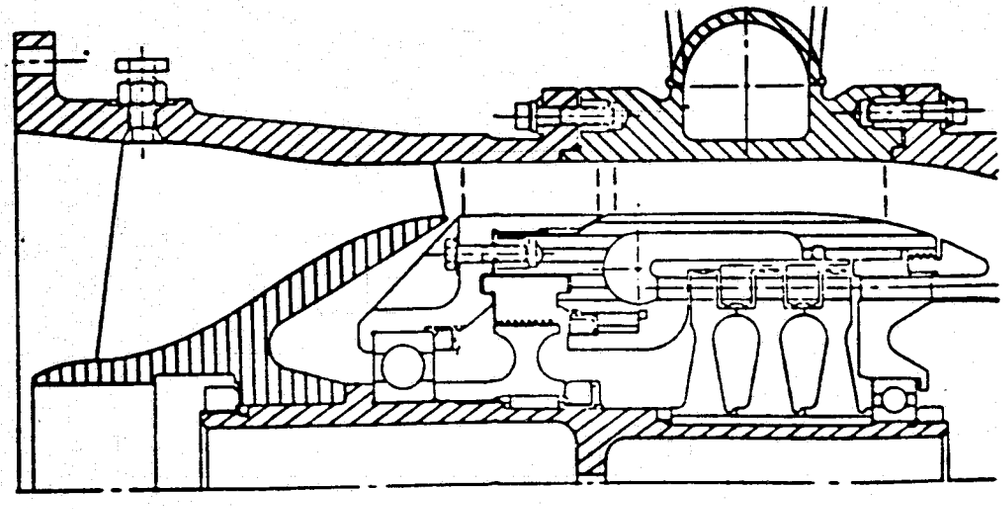

Figure 11. Partial Flow Hydraulic Boost Pump Drive

is described in Ref. 3. The advantages of the partial-flow hydraulic drive are flexible packaging, good life capability, and no nonpropulsive propellant loss. The disadvantages are that the start lags the main pump (no chilldown benefit) and that the flow returned to the main pump may be near the saturation point.

Hydrogen Gas Turbines

The GH_2 drives for the oxygen and hydrogen inducers are shown in Fig. 12 and 13. They consist of gas turbines driven by gaseous hydrogen heated in the thrust chamber cooling jacket. A small portion of the cooling jacket flow is diverted to drive the inducers prior to being routed to the preburner. The gas inlet pressure and temperature are approximately 4000 psi and 400 R, respectively based on some preliminary Rocketdyne studies. The advantages of the gas turbine drive are good life capability, flexibility, and more control over the start transient by helping the chilldown. The disadvantages are a purged seal package in the oxygen inducer, gas leakage into the hydrogen inducer, high-pressure GH_2 lines and a high axial shaft load.

It was concluded that because of the early benefit to the engine start process, the packaging flexibility, the flexibility for off-design operation, and the good life potential, the GH_2 drive method was the most desirable.

Fuel Turbopump Configurations

Two configurations were made of the gas-turbine-driven hydrogen inducer; these are shown in Fig. 14 and 15. The symmetrical arrangement of the seal package was used to balance the end thrust which could amount to 4000 pounds.

Configuration 1 was analyzed as having too much gas being returned to the inducer and was rejected. Configuration 2 with three seals on each side of the turbine was recommended. Note that the gas bleed between seals is vented into the inducer manifold and the liquid cooling the bearing returns to the inducer through the shaft.

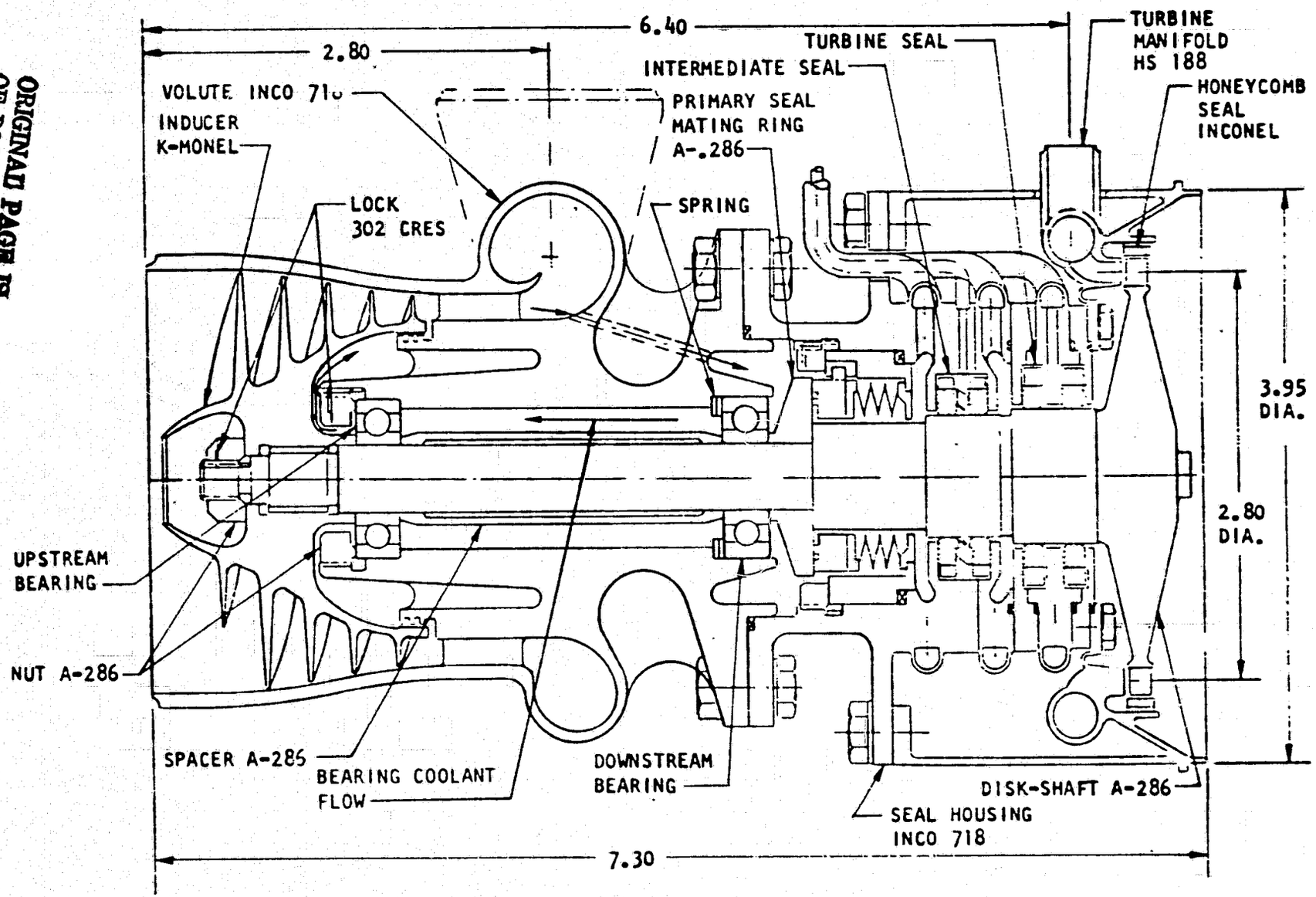

Figure 12. LO_2 Boost Pump (GH_2 Turbine Drive)

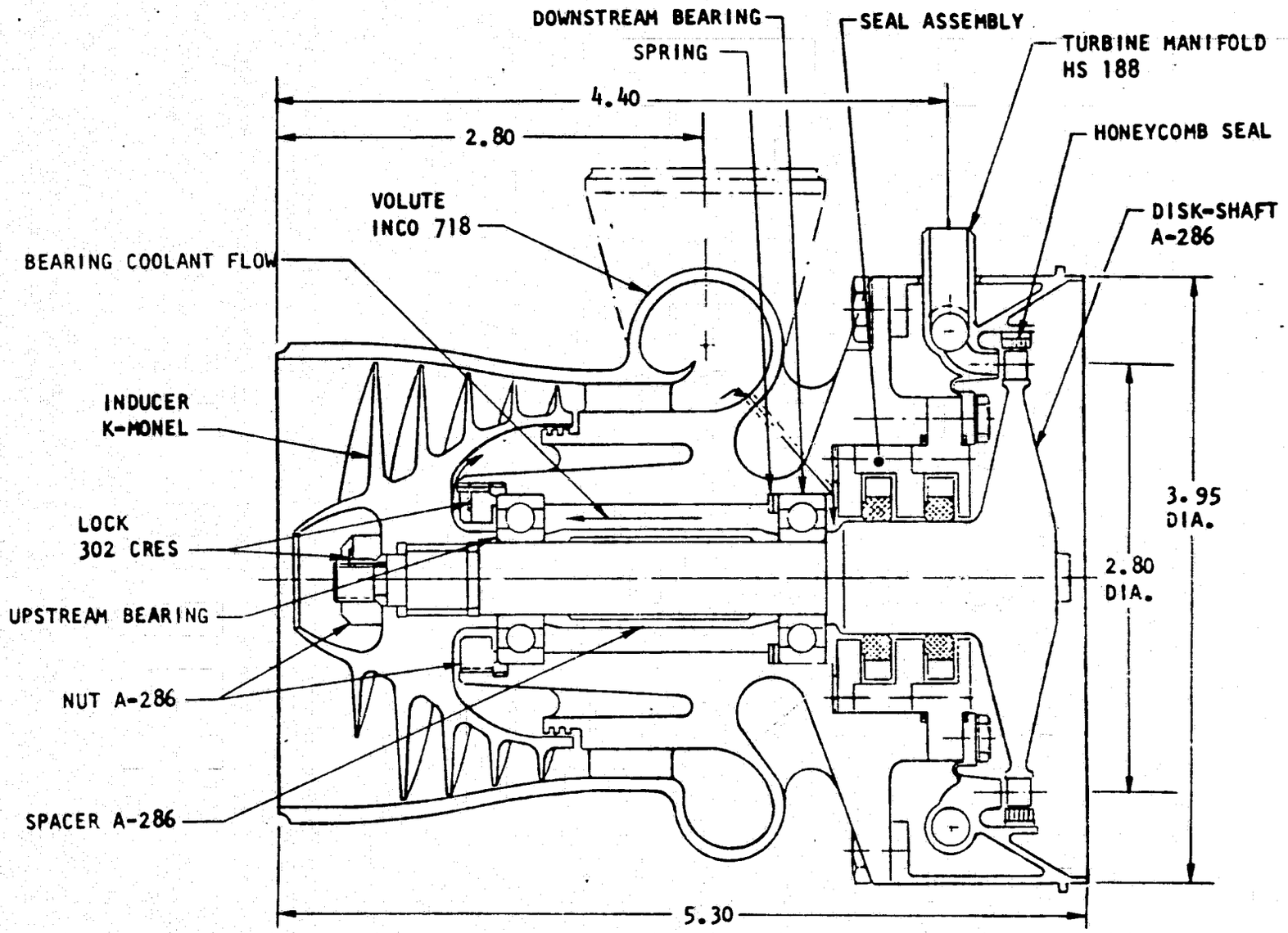

Figure 13. LH_2 Boost Pump (GH_2 Turbine Drive)

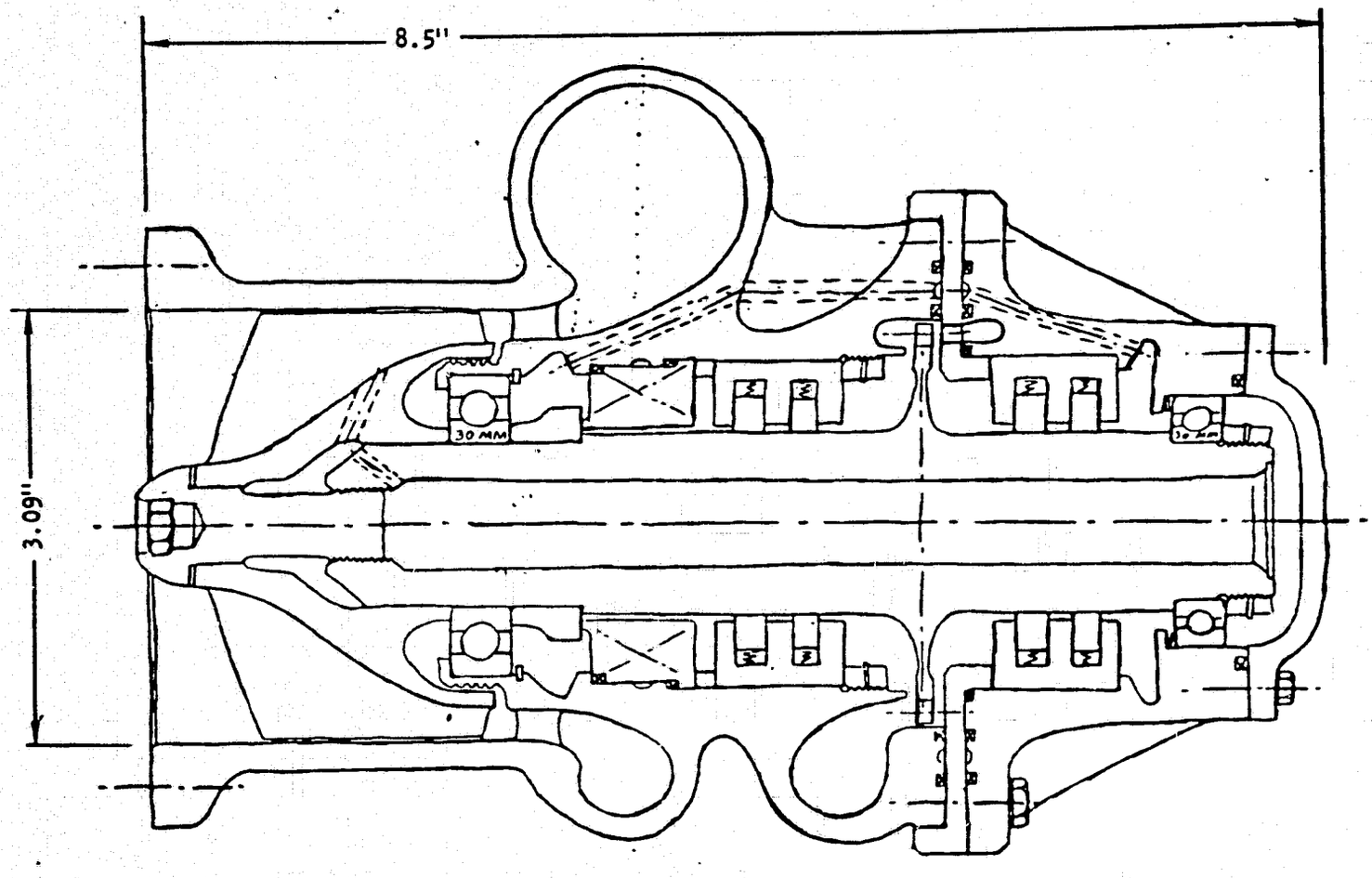

Figure 14. Low-Pressure Fuel Turbopump (Configuration No. 1)

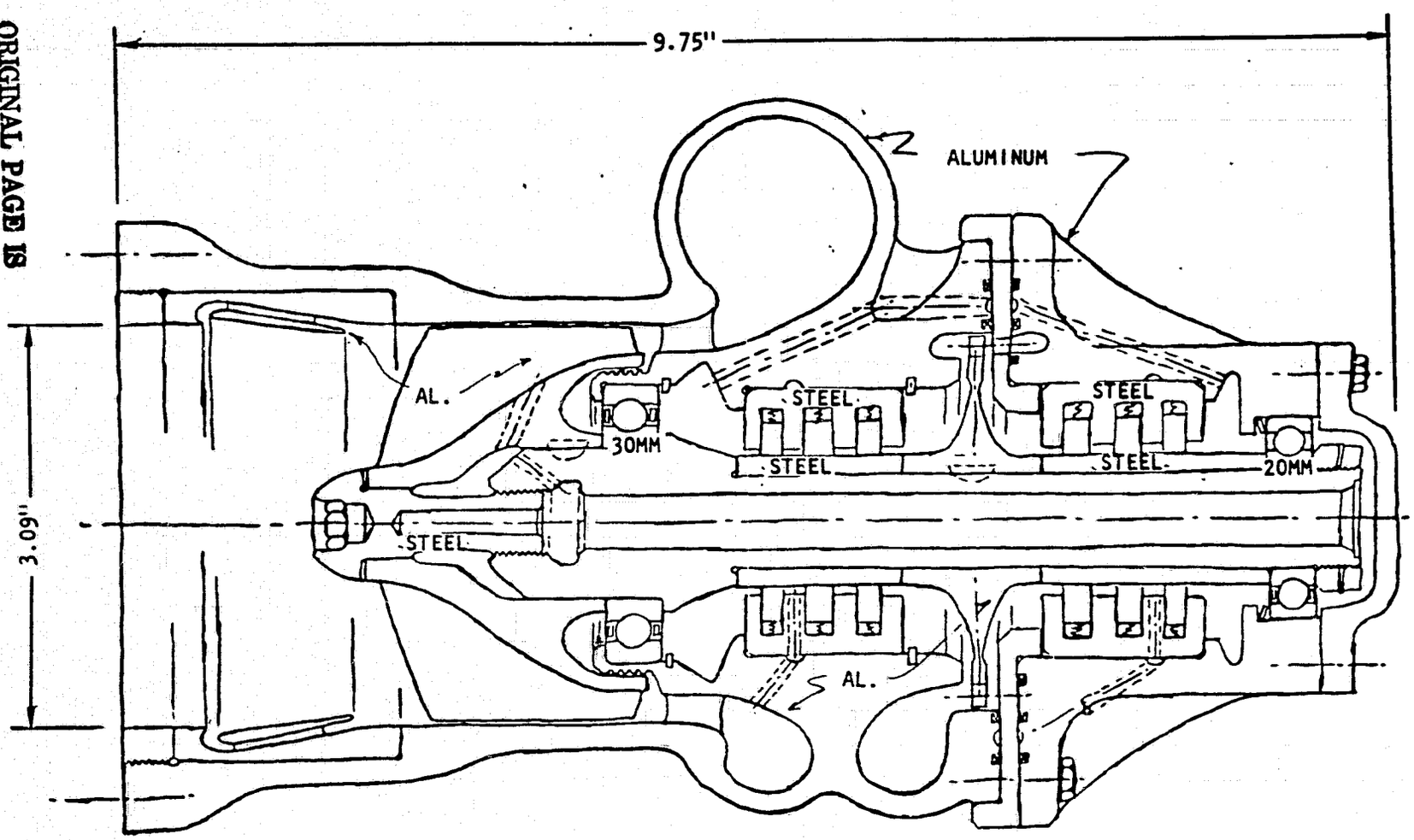

Figure 15. Low-Pressure Fuel Turbopump (Configuration No. 2)

Oxidizer Turbopump Configurations

Configuration 1 (Fig. 16) for the oxygen turbopump had a 30-mm bearing aft of the turbine that was either grease-packed or lubricated with GH_2. The symmetrical seal package was again necessary because of the high axial thrust. In the second oxidizer turbopump configuration (Fig. 17), the thrust bearing was put in front of the pump and the turbine was overhung. The effects of the front bearing housing, the struts, and the front bearing cooling flow on the two-phase pumping capability of the inducer were the major objections.

The critical speeds of the first two configurations were substantially higher than the operating speed. The turbine shaft diameter was therefore reduced to minimize the axial thrust and a 60-mm bearing was used to take the end thrust. This recommended configuration is shown in Fig. 18.

Revision of Design Points

At the Conceptual Design Review it was decided that making the inducer capable of operating on the 20K Space Tug design with its relatively high head requirements and high gas pressures placed too many restrictions on the design; the result was long and complicated seal packages and relatively large pumps. The program was therefore redirected to satisfy only the 15K and the RL-10 requirements.

Studies made on the 15K RL-10 indicated that during the start transient, the main hydrogen pump required 381 feet of head at the inlet when the flow was 2.76 lb/sec and during mainstage operation it required 182 feet at 4.87 lb/sec. The RL-10, Category III engine required 53.6 feet at mainstage. The two-phase inducer that satisfies these requirements has a constant tip diameter of 3.078 inches and an inlet hub diameter of 0.727 inch. It runs at a speed of 14,085 rpm with a peak efficiency estimated to be 74 percent.

The studies also indicated that during the start transient, the main oxygen pump required 44.7 feet of head at the inlet where the flow was 13.0 lb/sec and during mainstage operation it required 18.2 feet at 29.2 lb/sec. The RL-10, Category III

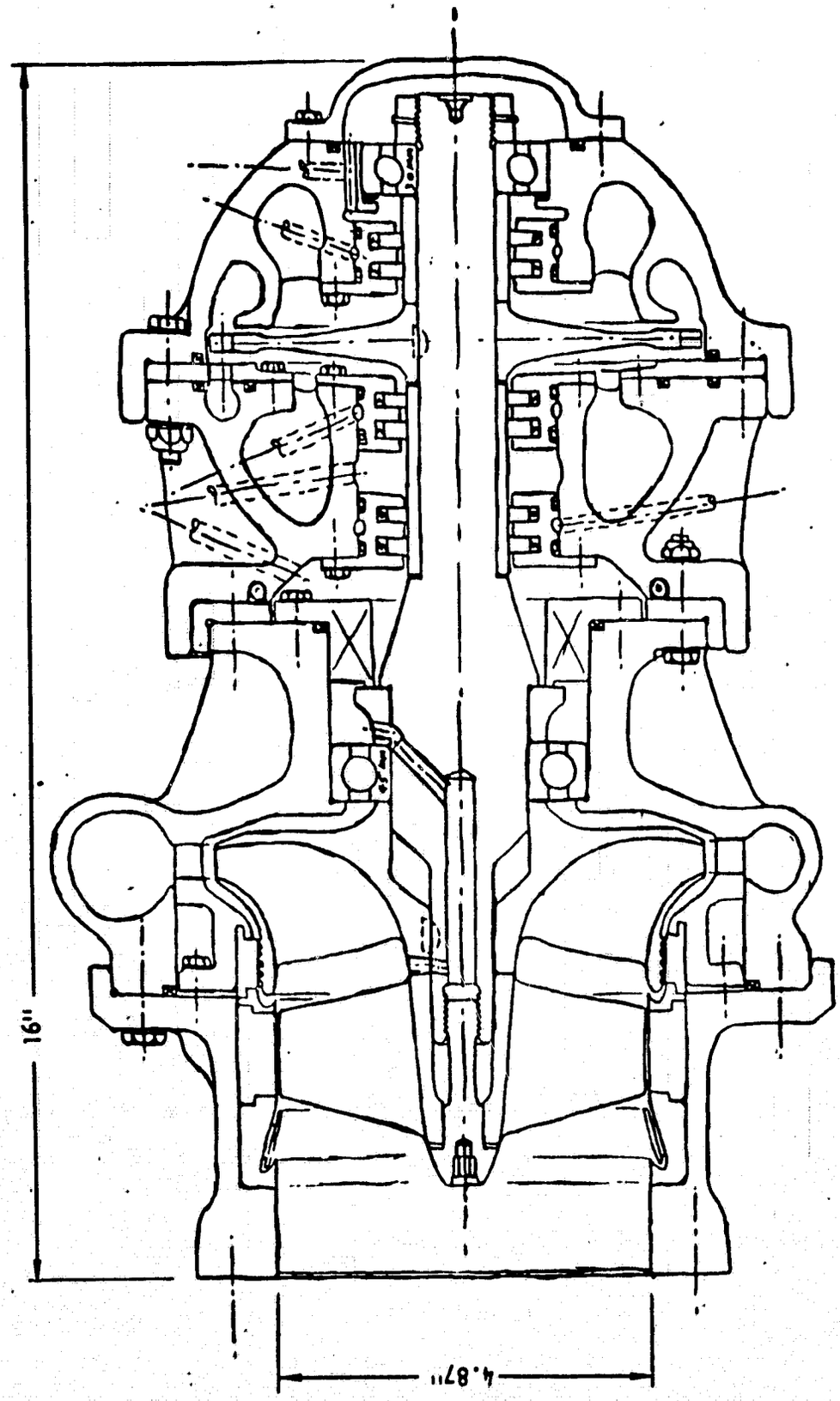

Figure 16. Low-Pressure Oxidizer Turbopump (Configuration No. 1)

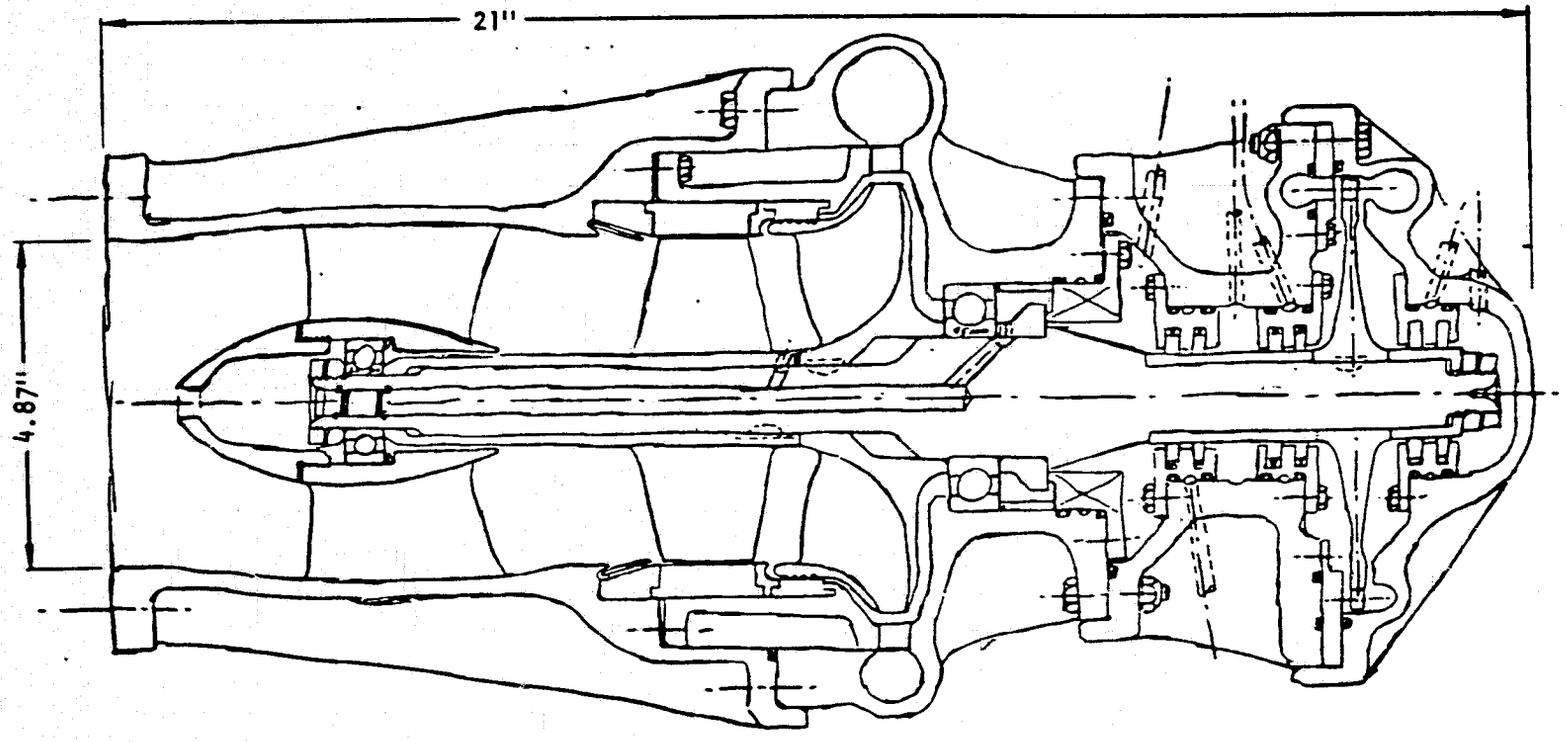

Figure 17. Low-Pressure Oxidizer Turbopump Forward Bearing (Configuration No. 2)

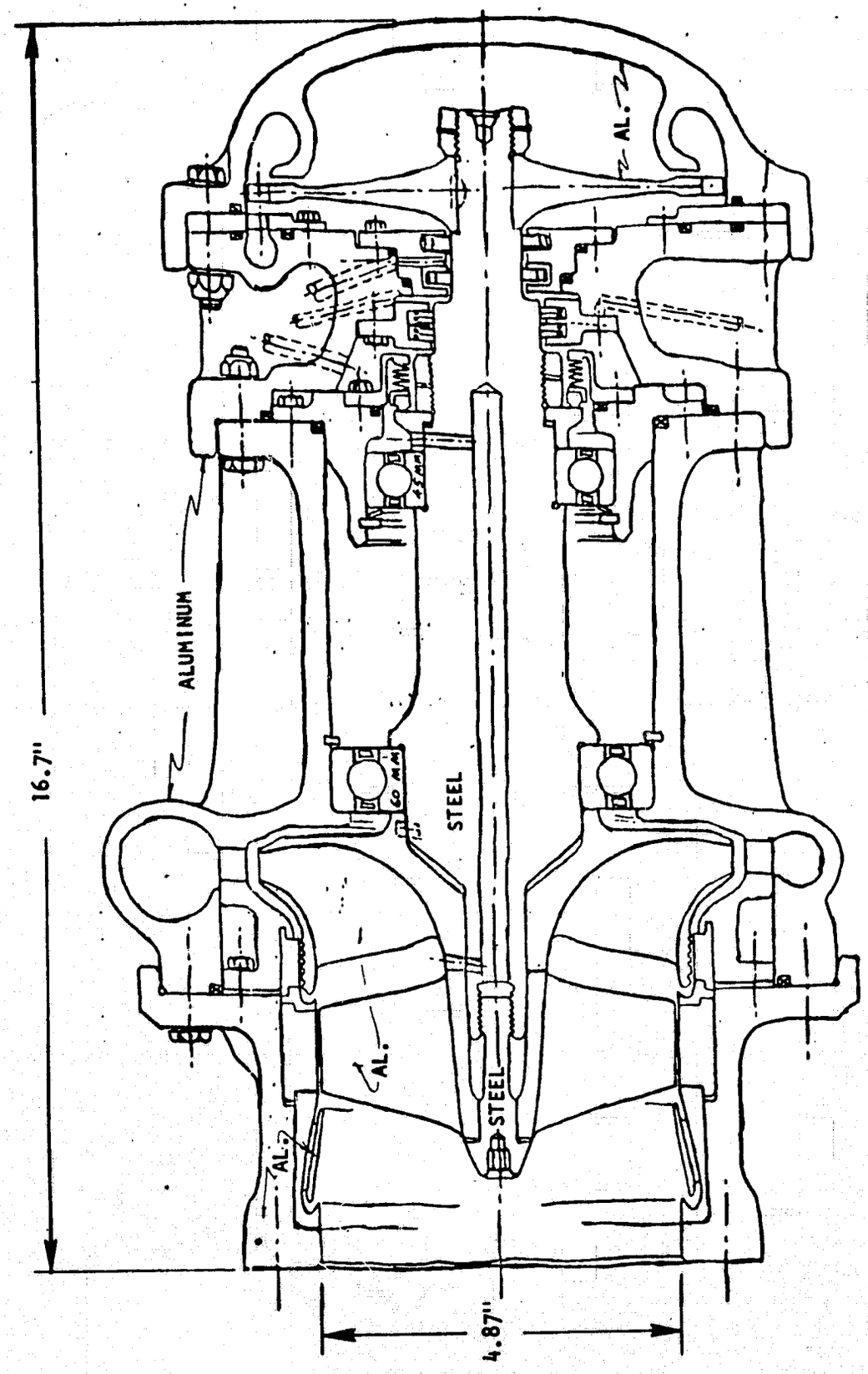

Figure 18. Low-Pressure Oxidizer Turbopump (Configuration No. 3)

ORIGINAL PAGE IS
OF POOR QUALITY

engine required 9.5 feet at mainstage. The two-phase inducer that satisfies these requirements has a constant tip diameter of 4.849 inches and an inlet hub diameter of 1.460 inches. It runs at 3008 rpm with a peak efficiency estimated to be 63 percent.

Comparison of Electric Motors with Hydrogen Gas Turbines

With the reduced power requirements, it became possible to drive the inducers with electric motors. Such motors could be provided with electricity from fuel cells on the Space Tug with inverters being used to provide alternating current. Rocketdyne was therefore directed by MSFC to study and compare electric motor drives with hydrogen gas turbines. The comparison is shown in Table 1.

Final Configuration Selection

The tradeoff studies showed that there was no great difference between the hydrogen gas turbine drive and the electric motor drive as to size and weight. It was apparent, however, that the electric motor drive would be more flexible in its application to a "breadboard" turbomachinery package. It was therefore decided by both Rocketdyne and MSFC to use the electric motor drive.

TABLE 1. COMPARISON OF GH_2 TURBINE DRIVE TO ELECTRIC MOTOR DRIVE

	GH_2 Turbine Drive	Electric Motor Drive
Weight	Hydrogen turbine ≅ 3 pounds; oxygen turbine ≅ 8 pounds • Oxygen turbine requires a helium purge, so add the weight of the helium plus bottle.	Hydrogen motor ≅ 9.6 pounds, oxygen motor ≅ 20 pounds • Hydrogen gas lines, engine tapoff and valves probably offset weight of wires and inverters.
Size	Approximately the same. Motors are slightly longer; turbine plus manifolds have a larger OD	
Seals	• Turbines have complicated seal packages particularly the oxygen turbine which has a helium purge. There is a slight danger of seal failure and oxygen and hydrogen mixing. • There are also overboard vents on the oxygen turbine. • In the hydrogen turboinducer, the turbine gases mix with pump flow reducing NPSH. Amount of reduction can be substantial. • End thrust can be high at start or at high speed. • Breakaway torque can be critical if only low-pressure gas is available at start.	• Motors are hemetically sealed--no seal packages. • No turbine end thrust at either start or steady state • No breakaway torque caused by rubbing seals. • Heat from motors has only small effect on NPSH.
Operational Features	• Turbines are engine-mounted only. • Turbines need a pressure bottle for starting. • Turbines could operate at a variety of speeds during the start transient to satisfy peak requirements. However, they would have to be sequenced and controlled. Control system could be complicated if the start is from a bottle and then to the engine bypass which pressure is changing during the transient. • Turbines could "run away" (particularly during the test program) when pump head drops suddenly at the two-phase pumping limits. An overspeed trip would be necessary.	• Motors can be mounted at the engine, in the pipe or in the tank. • Motors can operate before engine start to chilldown system. • Motors are constant-speed even at no load. Control is possible only by the shape of the H-Q map. • Motors will not "run away."
Testing	• Turbines are more difficult to control because of the variable supply pressure. • Hydrogen gas at high pressures is available at only a few locations. Burnoff stacks are necessary. Gas must be replenished at intervals. • Hydrogen gas lines.	• Electrical motors are more flexible. They can be controlled to the exact speed required by varying the frequency of the inverter. • Electricity is in constant supply at many locations. • Wires.
Technology Advancement	• Turbines would provide partial admission turbine efficiency data, acceleration rates, breakaway torque information and control and sequencing data plus cost and weight data. • Future tradeoff studies would include weight and cost of helium and tanks for purges and hydrogen and bottle weights and costs for starting purposes.	• Only a few experimental cryogenic motors have been tested and the data are not readily available. Weights and particularly costs are very approximate. Acceleration rates (zero to full speed) are not known. Motor and system efficiencies are vague. Methods of getting the lead wires out of the motor have not been studied. Motor running temperature and resultant heat soakback are unknowns. • Future tradeoff studies might include the weight and cost of 400 cps current and a 16-pole motor versus a 4-pole motor and extra inverter weight.

PHASE II--DETAILED ANALYSIS AND DESIGN

TWO-PHASE OXYGEN INDUCER LAYOUT

Figure 19 is a reproduction of the oxygen inducer layout. The inducer adds rotation and pressure to the two-phase oxygen, the pressure causing the vapor to collapse into a liquid. The inducer has a constant tip diameter of 4.849 inches and the diameter of the wall surrounding it is 4.868 inches. The inducer inlet diameter and blade angles were chosen to handle two-phase flow over a wide flow range with the nominal vapor content being 25.2 percent by volume. The solidity of the inducer blades at the tip was fixed at 2.5 to achieve the design head. The inducer has four blades with no splitters. The blade discharge angles were chosen to achieve free-vortex flow which produces constant head from hub to tip.

The stator vanes that remove the rotation put in by the inducer act as supports for the electric motor and the bearings. Their basic length and diameters were dictated by the motor size. Two stator rows, each with 11 vanes, were required to accomplish the diffusion. Figure 20 shows the profiles of these vanes. They are machined integral with the inner wall, and the outer wall is then shrunk around them. As can be seen from Fig. 20, the diffuser vanes are pinned to the outer wall to prevent movement and fretting in liquid oxygen. The vanes have an outer diameter of 4.7 inches and an inner diameter of 4.0 inches. The vanes remove all the rotation put in by the rotor, and the liquid oxygen is then discharged into a 2.5-inch pipe, this size being sufficient for removal of the rear bearing assembly.

The electric motor stator windings are "canned" in a 304 series stainless steel housing with all parting lines sealed with an inert gas fusion weld. The final assembly is checked for leaks with a helium mass spectrometer. The nominal wall thickness for the can is 0.040 inch except for the cylinder in the motor air gap which is machined after welding to a nominal wall thickness of 0.010 inch. As shown in Fig. 19, the "can" is shrunk into the aluminum diffuser housing with 0 to 0.004-inch interference at ambient temperature. This provides a 0.007-inch interference fit at cryogenic temperatures. The can makes contact with the housing

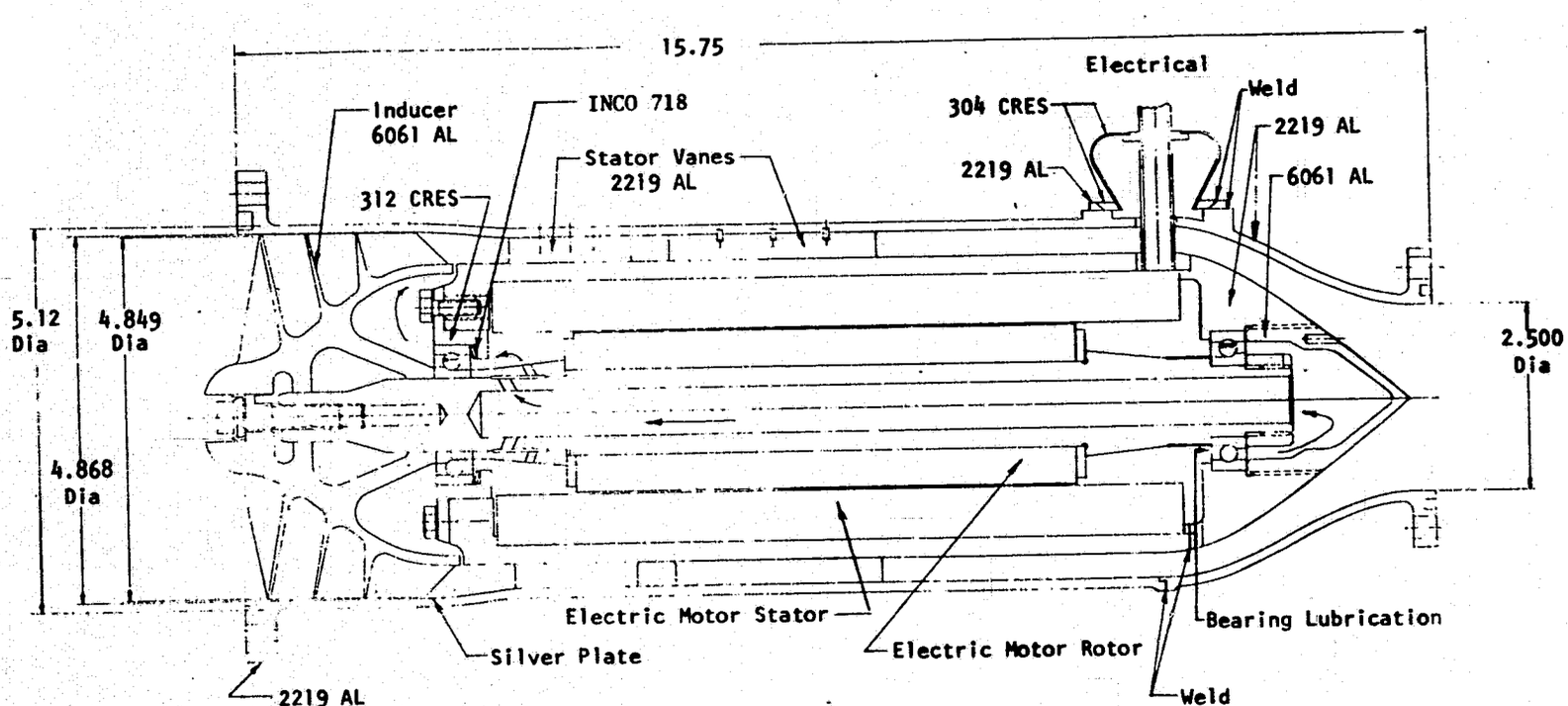

Figure 19. Oxygen Inducer Layout

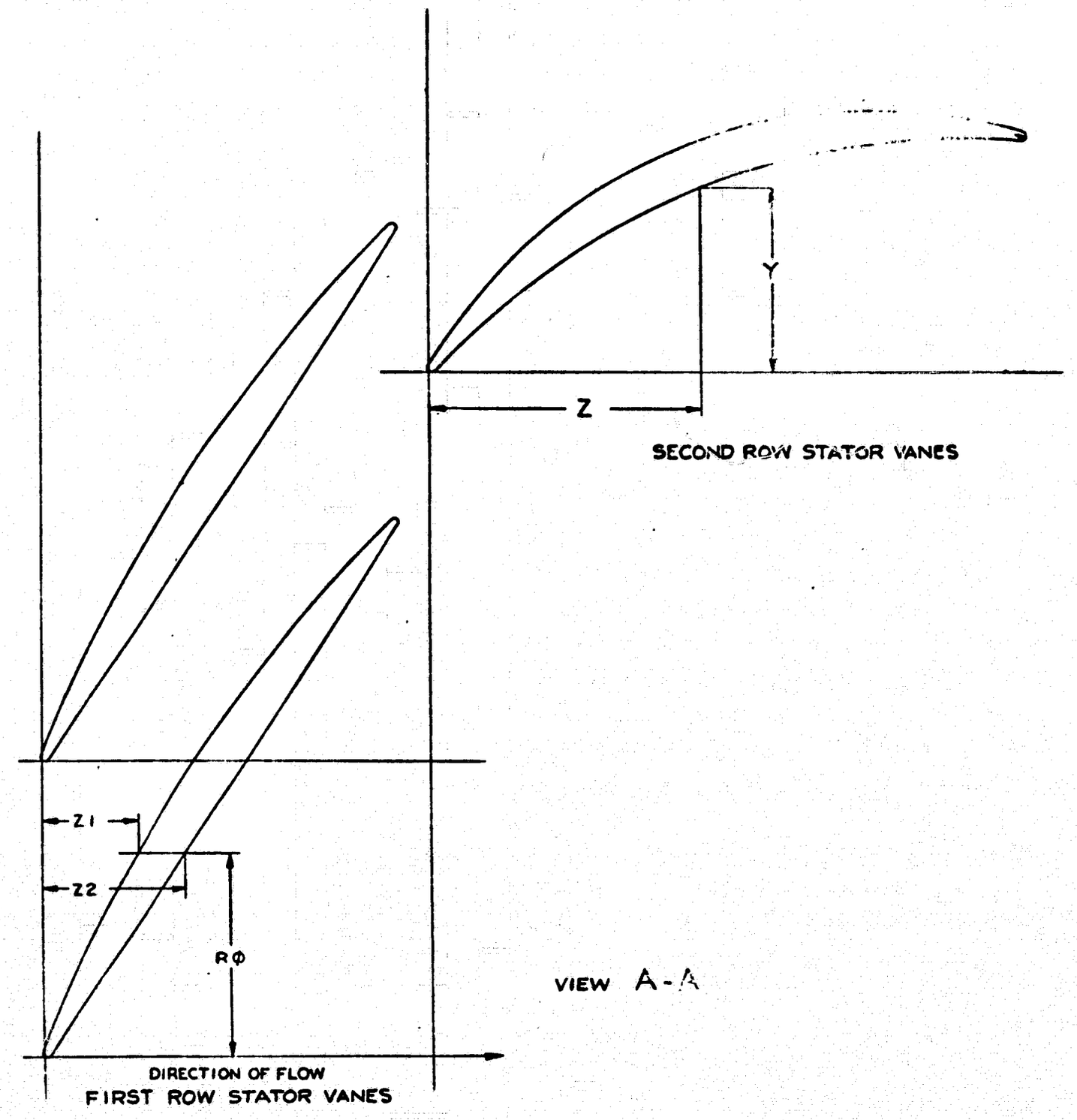

Figure 20. Stator Vane Profiles

along its entire length to provide good heat transfer out of the motor windings. The can has an integral radial tube through which the three-phase, wye-connected leads emerge from the motor. As shown in Fig. 19, the tube has a flange to which the LOX diaphragm seal is welded. This diaphragm allows for the differential expansion between the steel can and tube and the aluminum housing. The tube extends 6 inches beyond the flange so that the electrical connector at the terminal is separated from the LO_2 thermal cold sink. The connector is waterproof for Fire-X considerations.

The electric motor rotor has a press fit onto the shaft and makes contact with the shaft over its entire length so as to provide good heat transfer to the fluid inside the shaft.

The bearings are lubricated with liquid oxygen that enters through the slot underneath the rear bearing (see Fig. 19). Approximately 0.3 lb/sec of oxvgen flows rearward through the rear bearing, turns 180 degrees into the end of the shaft, flows through the shaft, out the two metering holes, through the front bearing, and re-enters the mainstream between the inducer and its inner cavity; two metering holes are used so as not to affect the balance of the shaft. Both bearings are 25-mm ball bearings. The rear bearing is locked in place and the bearing preload is fixed by the front bearing acting through a spring. Support is provided through the front flange acting as a cantilever or through both front and rear flanges.

The primary design parameters for the oxygen pump are given in Table 2. The predicted performance of the inducer-stator combination is shown in Fig. 21 with the different operating points shown on the curve. Table 3 gives the various stator operating parameters and Table 4 gives the electric motor characteristics.

TABLE 2. OXYGEN PUMP DESIGN PARAMETERS

Overall Pump	
Design Flow, lb/sec	23.51
Head Rise, feet	37.2
Efficiency, percent	68.0
Horsepower	2.34
Inducer	
Wall Diameter, inches	4.868
Speed, rpm	3008
Number of Blades	4
Inlet Tip Blade Angle, degrees	9.02
Inlet Design Incidence Angle, degrees	5.97
Stators	
Number of Rows	2
Number Blades per Row	11
Tip Diameter, inches	4.7
Hub Diameter, inches	4.0

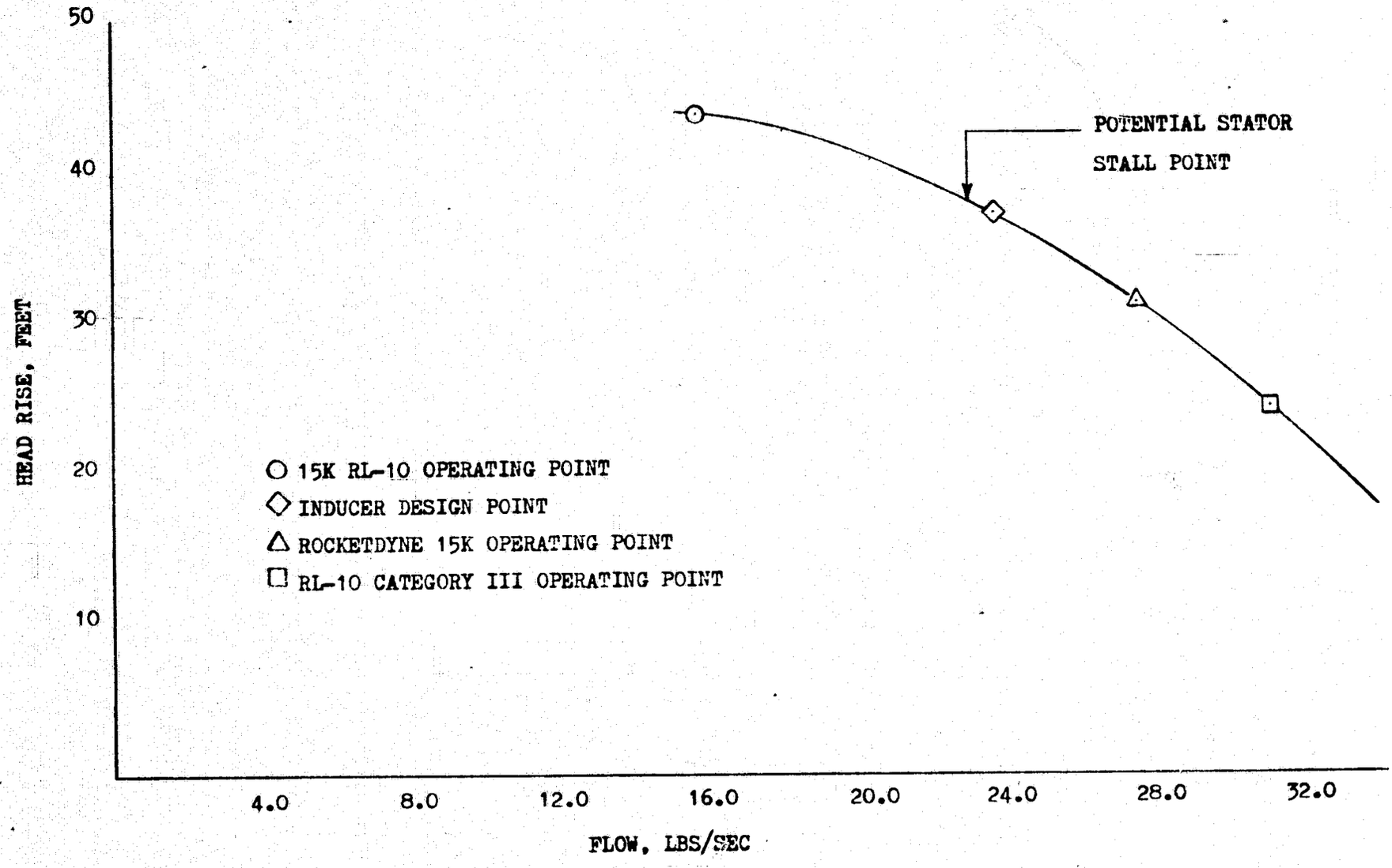

Figure 21. Oxygen Inducer Performance, Speed = 3008 rpm

TABLE 3. OXYGEN PUMP STATOR HYDRODYNAMIC FEATURES

	Minimum 15K RL-10 Operating Point	Inducer Design Point	Rocketdyne 15K Operating Point	RL-10 Category III Operating Point
Flowrate, lb/sec	15.57	23.51	27.35	30.80
Stator 1 Hub Diffusion Factor	0.8529	0.5792	0.4193	0.2560
Stator 1 Tip Incidence Angle	17.45	6.67	-1.66	-12.18
Stator 1 Cavitation Region	Hub-Tip Nose	None	Hub Nose	Tip-Nose, Hub Nose and Surfaces
Stator 2 Diffusion Factor	0.5961	0.5961	0.5961	0.5961
Stator 2 Cavitation Region	None	None	None	Nose if Stator 1 Separates

TABLE 4. PERFORMANCE CHARACTERISTICS OF OXYGEN MOTOR

SLIP	TORQUE IN.LB.	RPM	HP	I AMPS	EFF	PF	WATTS	VA	PRI LOSS	SEC LOSS	IRON LOSS	F W LOSS
0.20	0.97	3326	0.051	3.623	20.68	14.81	185	1250	11.8	0.1	105	29.9
0.40	2.70	3320	0.142	3.660	41.87	20.07	253	1263	12.0	0.5	105	29.8
0.60	4.43	3313	0.233	3.711	53.93	25.13	322	1280	12.4	1.2	105	29.6
0.80	6.14	3306	0.322	3.774	61.66	29.95	390	1302	12.8	2.2	105	29.5
1.00	7.86	3300	0.411	3.848	67.00	34.49	458	1328	13.3	3.4	105	29.4
1.50	12.11	3283	0.631	4.082	75.02	44.54	627	1408	15.0	7.6	105	29.1
2.00	16.32	3266	0.846	4.372	79.32	52.73	795	1508	17.2	13.5	105	28.8
2.50	20.47	3250	1.055	4.706	81.87	59.23	962	1624	19.9	20.9	105	28.5
3.00	24.57	3233	1.260	5.075	83.46	64.32	1126	1751	23.1	29.9	105	28.2
3.50	28.59	3216	1.459	5.470	84.46	68.28	1289	1887	26.8	40.5	105	27.9
4.00	32.54	3200	1.652	5.884	85.07	71.36	1448	2030	31.1	52.5	105	27.6
4.50	36.41	3183	1.839	6.311	85.42	73.74	1606	2177	35.7	65.9	105	27.4
5.00	40.20	3166	2.019	6.748	85.59	75.60	1760	2328	40.9	80.7	105	27.1
5.50	43.89	3150	2.193	7.191	85.61	77.03	1911	2481	46.4	96.8	105	26.8
6.00	47.49	3133	2.360	7.637	85.53	78.14	2059	2635	52.3	114.1	105	26.5
6.50	50.99	3116	2.521	8.085	85.36	78.98	2203	2789	58.7	132.6	105	26.2
7.00	54.39	3100	2.674	8.533	85.13	79.61	2344	2944	65.3	152.1	105	25.9
7.50	57.68	3083	2.821	8.978	84.85	80.07	2480	3098	72.3	172.7	105	25.7
8.00	60.87	3066	2.961	9.422	84.53	80.39	2613	3250	79.7	194.3	105	25.4
8.50	63.95	3050	3.094	9.861	84.17	80.60	2742	3402	87.3	216.7	105	25.1
9.00	66.91	3033	3.220	10.296	83.78	80.71	2867	3552	95.1	240.0	105	24.8
9.50	69.77	3016	3.338	10.726	83.37	80.73	2987	3700	103.2	264.0	105	24.6
10.00	72.51	3000	3.451	11.150	82.94	80.68	3104	3847	111.6	288.7	105	24.3
20.00	105.60	2666	4.467	18.128	72.61	73.38	4589	6254	294.9	837.8	105	19.2
30.00	110.38	2333	4.085	22.439	61.80	63.71	4932	7741	451.8	1312.5	105	14.7
40.00	103.95	2000	3.298	25.024	51.41	55.43	4785	8633	561.9	1647.3	105	10.8
50.00	94.64	1667	2.502	26.625	41.58	48.87	4489	9186	636.1	1874.0	105	7.5
60.00	85.44	1333	1.807	27.864	32.30	43.73	4174	9544	686.8	2029.2	105	4.8
70.00	77.22	1000	1.225	28.371	23.54	39.66	3882	9788	722.3	2138.5	105	2.7
80.00	70.13	667	0.742	28.871	15.26	36.39	3625	9960	748.0	2217.7	105	1.2
90.00	64.06	333	0.339	29.237	7.43	33.73	3402	10087	767.1	2276.8	105	0.3
100.00	58.87	0	0.000	29.514	0.00	31.51	3209	10182	781.7	2322.0	105	0.0

TWO-PHASE HYDROGEN INDUCER LAYOUT

Figure 22 is a reproduction of the hydrogen inducer layout. The hydrogen inducer is similar in function and construction to the oxygen inducer. The hydrogen inducer will probably be located near the tank with a moderately long discharge line to the main pump which will be engine-mounted. Calculations have shown that a 3-inch line will be adequate to keep the line losses at a minimum. The area of this line is large compared to the inducer discharge area so a moderate amount of axial diffusion is necessary. From Fig. 22, it can be seen that this takes place at the rear of the unit between the stator exit and the pipe.

The electric motor is not "canned" but is still held by the aluminum housing with an interference fit. The electrical lead tube is part of the pump housing and is therefore, aluminum.

Both bearings are 25-mm ball bearings and both are spring loaded. Support can be through both front and rear flanges, or the pump can be cantilevered from the front flange. They are cooled by a flow of approximately 0.25 lb/sec of hydrogen.

The primary design parameters for the hydrogen pump are shown in Table 5. The predicted performance of the inducer-stator combination is shown in Fig. 23 with the operating points shown on the curve. Table 6 gives the stator operating parameters and Table 7 the electric motor characteristics.

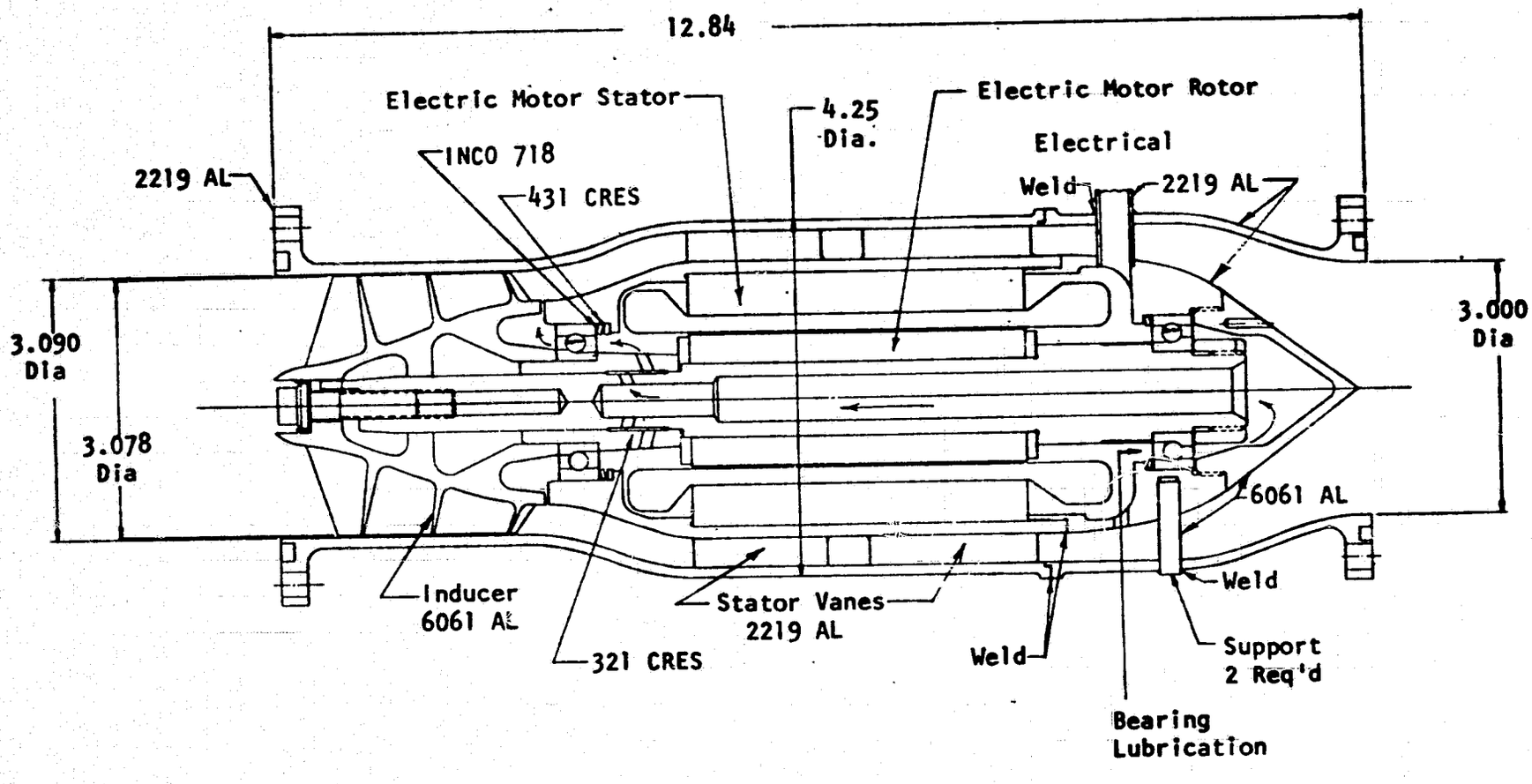

Figure 22. Hydrogen Inducer Layout

TABLE 5. HYDROGEN PUMP DESIGN PARAMETERS

Overall Pump	
Design Flow, lb/sec	4.025
Head Rise, feet	297
Efficiency, percent	74.2
Horsepower	2.94
Inducer	
Wall Diameter, inches	3.09
Speed, rpm	14,058
Number of Blades	4
Inlet Tip Blade Angle, degrees	18.8
Tip Design Incidence Angle, degrees	11.9
Stators	
Number of Rows	2
Number Blades per Row	11
Tip Diameter, inches	4.0
Hub Diameter, inches	3.3

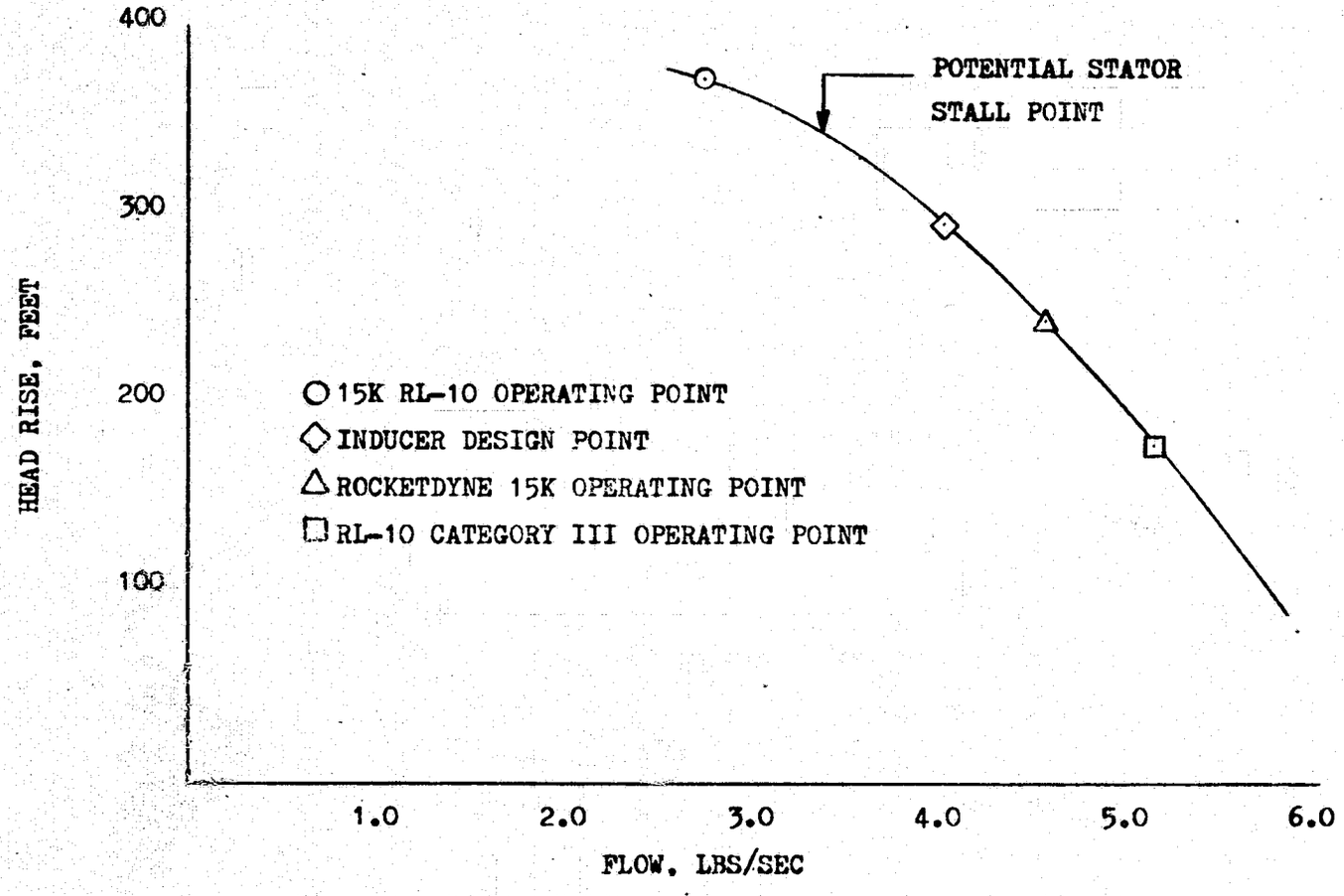

Figure 23. Hydrogen Inducer Performance, Speed = 14,058 rpm

TABLE 6. HYDROGEN PUMP STATOR HYDRODYNAMIC FEATURES

	Minimum 15K RL-10 Operating Point	Inducer Design Point	Rocketdyne 15K Operating Point	RL-10 Category III Operating Point
Flowrate, lb/sec	2.75	4.025	4.56	5.15
Stator 1 Hub Diffusion Factor	0.7426	0.4436	0.3087	0.1603
Stator 1 Tip Incidence Angle	28.56	10.73	0.0	-14.73
Stator 1 Cavitation Region	Hub-Tip Nose	Nose at Tip	None	Hub-Tip Nose
Stator 2 Diffusion Factor	0.4125	0.4125	0.4125	0.4125
Stator 2 Cavitation Region	None	None	None	Nose if Stator 1 Separates

TABLE 7. PERFORMANCE CHARACTERISTICS OF HYDROGEN MOTOR

SLIP	TORQUE IN.LB.	RPM	HP	I AMPS	EFF	PF	WATTS	VA	PRI LOSS	SEC LOSS	IRON LOSS	F W LOSS
0.50	2.14	14925	0.506	4.641	81.89	28.76	461	1601	1.7	2.0	50	29.7
1.00	4.43	14850	1.043	5.188	89.67	48.48	868	1790	2.1	8.2	50	29.4
1.50	6.70	14775	1.570	5.966	92.13	61.78	1272	2058	2.7	18.3	50	29.1
2.00	8.94	14700	2.085	6.891	93.13	70.26	1670	2378	3.7	32.3	50	28.8
2.50	11.15	14625	2.586	7.906	93.53	75.63	2063	2728	4.8	50.2	50	28.5
3.00	13.31	14550	3.071	8.974	93.62	79.05	2447	3096	6.2	71.7	50	28.2
3.50	15.41	14475	3.539	10.071	93.53	81.24	2823	3475	7.8	96.8	50	27.9
4.00	17.46	14400	3.989	11.182	93.34	82.64	3188	3858	9.6	125.1	50	27.6
4.50	19.44	14325	4.418	12.296	93.06	83.49	3542	4242	11.7	156.6	50	27.4
5.00	21.35	14250	4.827	13.405	92.74	83.96	3883	4625	13.8	190.9	50	27.1
5.50	23.19	14175	5.214	14.504	92.38	84.15	4211	5004	16.2	228.0	50	26.8
6.00	24.95	14100	5.580	15.589	91.99	84.14	4525	5378	18.7	267.4	50	26.5
6.50	26.62	14025	5.923	16.657	91.57	83.96	4825	5747	21.4	309.0	50	26.2
7.00	28.21	13950	6.243	17.704	91.14	83.66	5110	6108	24.2	352.5	50	25.9
7.50	29.72	13875	6.541	18.730	90.70	83.26	5380	6462	27.0	397.7	50	25.7
8.00	31.14	13800	6.817	19.732	90.24	82.78	5635	6808	30.0	444.4	50	25.4
10.00	35.96	13500	7.701	23.486	88.35	80.26	6503	8103	42.5	641.1	50	24.3
12.00	39.48	13200	8.268	26.813	86.38	77.19	7140	9251	55.4	844.2	50	23.2
14.00	41.86	12900	8.566	29.720	84.37	73.87	7574	10253	68.1	1043.9	50	22.2
16.00	43.28	12600	8.652	32.235	82.34	70.49	7839	11121	80.1	1233.4	50	21.2
26.00	42.25	11100	7.441	40.402	72.10	55.24	7699	13939	125.8	1956.1	50	16.4
36.00	36.85	9600	5.612	44,324	61.91	44.22	6762	15292	151.4	2361.9	50	12.3
46.00	31.63	8100	4.064	46.380	51.86	36.54	5846	16001	165.8	2590.1	50	8.7
56.00	27.35	6600	2.864	47.563	41.95	31.03	5092	16409	174.3	2726.2	50	5.8
66.00	23.95	5100	1.938	48.297	32.18	26.95	4491	16662	179.7	2812.5	50	3.5
76.00	21.23	3600	1.213	48.780	22.56	23.83	4010	16829	183.4	2870.2	60	1.7
86.00	19.04	2100	0.634	49.115	13.07	21.37	3620	16945	185.9	2910.6	50	0.6
96.00	17.24	600	0.164	49.356	3.71	19.38	3300	17028	187.7	2939.8	50	00

CRITICAL SPEEDS

The Rocketdyne Structural Dynamics Analysis Program was used to calculate the critical speeds of both oxygen and hydrogen units. Figure 24 is a plot of the first and second critical speeds of the oxygen unit as a function of the bearing stiffness. The circled point on the curve shows the first critical speed for the unit. This value of 25,257 rpm is far above the maximum design speed of 3167 rpm.

Figure 25 is a plot of the first- and second-critical speeds of the hydrogen unit as a function of bearing stiffness. Again the circled point on the curve is at the first critical speed of the unit. This value of 31,171 rpm is also well above the maximum design speed of 14,614 rpm.

TRANSIENT ANALYSIS

Figure 26 is a plot of the torque of the electric motor that drives the oxygen pump as a function of speed as per the Sundstrand computer printout. Also shown is the maximum pump torque along a constant Q/N line (constant resistance or throttle setting). The two lines cross at the pump operating speed of 3110 rpm.

At the start, the motor has a relatively high torque while the pump has no load other than its own inertia. The unit, therefore, will accelerate until it reaches equilibrium at 3110 rpm. The characteristics of the hydrogen unit are similar, with the maximum pump torque occurring at the pump operating speed of 14,526 rpm.

The moments of inertia of the rotating assemblies were calculated and found to be 29.36×10^{-3} in.-lb-sec^2 for the oxygen and 3.577×10^{-3} in.-lb-sec^2 for the hydrogen units. Because the torque is proportional to the product of the moment of inertia and the angular acceleration and as Rocketdyne has a computer program to handle the calculation, it was a simple matter to input the data for the two units. The results are shown in Fig. 27. The curves indicate that, without a speed control, the oxygen unit can accelerate to full speed in 0.16 second and the hydrogen unit in 0.24 second.

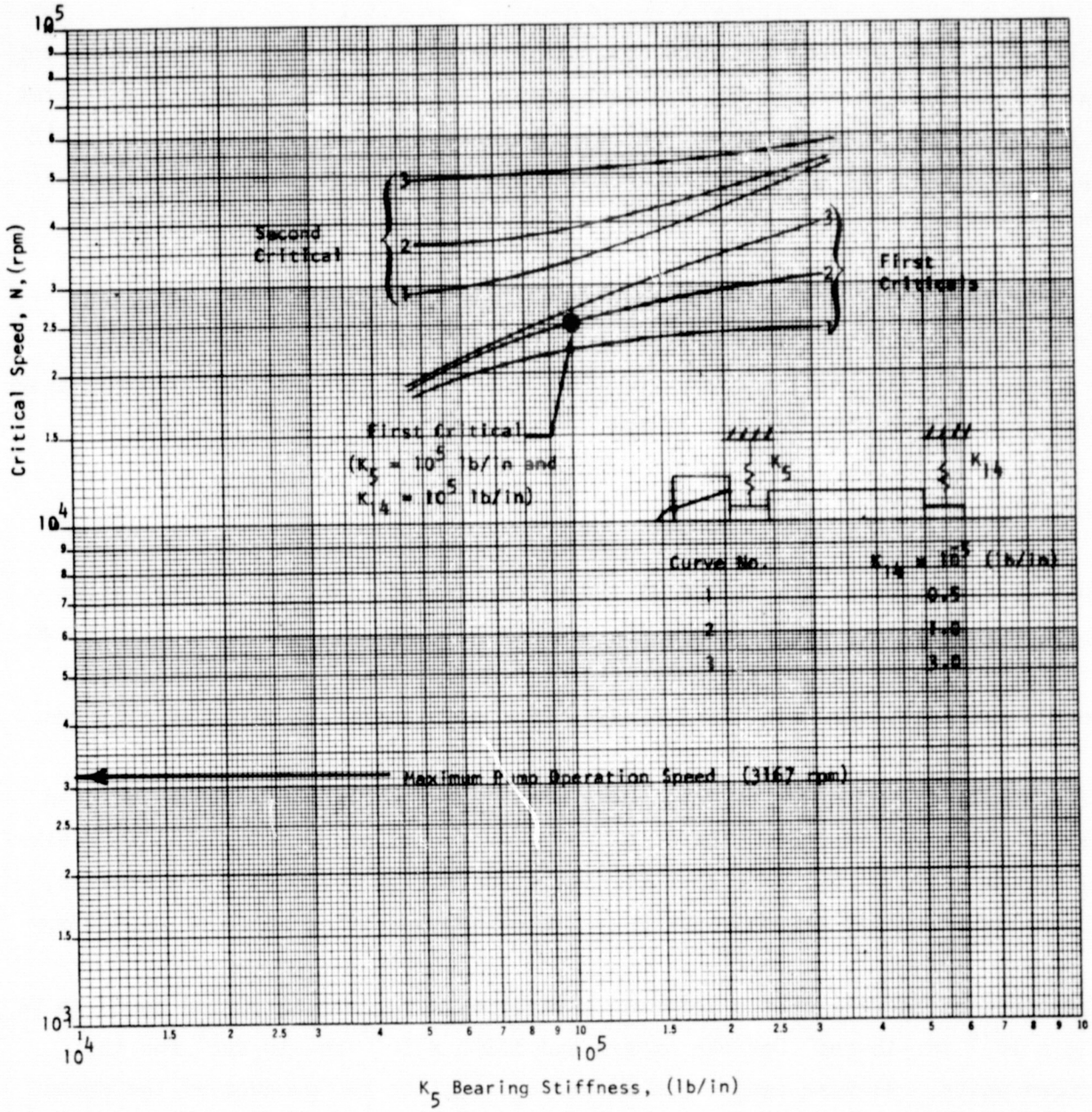

Figure 24. Oxygen Pump Critical Speed

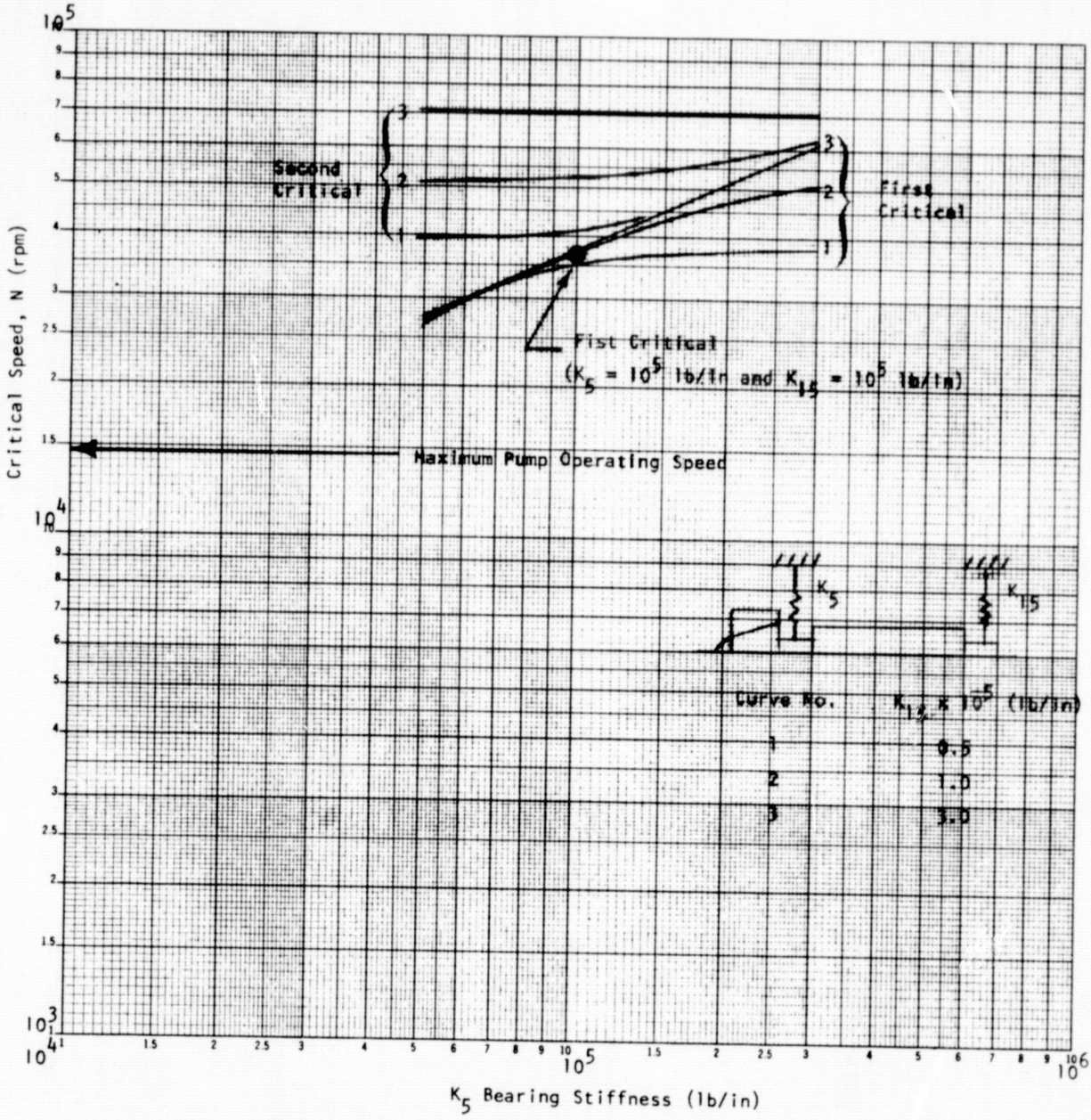

Figure 25. Hydrogen Pump Critical Speed

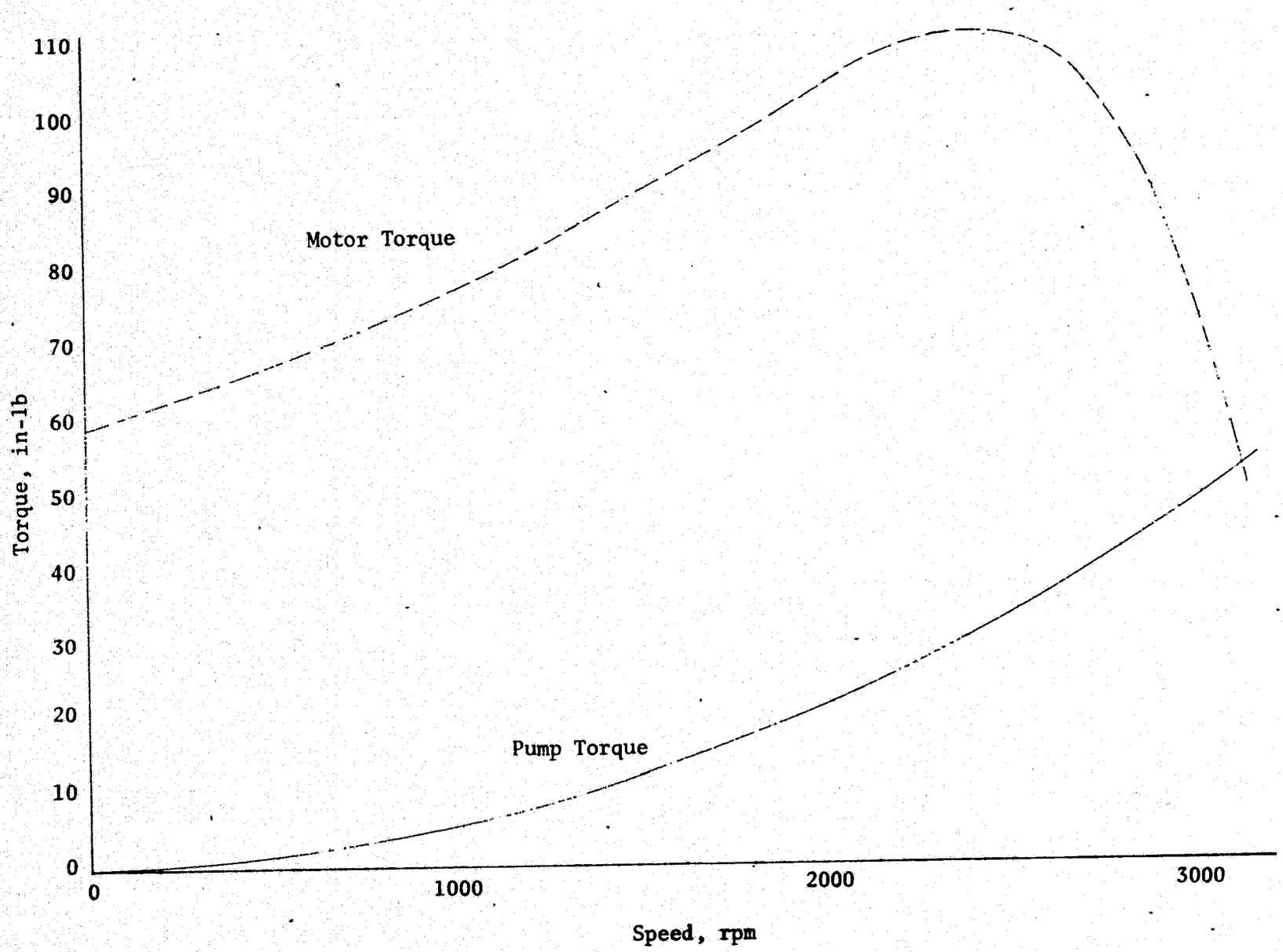

Figure 26 Motor and Oxygen Pump Torque as a Function of Speed

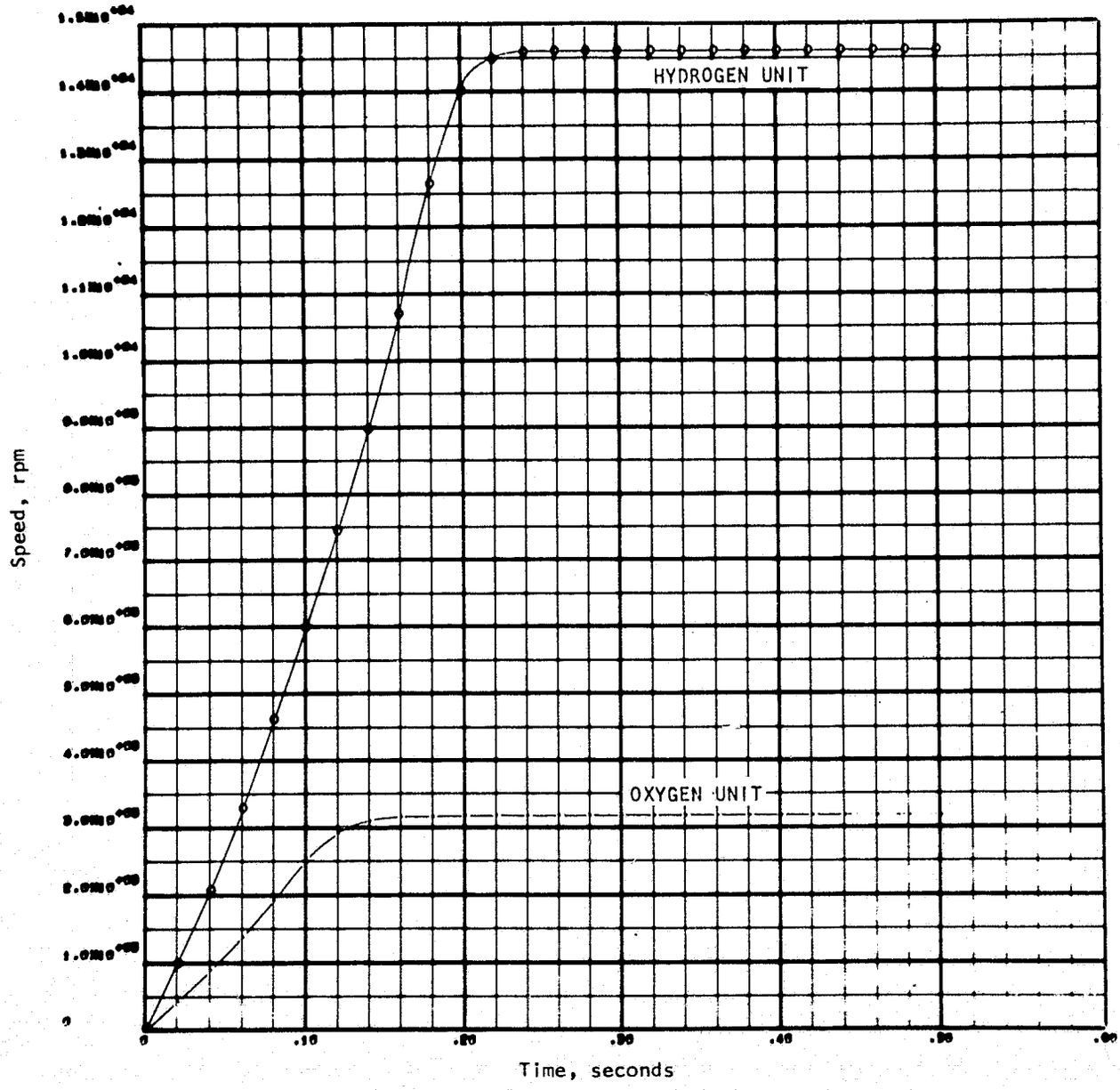

Figure 27. Acceleration Rates of the Units

PHASE III - FABRICATION

Both pump units utilize the same design concept and thus are fabricated similarly. In each case, the electric drive motor is installed within the pump package so that the inducer is connected directly to the motor shaft. Two bearings support the rotating assembly; one at the aft end of the motor shaft and the other between the inducer and the motor armature. Bearing lubrication is provided by a small bleed flow of each propellant circulating counter to the main flow. The motor stator section is contained within the downstream diffuser vanes. The hydrogen motor electrical windings are exposed to the liquid hydrogen while the oxygen windings are contained within a sealed steel shell. This complete assembly (rotating assembly, motor stator, diffuser vanes) is contained within a welded aluminum housing.

An accessory, a back-flow deflector, was also fabricated for each pump assembly. A drawing of the back-flow deflector mounted in front of the oxygen inducer is shown on Fig. 28. The back-flow deflector is designed to capture the flow that comes back through the clearance space around the inducer and prevent this flow from going any further upstream. Tests have shown that it can have a strong effect on head and cavitation performance particularly at high heads and low flows where the percentage backflow is high.

Figures 29 and 30 are the assembly drawings of the hydrogen and oxygen units, respectively. Photographs of the various components are included as Fig. 31 through 42.

The hydrogen units were assembled first, and the initial assembly was made with only one incident on Unit No. 1. The motor stator is a pressed fit within the diffuser. On installing the motor, it bound in the receiving bore and had to be pressed out. Subsequently, the bore assembly was heated and the motor cooled and the installation was made without difficulty.

Following initial assembly of the hydrogen units, it was found that the motors were wound incorrectly (see Test Section). This required the disassembly of each

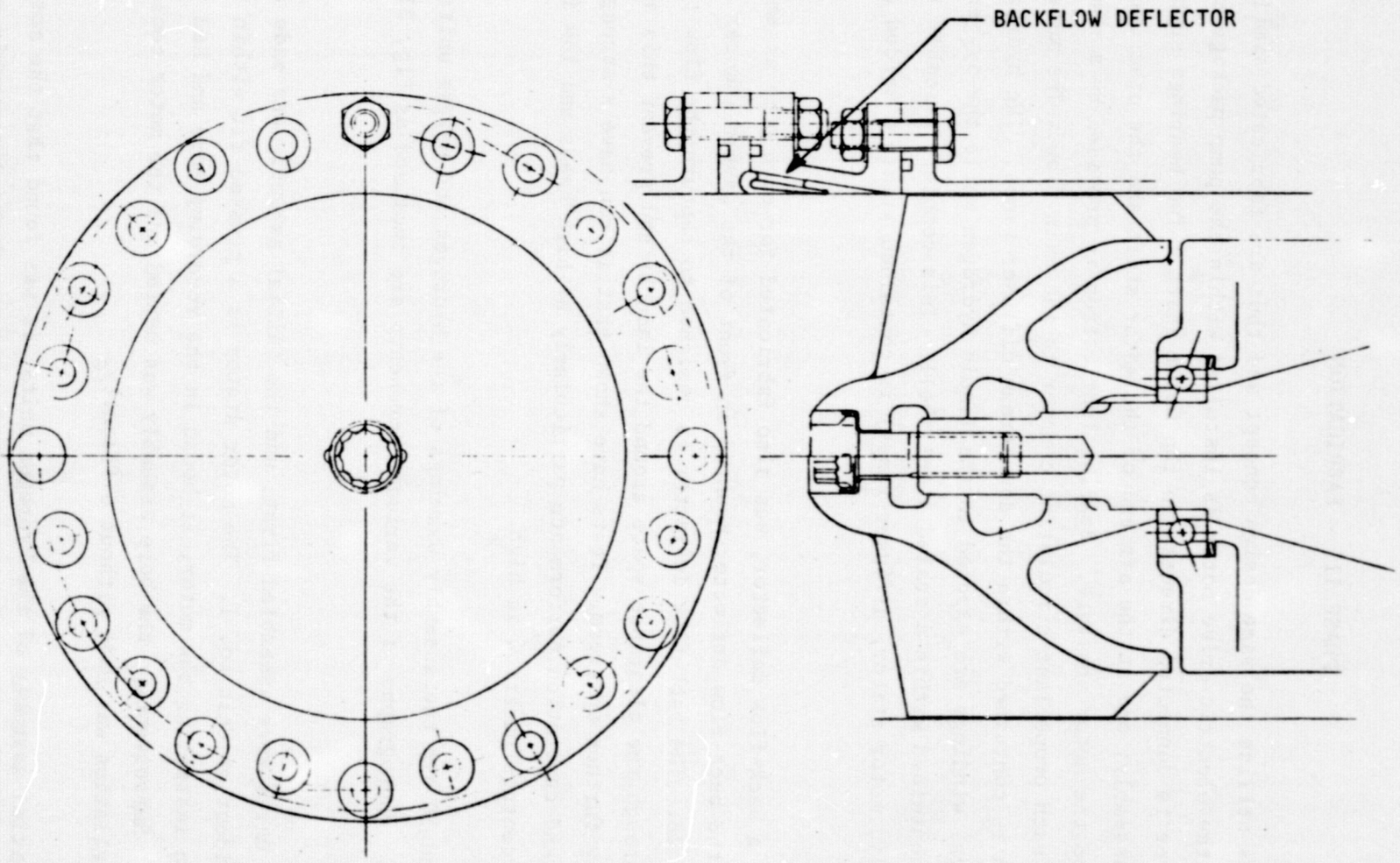

Figure 28. Two-Phase Oxygen Inducer Preliminary Layout With Backflow Deflector

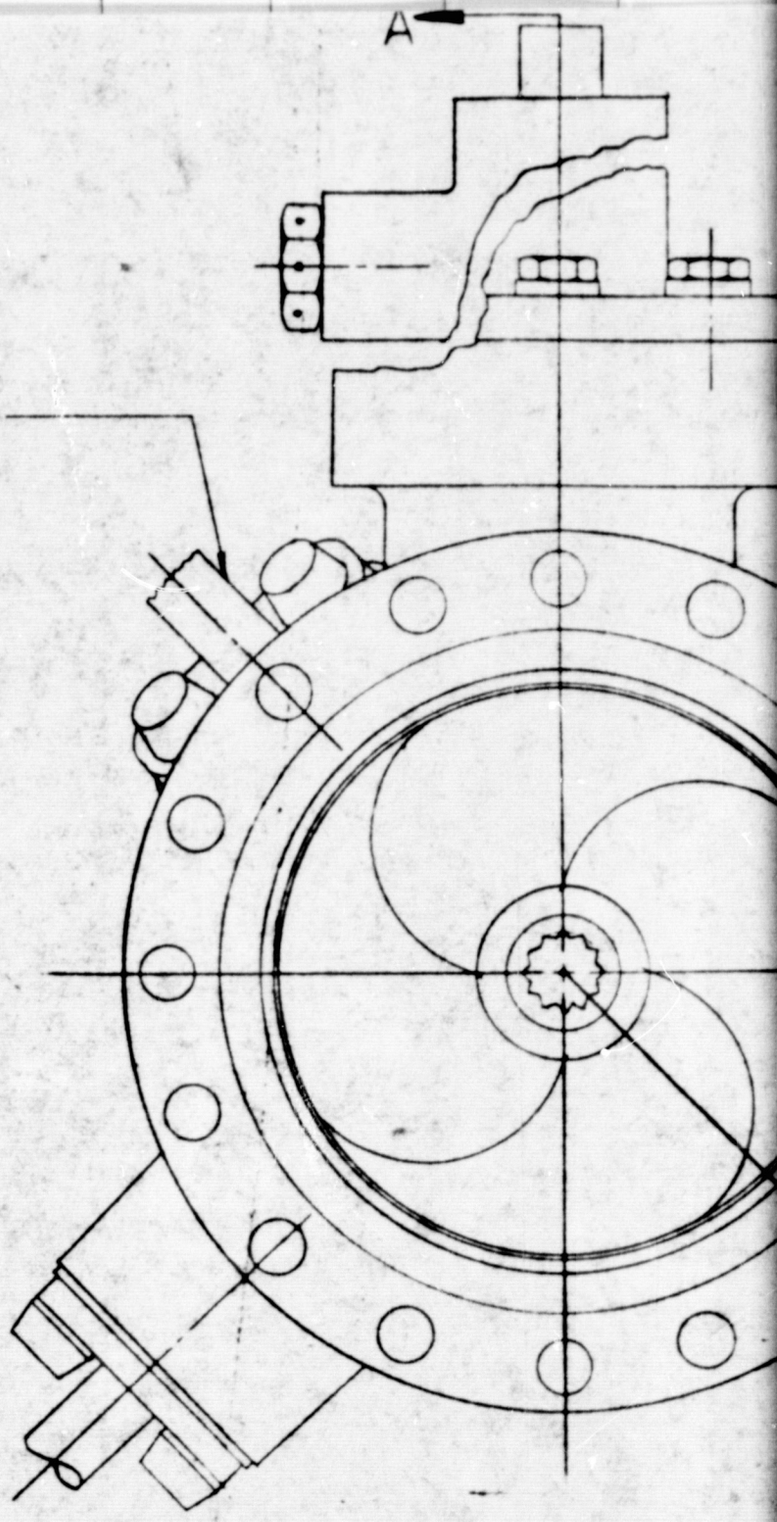

(5) (11)	NAS-27325T1	TRANSDUCER	1 REQD
	404664	SEAL	1 REQD
	RD111-3006-4208	BOLT	2 REQD
	TORQUE 46 ± 2 IN. LB.		
(8)	MEOR941226	PLUG REF	

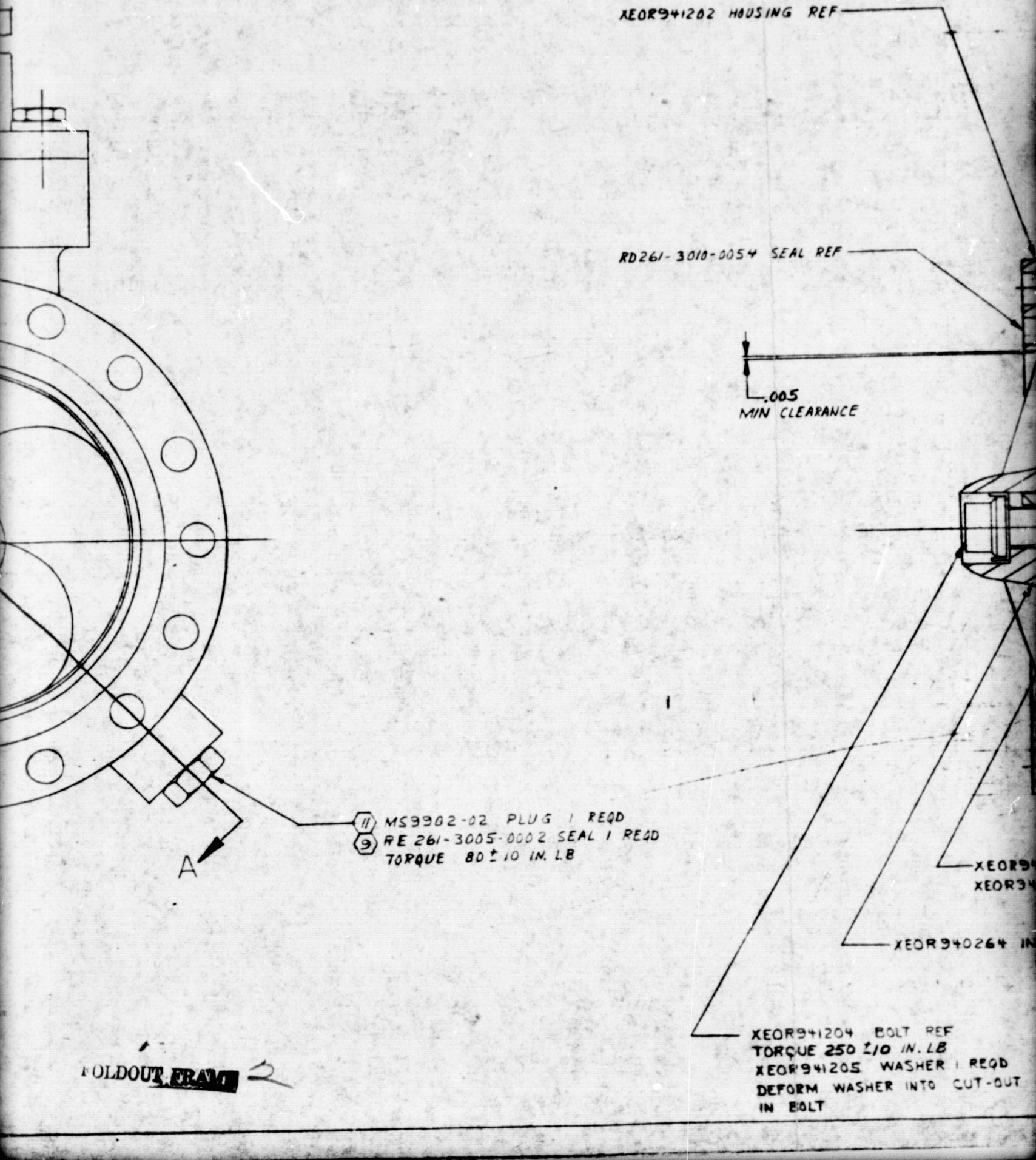

FOLDOUT FRAME 2

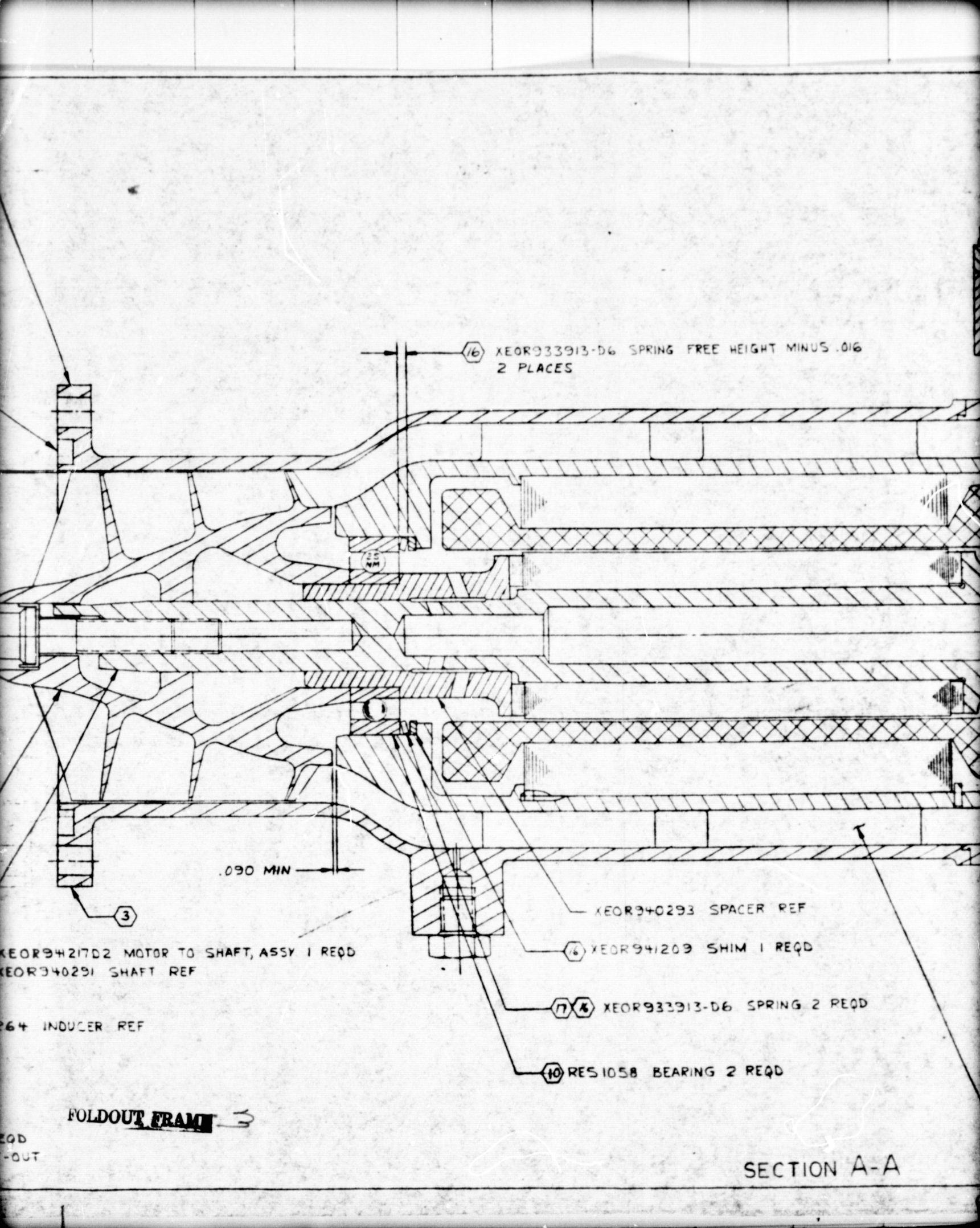
(16) XEOR933913-D6 SPRING FREE HEIGHT MINUS .016
2 PLACES
.090 MIN
3
XEOR940293 SPACER REF
(16) XEOR941209 SHIM 1 REQD
(17) (16) XEOR933913-D6 SPRING 2 REQD
(10) RES1058 BEARING 2 REQD
XEOR941217D2 MOTOR TO SHAFT, ASSY 1 REQD
XEOR940291 SHAFT REF
264 INDUCER REF
FOLDOUT FRAME 3
EQD
-OUT

SECTION A-A

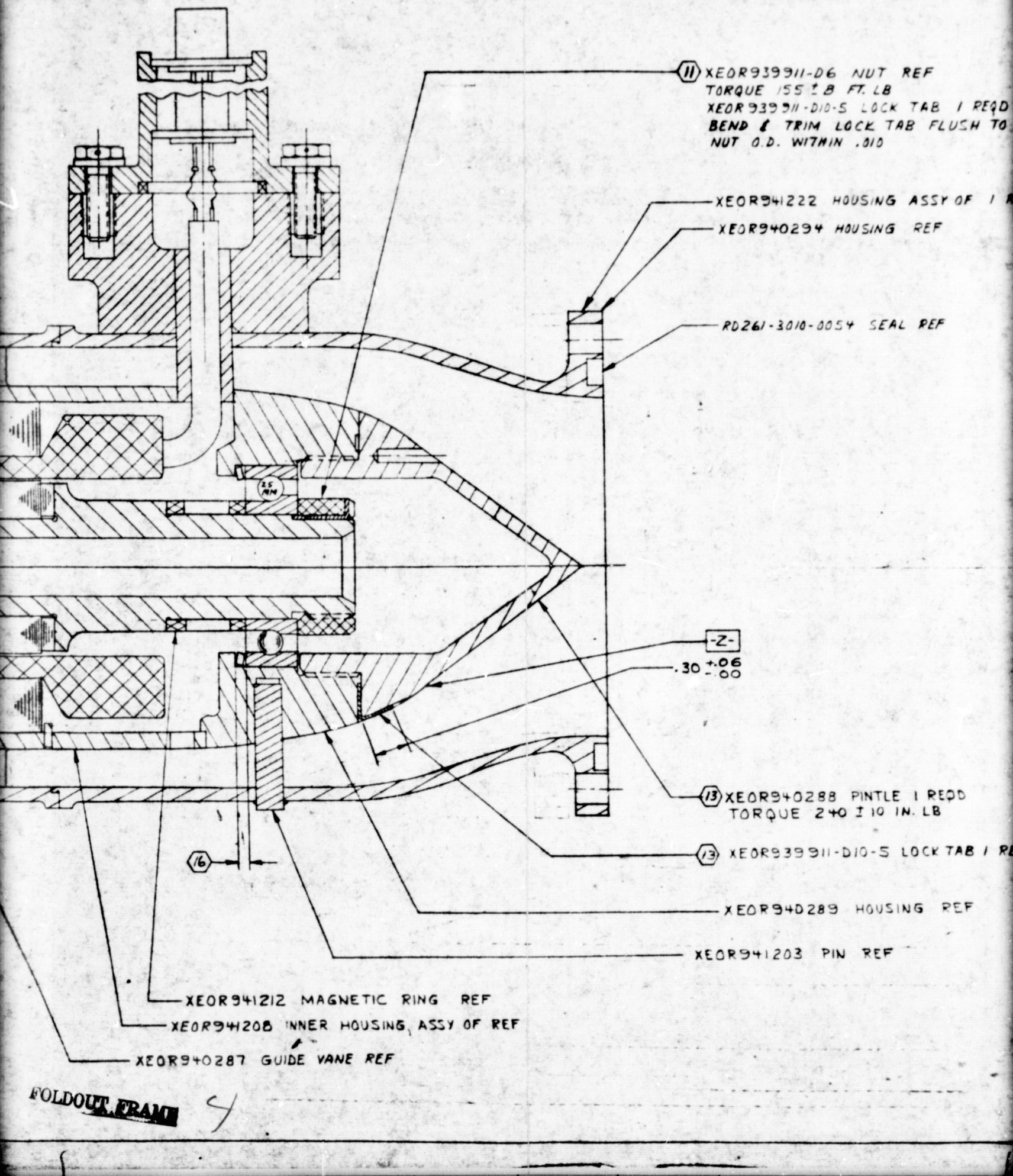

FOLDOUT FRAME 4

REQD
H TO

1 REQD

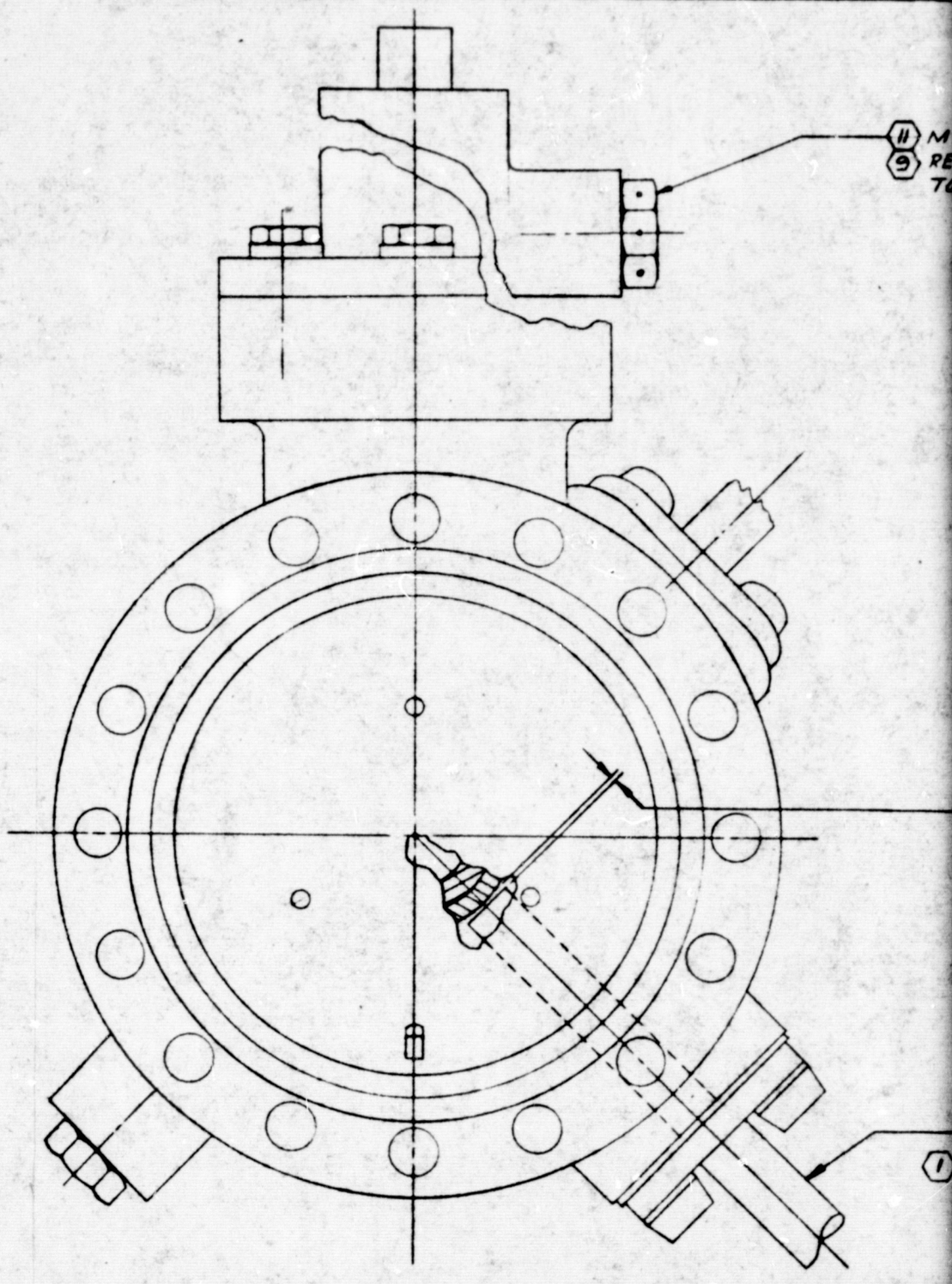

1 REQD

FOLDOUT FRAME 5

(11) MS9902-04 PLUG 1 REQD
(9) RE 261-3005-0004 SEAL 1 REQD
TORQUE 240 ± 10 IN. LB

.033 ± .003

SPEED TRANSDUCER

(1) MODEL 148W TRANSDUCER 1 REQD
404664 SEAL 1 REQD
RD111-3006-4208 BOLT 2 REQD
TORQUE 46 ± 2 IN. LB

(17) INSTALL SPRINGS AS SHOWN
(16) MACHINE SHIM TO OBTAIN .1160 ± .0005 SPRING COMPRESSION AS SHOWN.
15. ELECTRICAL CHECK OUT PER ENGINEERING INSTRUCTIONS
14. LEAK CHECK WITH NITROGEN GAS AT AMBIENT TEMP @ 30 ± 5 PSIG FOR 2 MINUTES MIN. THERE SHALL BE NO VISIBLE EVIDENCE OF LEAKAGE DURING THE TEST.
(13) INSTALL LOCK TAB AND TORQUE PINTLE. MARK PINTLE IN PREPARATION FOR MACHINING LOCK TAB SLOT. REMOVE PINTLE AND MACHINE LOCK TAB SLOT SO THAT THE BENT LOCK TAB IS .010 ± .010 BELOW SURFACE Z AND AS SHOWN. APPLY COLORED CHEMICAL FILM PER RA0109-031 TO BARE ALUM. INSTALL LOCK TAB AND TORQUE PINTLE. TRIM AND BEND LOCK AS SHOWN.
12. TORQUE PUMP PER ENGINEERING INSTRUCTIONS
(11) LUBRICATE PER RA0112-002 FOR SPECIAL CONDITIONS WITH MOLYKOTE TYPE Z, DOW CORNING, MIDLAND, MICHIGAN
(10) INSTALL BEARINGS AS SHOWN
(9) INSTALL SEALS PER RA0101-013
(8) REMOVE TRANSDUCER AND INSTALL PLUG AFTER TESTING
7. INSTALL FITTINGS AND LINE SUPPORT CLAMPS PER RA0102-005
6. INSTALL THREADED FASTENERS AND LOCKWIRE PER RA0101-002
(5) SUPPORT TRANSDUCER WITH CLAMPS AS NECESSARY
(4) PLUG BLEEDER TUBE WITH AN806-2 PLUG OR CRIMP AND WELD BLEEDER TUBE CLOSED
(3) ELECTROCHEMICAL ETCH IDENTIFY ASSY PER RA0104-008 AND SERIALIZE PER RA0107-004
2. CLEAN ALL COMPONENTS PER RA0110-004
(1) ROSEMOUNT ENGINEERING COMPANY, MINNEAPOLIS, MINN

LAYOUT FRAME 6

SSION

30 ± 5 PSIG
VCE OF

PARATION
INE LOCK
W
FILM
TORQUE

MOLYKOTE

005
02

D

AND

FOLDOUT FRAME 7

FIGURE 29. LOW SPEED INDUCER, HYDROGEN ASSEMBLY

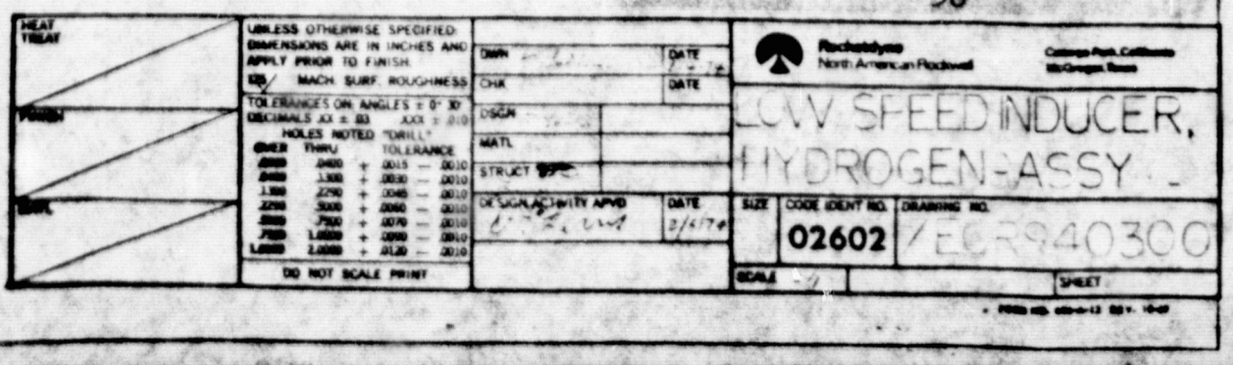

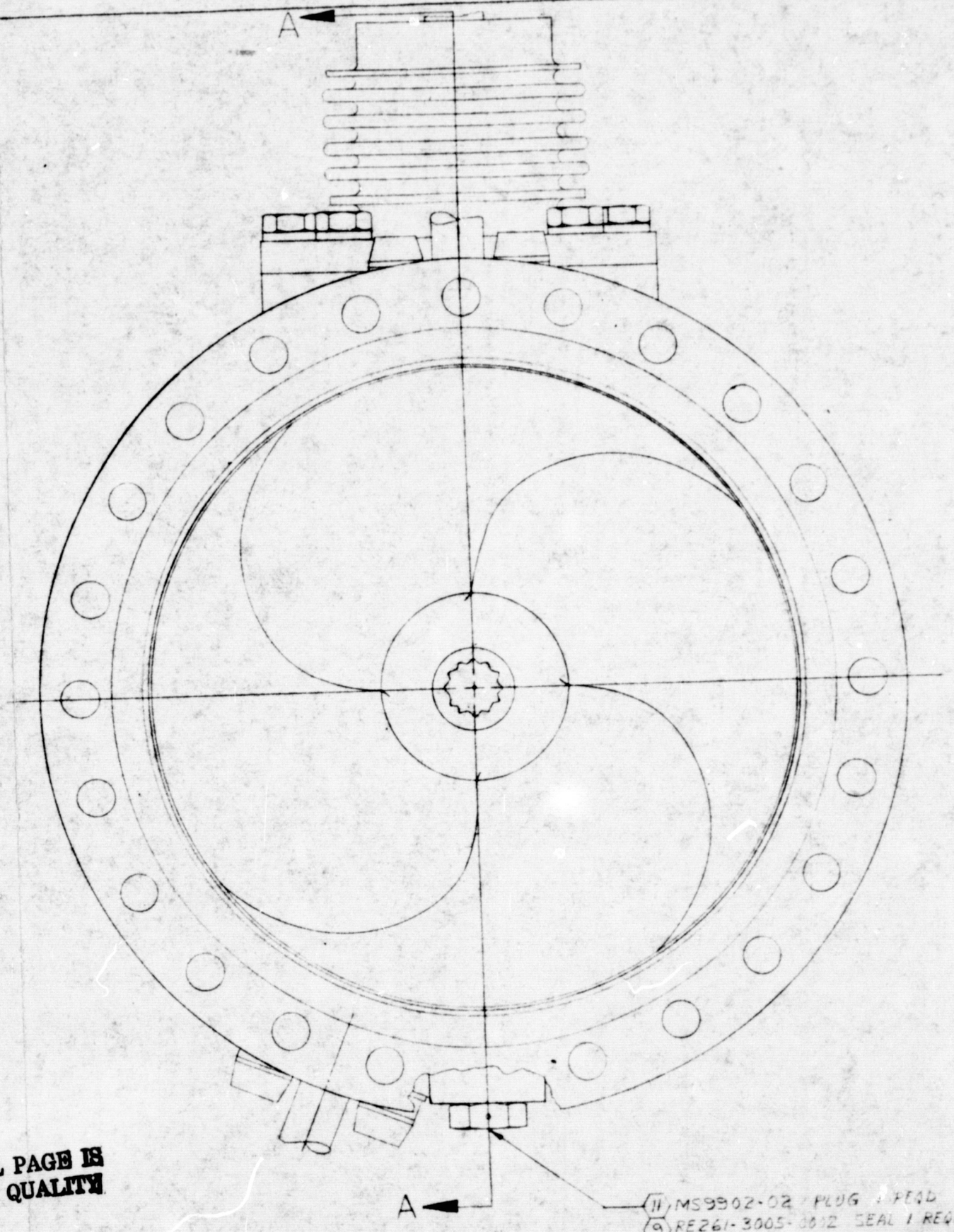

XEOR
TORQ
XEOR
DEFO
IN B

(16) X
N
N
N

FOLDOUT FRAME 1

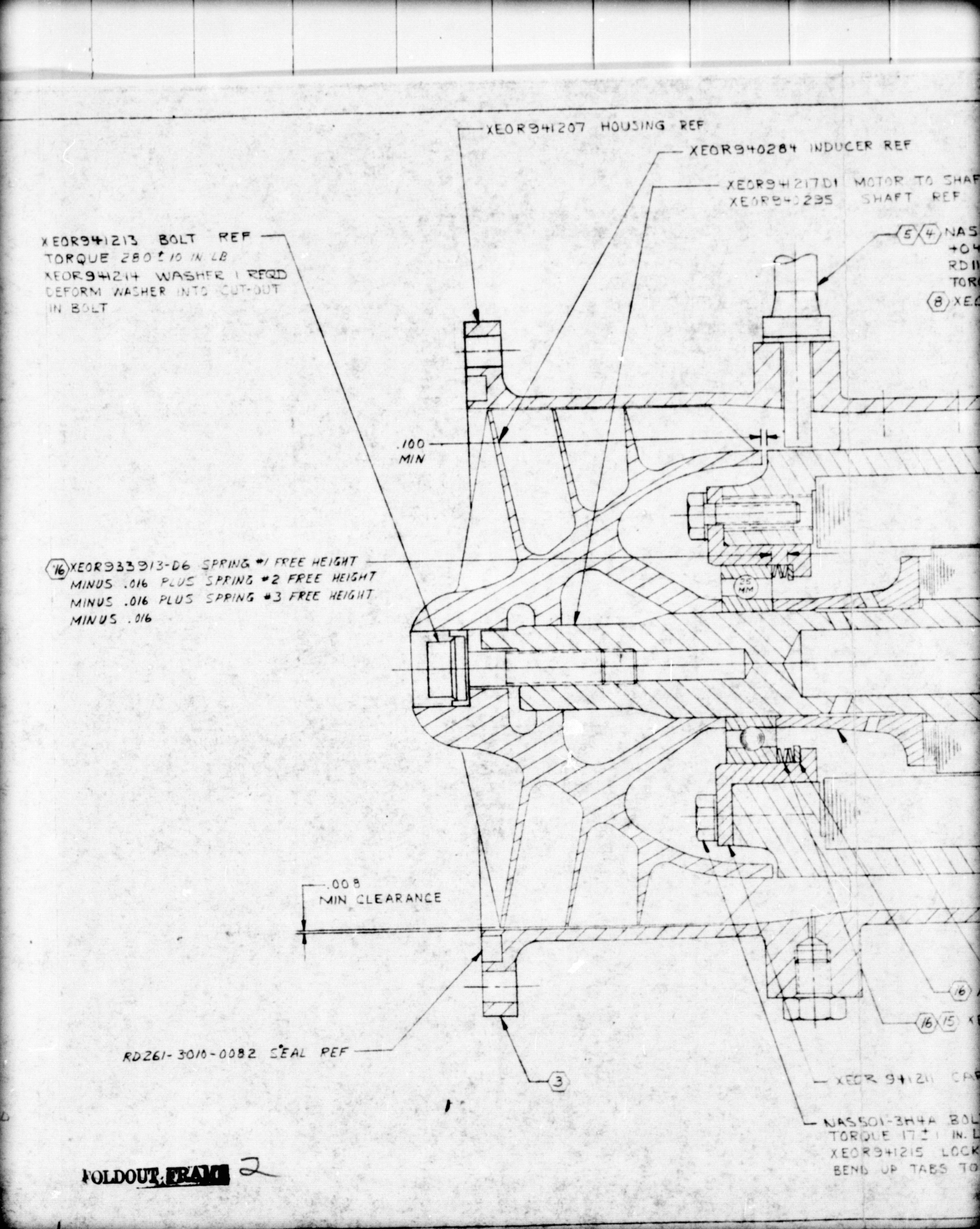

FOLDOUT FRAME 2

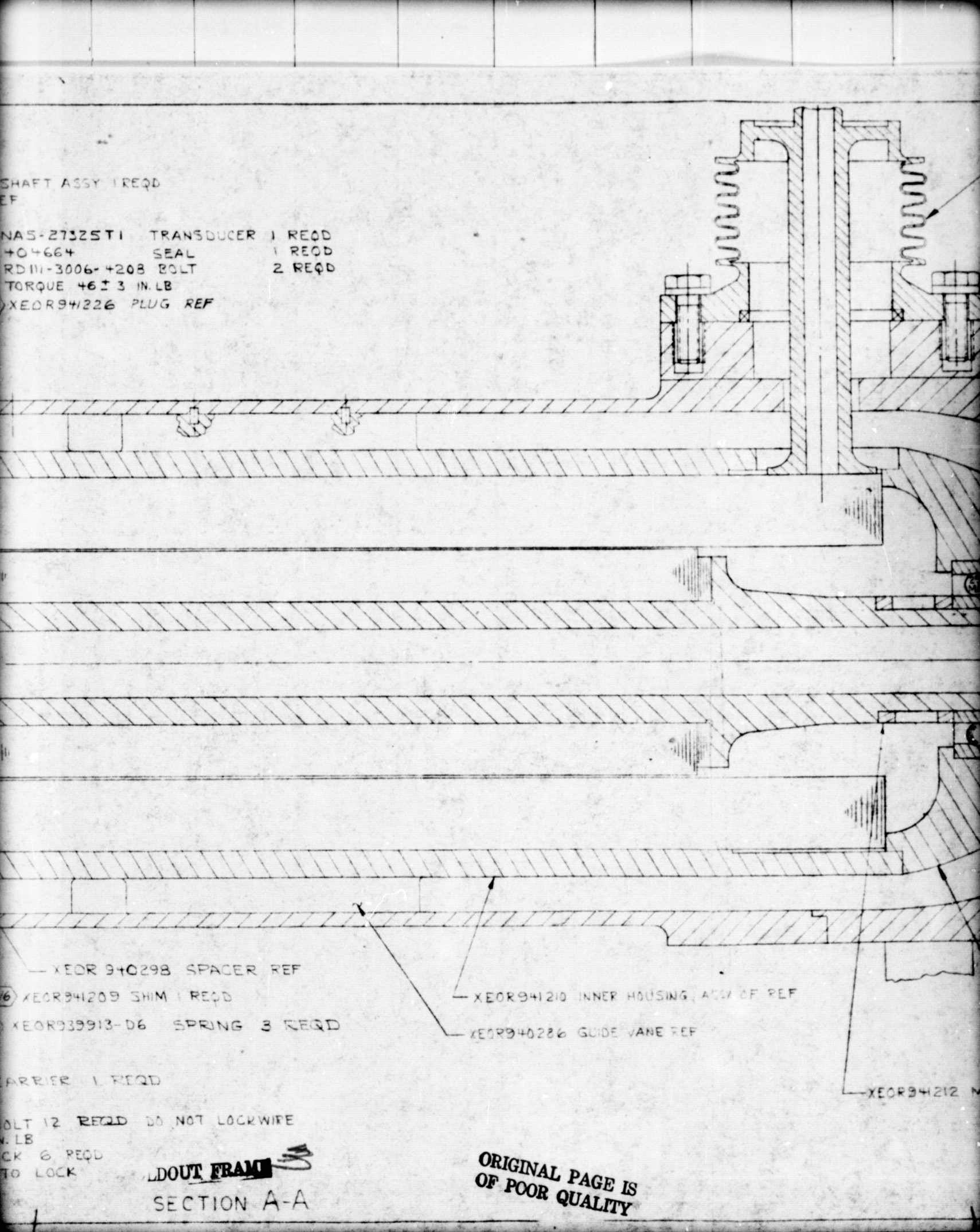

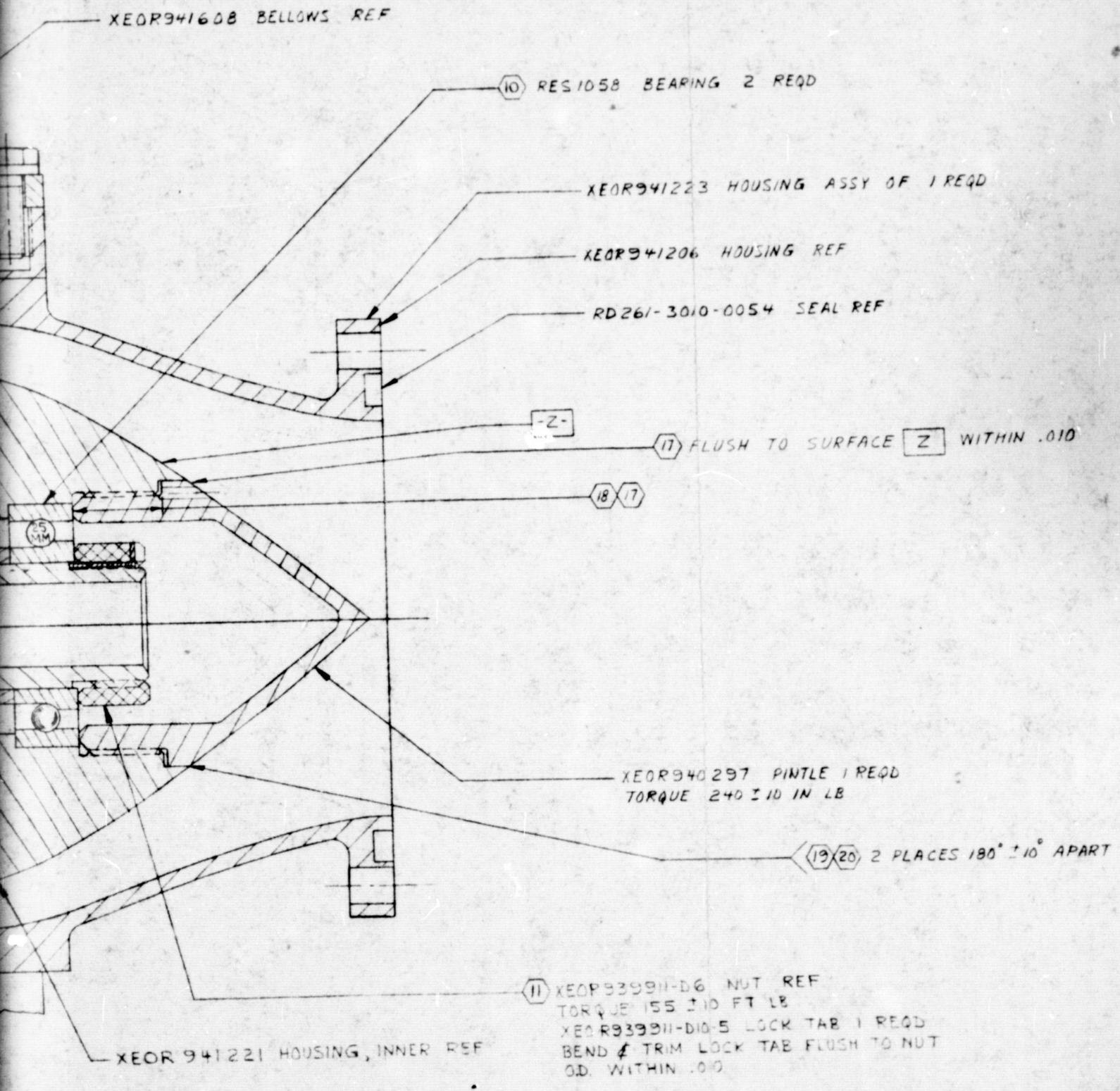

212 MAGNETIC RING REF

FOLDOUT FRAME

4

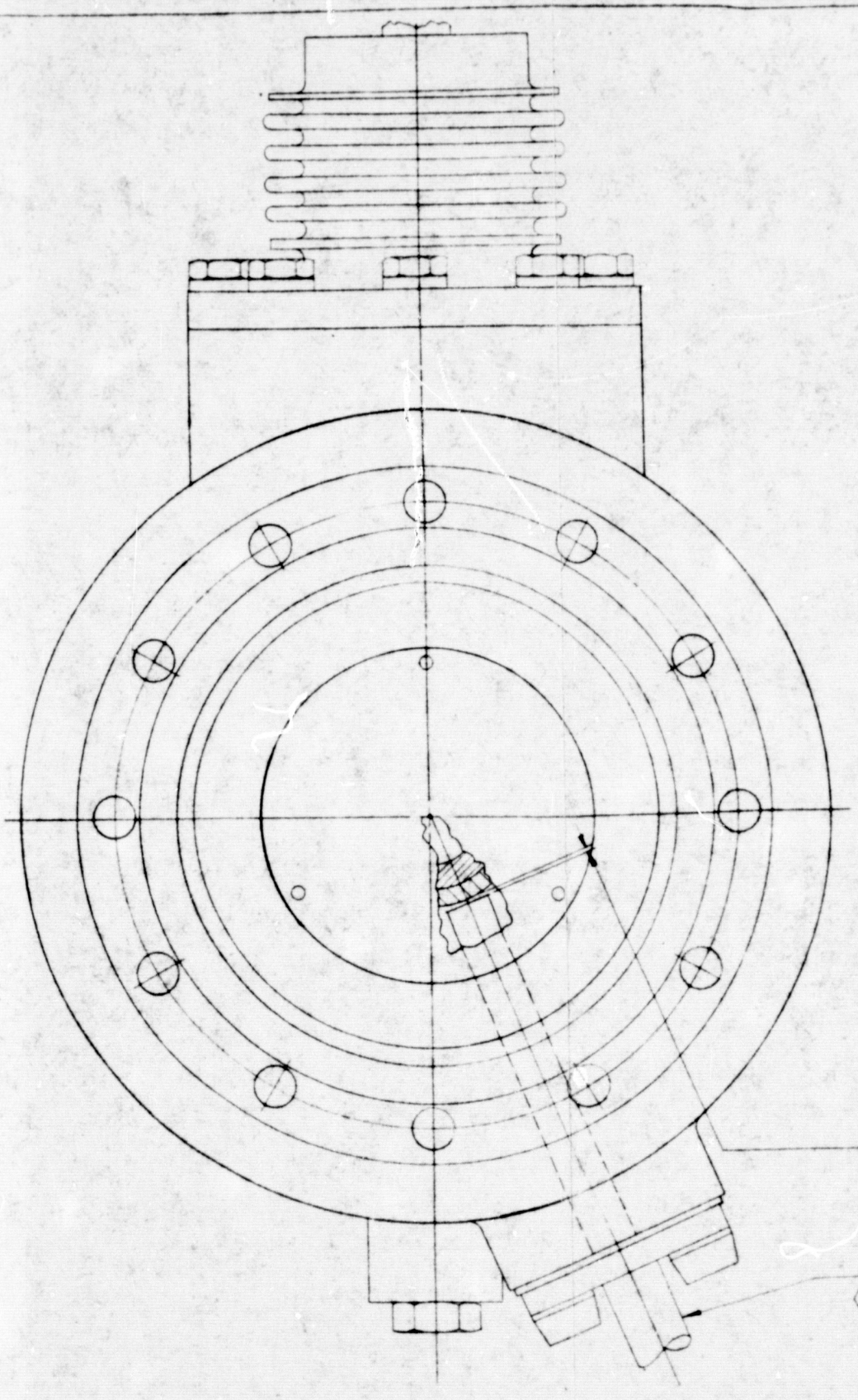

.033 ± .003

TACHOMETER PROBE

(1)	MODEL 148W	TRANSDUCER	1 REQD
	404664	SEAL	1 REQD
	RD111-3006-4208	BOLT	2 REQD

TORQUE 46 ± 3 IN LB

FOLDOUT FRAME 5

(20) COMPLETE ALL CHECK-OUTS PRIOR TO TACK WELDING PINTLE

(19) GTA TACK WELD PER RA0107-027 EXCEPT USE 2319 ALUM FILLER, TO LOCK PINLTE. CLEAN LOCALLY FOR WELDING.

(18) APPLY COLORED CHEMICAL FILM PER RA0103-031 TO BARE ALUM

(17) DIMENSION MAY BE MODIFIED TO MEET THE REQUIREMENT OF FLUSH TO SURFACE [Z]

(16) MACHINE SHIM TO OBTAIN .0160 ± .0005 SPRING COMPRESSION FOR EACH SPRING AS SHOWN

(15) INSTALL SPRINGS AS SHOWN

14. ELECTRICAL CHECK OUT PER ENGINEERING INSTRUCTIONS

13. LEAK CHECK WITH NITROGEN GAS AT AMBIENT TEMP & 30 ± 5 PSIG FOR 2 MINUTES MIN. THERE SHALL BE NO VISIBLE EVIDENCE OF LEAKAGE DURING THE TEST

12. TORQUE PUMP PER ENGINEERING INSTRUCTIONS

(11) LUBRICATE PER RA0112-002 FOR SPECIAL CONDITIONS WITH MOLYKOTE Z, DOW CORNING, MIDLAND, MICHIGAN

(10) INSTALL *BEARINGS AS SHOWN

(9) INSTALL SEALS PER RA0101-003

(8) REMOVE TRANSDUCER AND INSTALL PLUG AFTER TESTING

7. INSTALL FITTINGS AND LINE SUPPORT CLAMPS PER RA0102-005

6. INSTALL THREADED FASTENERS AND LOCKWIRE PER RA0101-002

(5) SUPPORT TRANSDUCER WITH CLAMPS AS NECESSARY

(4) PLUG BLEEDER TUBE WITH AN806-2 PLUG OR CRIMP AND WELD BLEEDER TUBE CLOSED

(3) ELECTROCHEMICAL ETCH IDENTIFY ASSY PER RA0104-008 AND SERIALIZE PER RA0104-007

2. CLEAN ALL COMPONENTS PER RA0110-004

(1) ROSEMOUNT ENGINEERING COMPANY, MINNEAPOLIS, MINN

1 REQD
1 REQD
2 REQD

FOLDOUT FRAME

FOLDOUT FRAME 7

FIGURE 30. LOW SPEED INDUCER, OXYGEN ASSEMBLY

HEAT TREAT	UNLESS OTHERWISE SPECIFIED: DIMENSIONS ARE IN INCHES AND APPLY PRIOR TO FINISH.	DWN	DATE
FINISH	125/ MACH SURF. ROUGHNESS.	CHK	DATE
MATL	TOLERANCES ON ANGLES ± 0° 30' DECIMALS .XX ± .03 .XXX ± .010 HOLES NOTED "DRILL"	DSGN	
	OVER THRU TOLERANCE .0008 .0400 + .0025 — .0010 .0400 .1300 + .0030 — .0010 .1300 .2290 + .0045 — .0010 .2290 .5000 + .0060 — .0010 .5000 .7500 + .0070 — .0010 .7500 1.3000 + .0090 — .0010 1.0000 2.0000 + .0120 — .0010	MATL	
	DO NOT SCALE PRINT	STRUCT CKD	
		DESIGN ACTIVITY APVD	DATE 4/6/70

Rocketdyne, North American Rockwell — Canoga Park, California; McGregor, Texas

LOW SPEED INDUCER, LOX-ASSY

SIZE	CODE IDENT NO.	DRAWING NO.
	02602	XEOR 740290

SCALE — SHEET

FORM NO. 68B-4-13, REV. 10-69

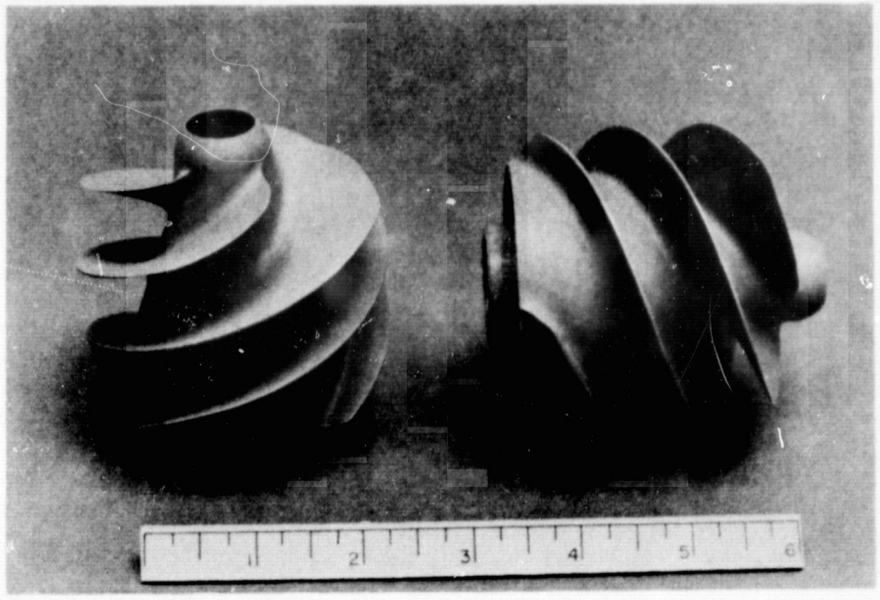

5AJ33-10/11/73-C1A

Figure 31. Two-Phase Hydrogen Inducers

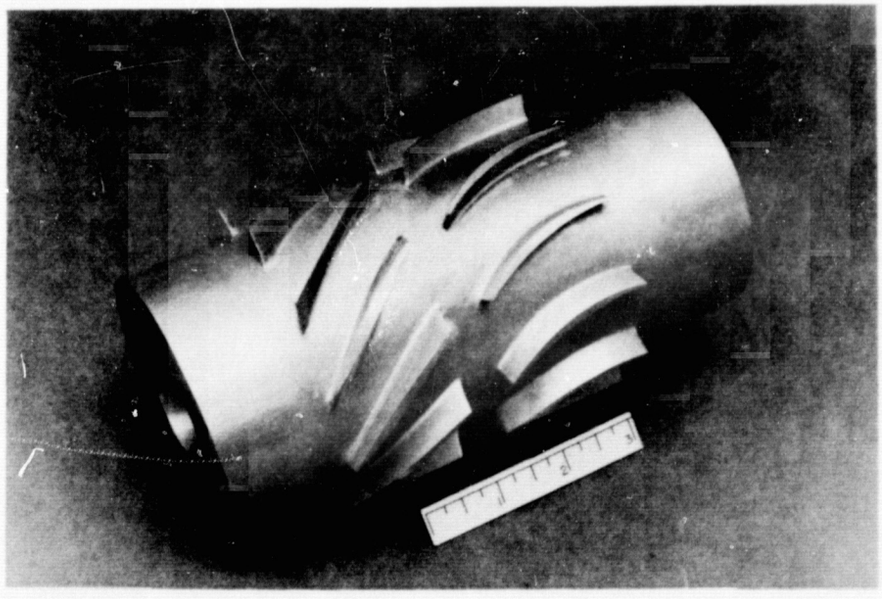

1XZ52-11/9/73-C1A

Figure 32. Two-Phase Hydrogen Guide Vane

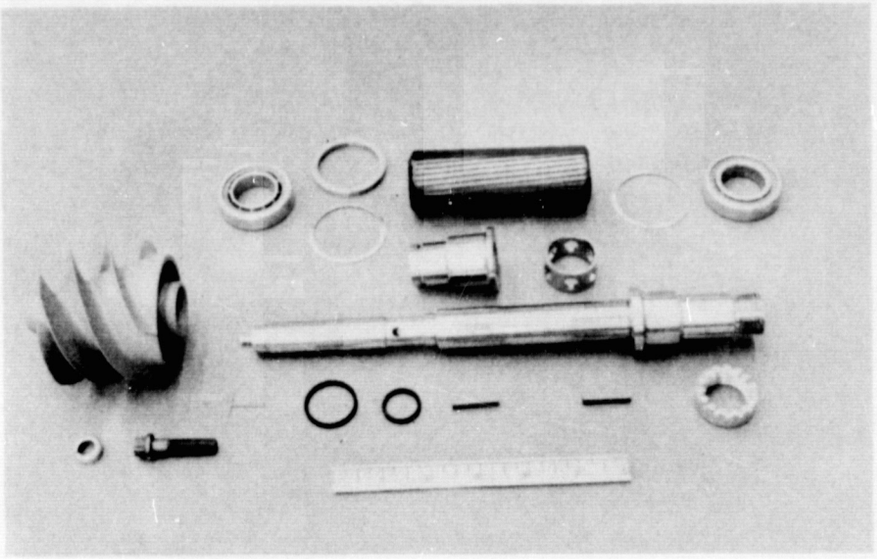

5AJ33-1/30/74-C1C

Figure 33. Rotating Assembly, LH_2 Unit

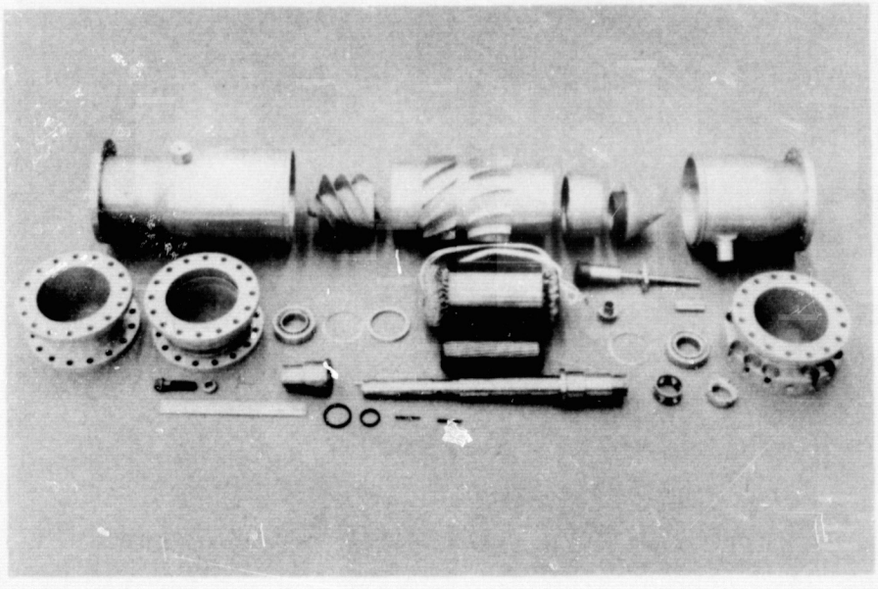

5AJ33-1/30/74-C1A

Figure 34. Complete Assembly, LH_2 Unit

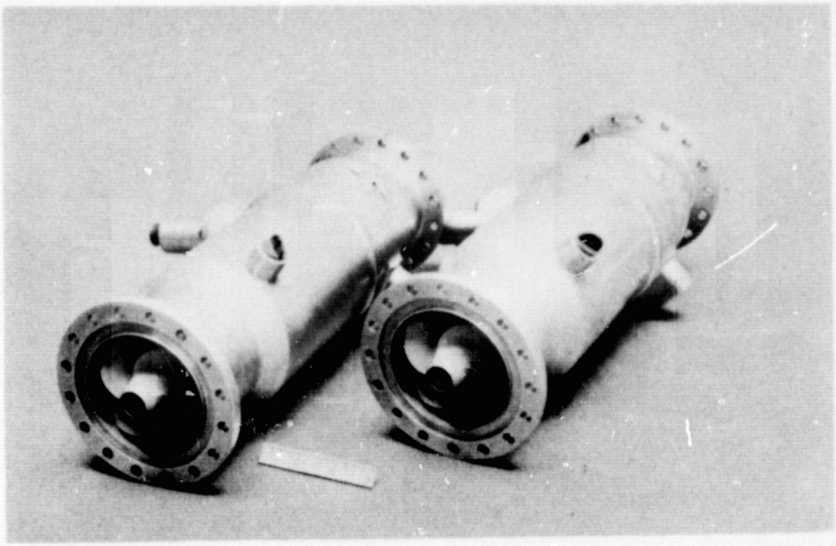

1XY51-6/27/74-C1C

Figure 35. Inlet View of Hydrogen Pump Assemblies

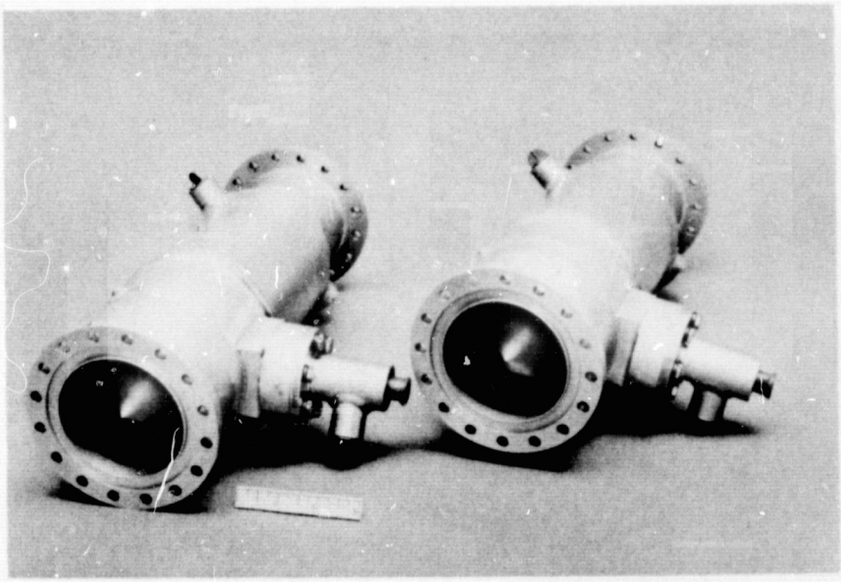

1XY51-6/27/74-C1B

Figure 36. Discharge View of Hydrogen Pump Assemblies

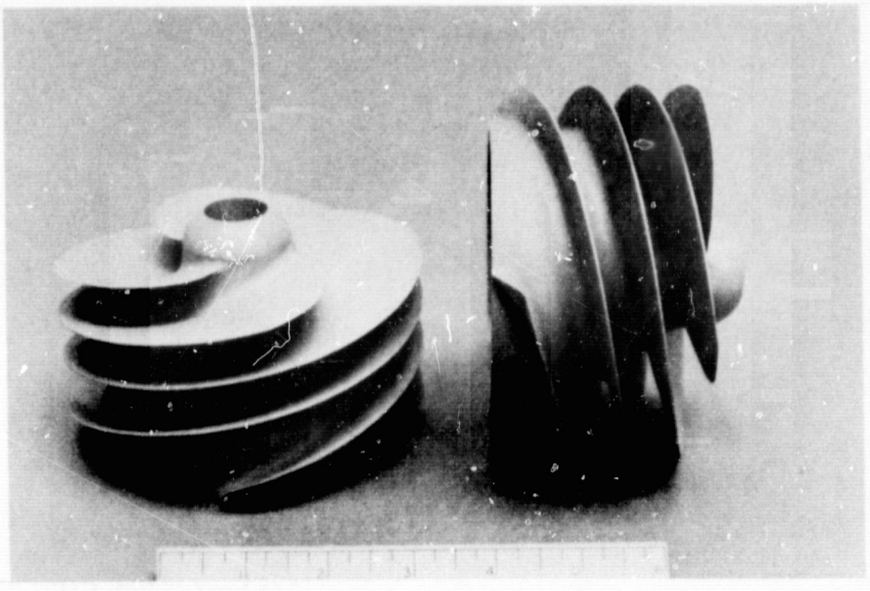

5AJ33-10/11/73-C1B

Figure 37. Two-Phase Oxygen Inducers

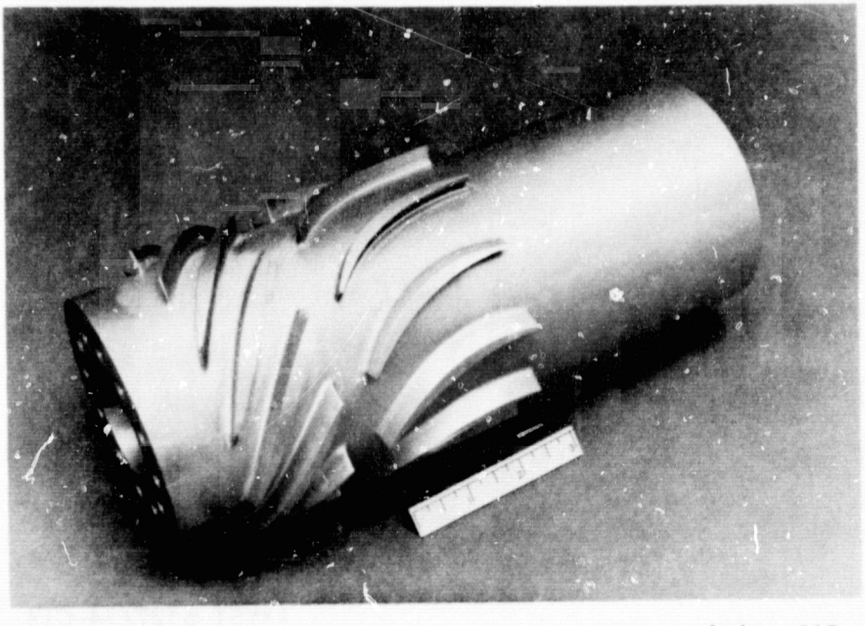

1XZ52-11/9/73-C1B

Figure 38. Two-Phase Oxygen Guide Vane

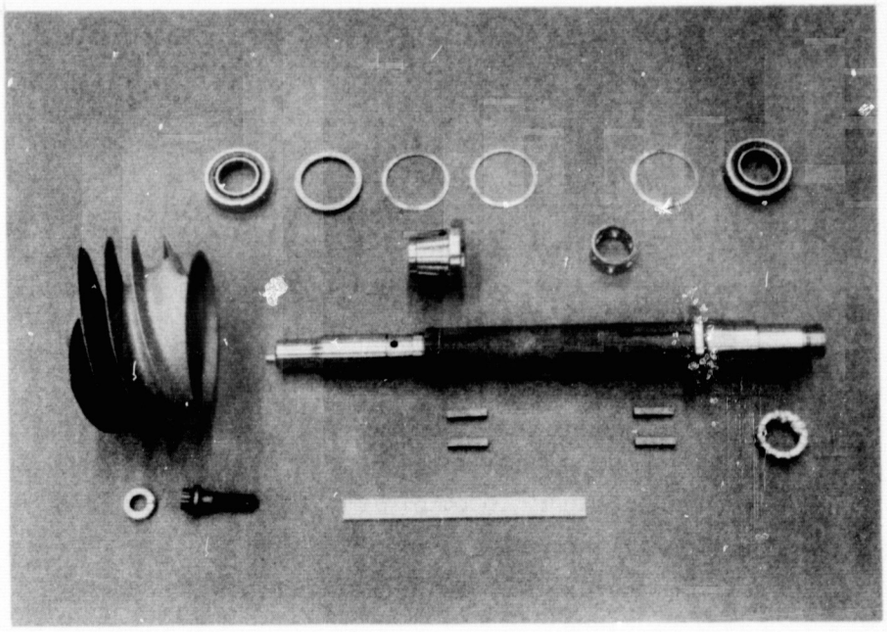

4MA62-3/18/74-C1A*

Figure 39. Rotating Assembly, LO_2 Unit

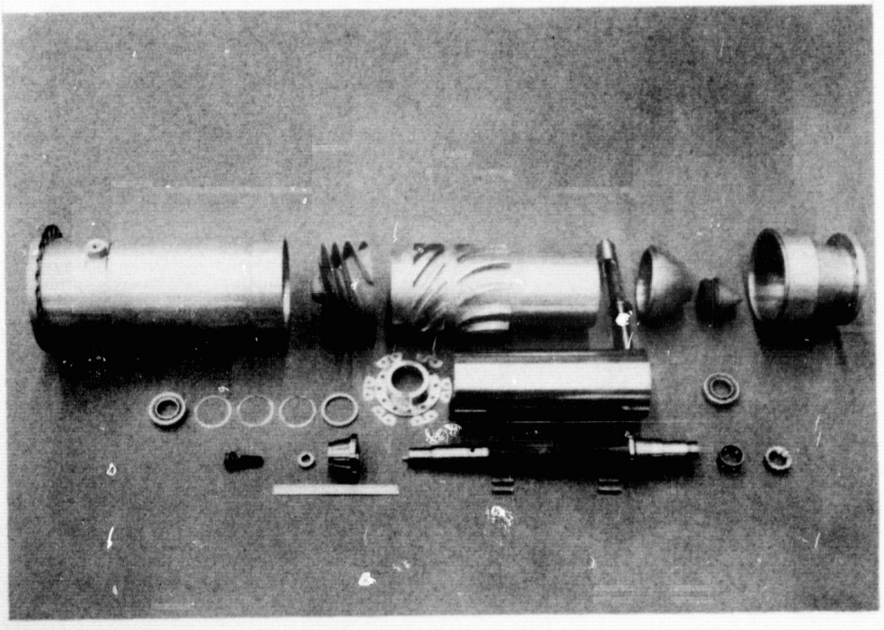

4MA62-3/18/74-C1C*

Figure 40. Complete Assembly, LO_2 Unit

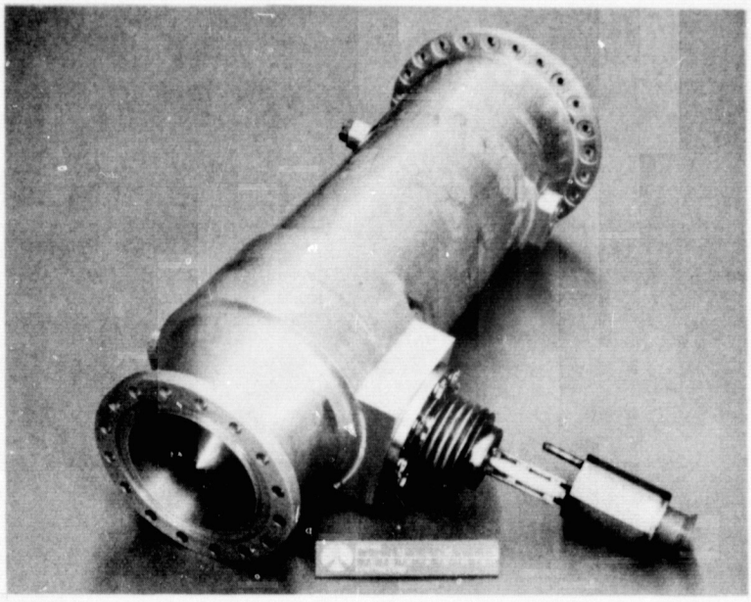

5AJ33-10/16/74-C1B

Figure 41. Discharge View of Oxygen Pump

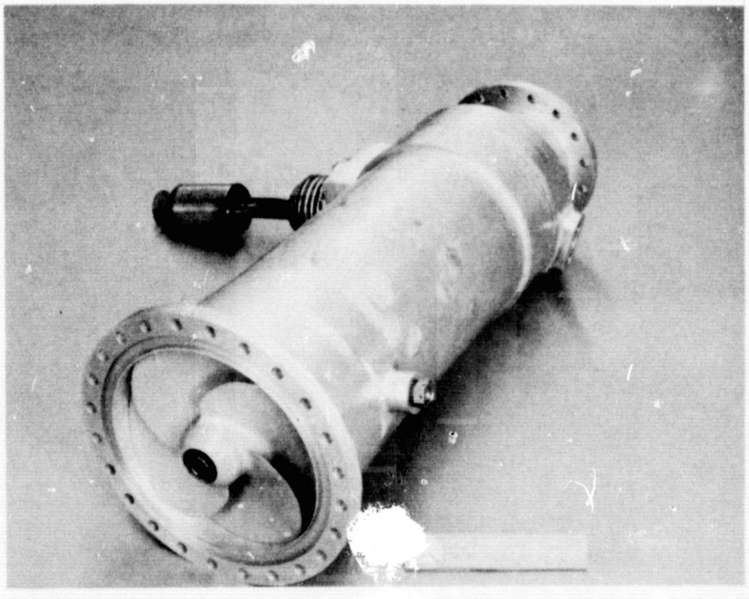

5AJ33-10/16/74-C1A

Figure 42. Inlet View of Oxygen Pump

unit, removal of the motor, and its return to the vendor. New outer and inner spacer rings were made and the units reassembled as initially done, following rewinding of the motors.

Difficulty was also encountered with the electrical connector on each motor assembly. The connectors originally specified, and installed on the oxygen units by Sundstrand, were too small to carry the required current. These connectors were replaced with connectors qualified for the Saturn program and used on the S-II stage hydrogen recirculation pump. For the hydrogen units, this replacement was done by Rocketdyne. On the oxygen motors, the replacement was done at the Sundstrand Perry, Ohio facility.

Oxygen Unit No. 2 was found to have a leak in the electrical motor steel housing. This housing is filled with helium and sealed as a safety feature. A small hole was discovered when the helium was admitted, prior to final sealing, and following the electrical connector replacement. This leak was caused by too deep a penetration of an electron-beam weld on the inner housing assembly. It was decided to cut two access holes, one each in the outer and inner housing assemblies to expose the leak. The leak was then sealed by a hand tack weld and the access holes closed. After the seal was satisfactorily made, it was decided not to close the inner housing access hole since this section is open to flow anyway. The outer housing access hole was then sealed.

Each rotor assembly was dynamically balanced (Fig. 43 and 44) prior to installation in the pumps. Slave bearings were used for this operation. Each unit was balanced to within 0.005 inch-ounces (0.36 cm-gram).

After final assembly, the units were pressurized to 30 psig with gaseous nitrogen and checked for leaks. Each unit was then cold torque checked using LN_2. Results are listed in Table 8. Each unit was then vacuum dried at 130 F for 36 hours. The final weights for each unit are given in Tables 9 and 10.

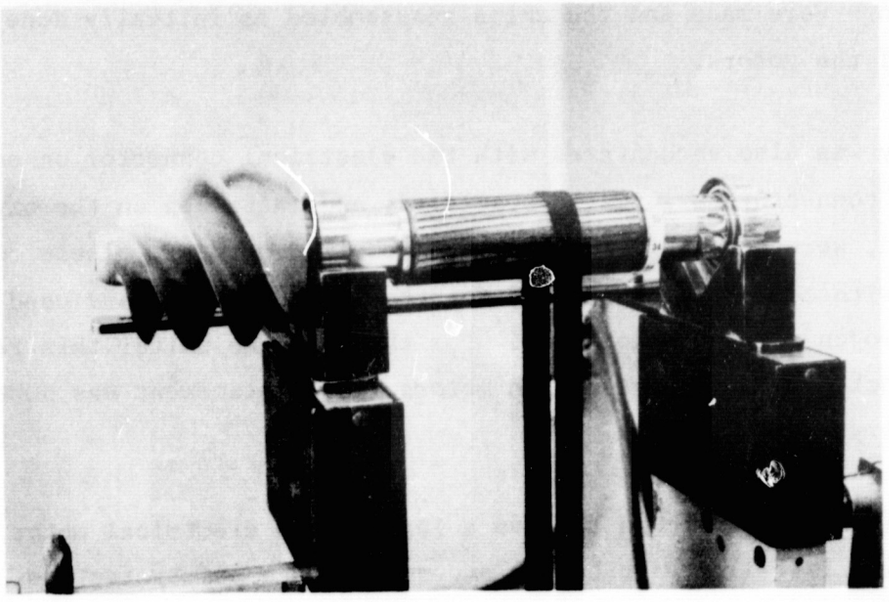

1XY52-5/23/74-C1A

Figure 43. Balancing Setup for H_2 Pump Rotating Assembly

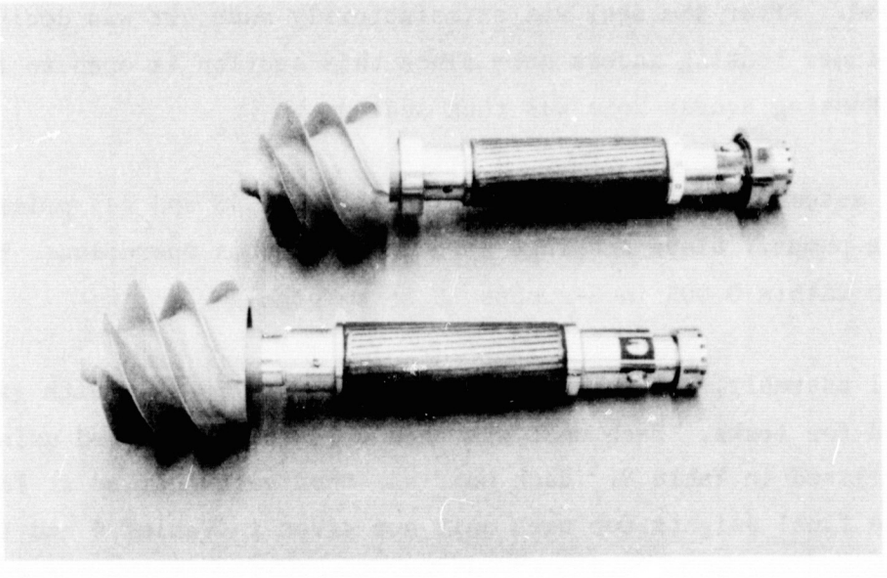

1XY52-5/23/74-C1B

Figure 44. H_2 Pump Rotating Assemblies After Balancing

TABLE 8. PUMP TORQUE CHECK RESULTS

Pump	Torque			
	Ambient Temperature		LN_2 Temperature	
	Breakaway in. oz (cm kg)	Running in. oz (cm kg)	Breakaway in. oz (cm kg)	Running in. oz (cm kg)
No. 1 LH_2	5 (0.36)	4 (0.29)	14 (1.01)	10 (0.72)
No. 2 LH_2	3 (0.22)	2 (0.14)	12 (0.86)	10 (0.72)
No. 1 LO_2	N/A*	N/A*	N/A*	N/A*
No. 2 LO_2	3 (0.22)	3 (0.27)	10 (0.72)	10 (0.72)

* Not Available

TABLE 9. HYDROGEN PUMP WEIGHT SUMMARY

Major Component	Estimated Weight lb (kg)	Actual Weight	
		Pump No. 1 lb (kg)	Pump No. 2 lb (kg)
Inducer	0.6 (0.272)	0.5 (0.227)	0.5 (0.227)
Electric Motor Rotor	1.5 (0.680)	1.1 (0.499)	1.1 (0.499)
Entire Rotating Assembly	3.8 (1.72)	3.83 (1.74)	3.84 (1.74)
Electric Motor Stator	5.5 (2.50)	5.6 (2.54)	5.6 (2.54)
Entire Housing Assembly	12.2 (5.54)	12.42 (5.63)	12.66 (5.74)
Total Pump Weight	16.0 (7.26)	16.25 (7.37)	16.50 (7.48)

TABLE 10. OXYGEN PUMP WEIGHT SUMMARY

Major Component	Estimated Weight lb (kg)	Actual Weight	
		Pump No. 1 lb (kg)	Pump No. 2 lb (kg)
Inducer	1.2 (0.544)	0.954 (0.433)	0.975 (0.442)
Electric Motor Rotor	4.2 (1.909)	4.22 (1.914)	4.22 (1.914)
Entire Rotating Assembly	8.9 (4.03)	8.97 (4.069)	8.75 (3.969)
Electric Motor Stator	10.8 (4.898)	10.8 (4.898)	10.8 (4.898)
Entire Housing Assembly	18.9 (8.573)	23.53 (10.68)	24.25 (11.0)
Total Pump Weight	27.8 (12.61)	32.5 (14.74)	33.0 (14.98)

PHASE IV - TESTING

TEST OBJECTIVES

The original test objectives of the program called for extensive testing of both the hydrogen and oxygen inducers. Upon initiation of the hydrogen unit test activity, it was determined that the hydrogen unit electric motors had been incorrectly designed. A re-evaluation of program objectives at that time eliminated any additional hydrogen unit testing, and the testing emphasis was directed solely to the No. 1 oxygen unit. The objectives of the revised test program were defined as:

1. The mechanical and hydrodynamic integrity of one of the oxygen inducers shall be verified in this phase of the program. A minimum of 2500 seconds run-time shall be accumulated on the machine.
2. The inducer's suction performance shall be verified over a flow range of 55 to 232 gpm with and without an inlet backflow deflector. Transient performance shall also be verified over the required operating range.
3. In addition to suction performance, chilldown thermal characteristics shall be evaluated. Drive system efficiency will also be evaluated.

Following a review of proposals by several independent testing laboratories, as well as Rocketdyne facilities, it was decided to do the testing at the Saugus, California, facility of Approved Engineering Test Laboratories (AETL). A subcontract was executed and AETL assembled the flow test circuit.

HYDROGEN TESTING

The No. 1 LH_2 unit was installed and following several LH_2 blowdowns, the pump was started. The first test resulted in a failed electrical connector. It was determined that the connector size was too small to carry the current required, and an interim fix was made to allow testing to continue.

A second test was attempted and it was determined that the pump did not reach design operating speed. In addition, the motor currents were excessive (all phases greater than 40 amperes with no load). The initial analysis of this problem indicated that the motors had been designed incorrectly. Analysis by Sundstrand of the high current problem showed that the most probable cause was that the "throw" of the stator windings was unsuitable for a 2-pole machine. The throw of this stator was 1 to 6 as opposed to 1 to 10 or 1 to 13, which would have been a more conventional design. This design error was attributed to taking notes from a drawing for a 4-pole machine and using them for the 2-pole design. It was decided that the stators would have to be rewound. The lack of ability to attain design speed was also thought to be due to this winding error although subsequent tests showed that the motor would achieve the design speed of 14,550 rpm at excessive current input. The stators were removed from the pumps and returned to Sundstrand.

OXYGEN TESTING

Test Facility

Following the failure of the hydrogen motors to operate properly, oxygen testing was initiated. The AETL facility was converted to LO_2 use, and the oxygen pump was installed. The test flow circuit is shown in Fig. 45, flow direction being from the run tank to the storage tank. Figure 46 is a photograph of the facility. From Fig. 46, it can be seen that only a portion of the facility lines are insulated. The inlet line, beginning at the inlet valve and including the filter and flowmeter, and the pump and part of the discharge line are not insulated. There are indications in the test data that this lack of insulation resulted in sufficient heat being added to the fluid to create vapor bubbles in the line. This was especially noticeable in the flow data, which was somewhat erratic. Figure 47 shows flow and speed data from two tests, one being a start transient, the other a segment of a long-duration run. In both cases, the flow is erratic and at times completely drops out. This could be indicative of a bad flowmeter connection but is more likely an indication that a gas pocket passed through the turbine. The loss of flow is usually accompanied by some speed increase

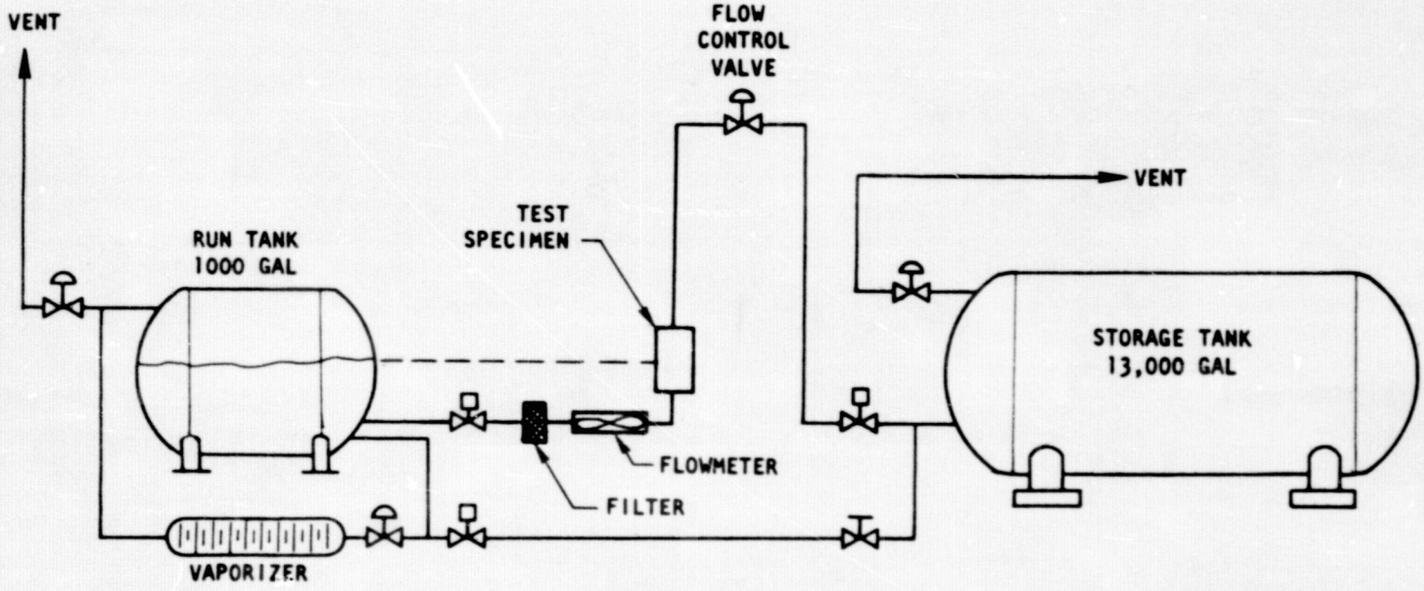

Figure 45. Oxygen Pump Facility Schematic

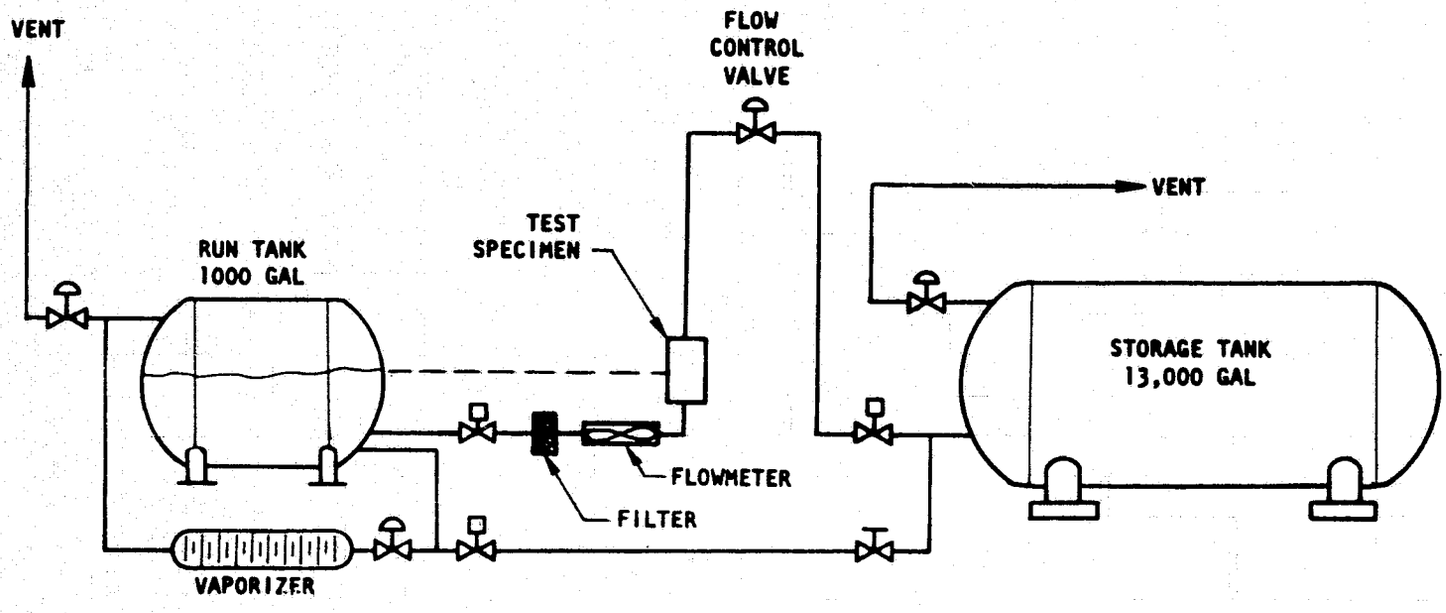

Figure 45. Oxygen Pump Facility Schematic

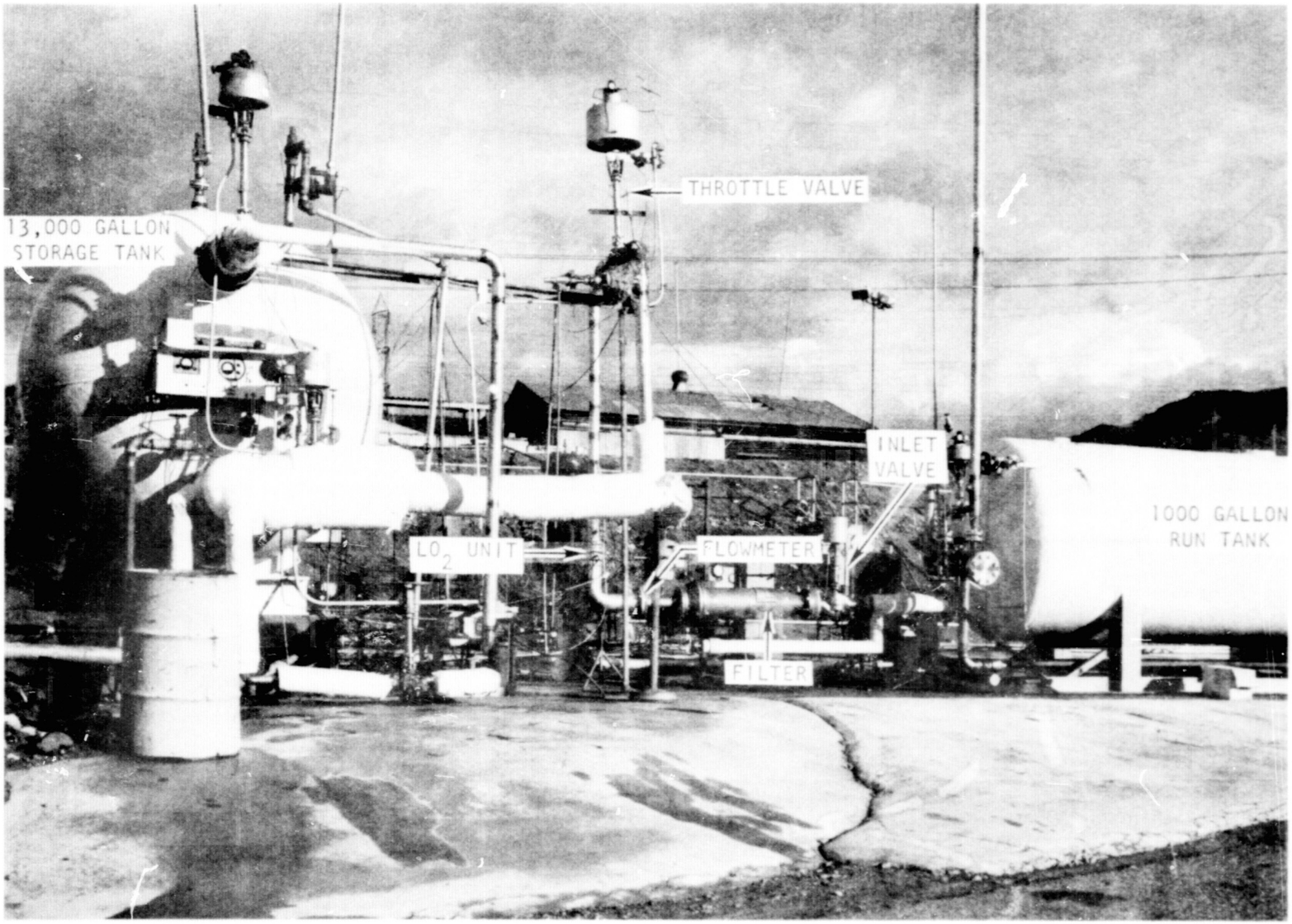

Figure 46. LO_2 Flow Facility With LO_2 Unit No. 1 Installed

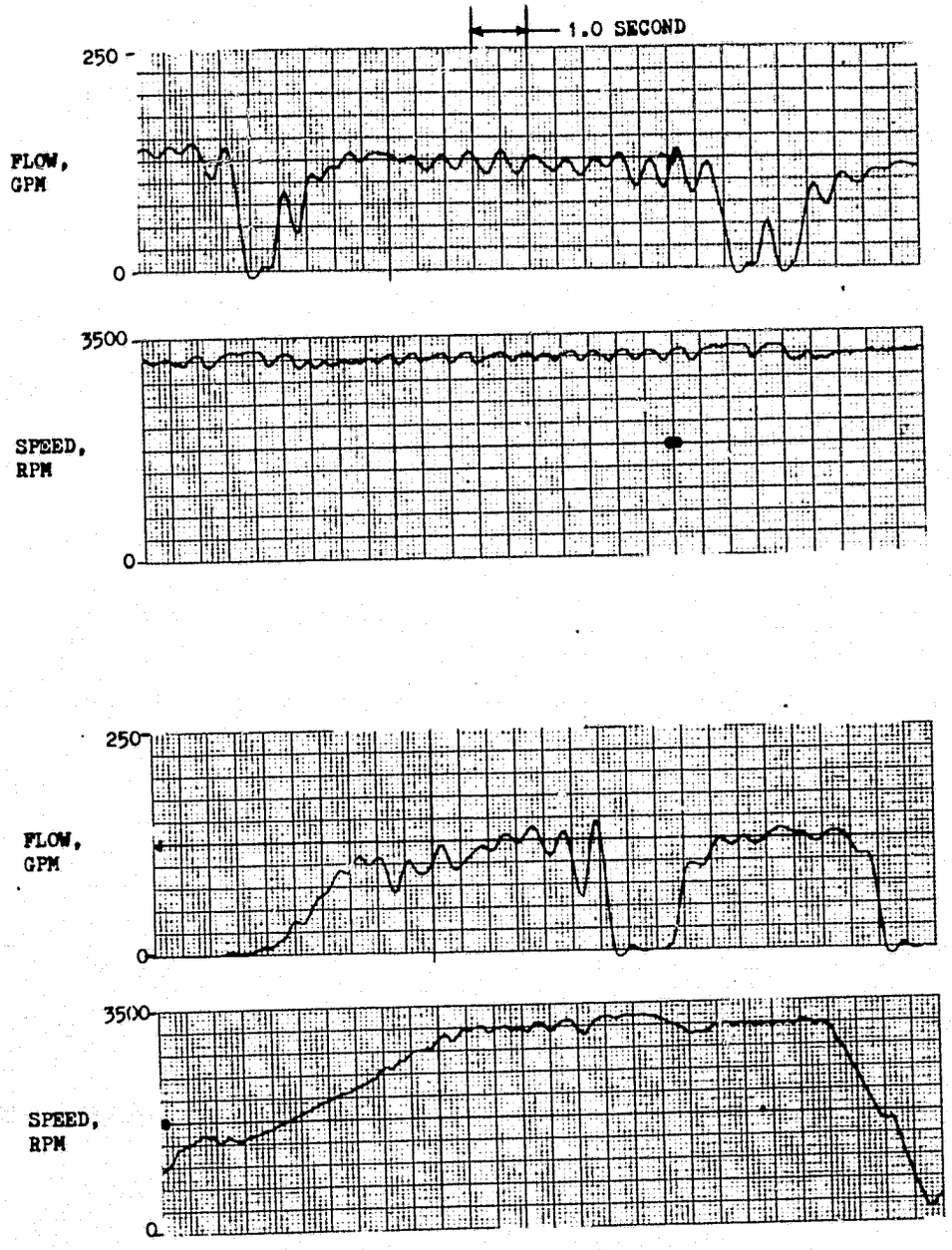

Figure 47. Data Slice From Test Series 4b and 4c (Top)

in the motor as if the pump began to unload. The speed change is not large, but the motor efficiency drops so rapidly with speed increases above 3000 rpm that very little speed increase is possible. (Based on the data supplied with the motor, an increase in speed from 3150 to 3290 rpm represents a 75-percent drop in horsepower required by the pump.) This again would indicate a gas pocket in the line. There were some tests in which the flow was at least stable enough to establish pump performance.

The temperature measurements did not tend to show any erratic behavior. However, they would not be expected to follow the flow variations because the vapor and liquid are at essentially the same temperature, slight variations locally causing gas pockets, and a resistance bulb probe will not indicate any difference in liquid and vapor with a two-phase flow at the same temperature for each phase.

The run tank pressure in the facility is regulated manually as well as the throttle valve in the facility discharge line. This also presented problems in obtaining accurate data in that the flow and inlet pressure could not be adjusted independently. It was desired to run tests with either flow or suction pressure held constant while the other varies, but this was not possible. The flow changes would cause corresponding drops in suction pressure due to extra inlet line losses that were large percentage changes with such low operating suction pressures. This will be demonstrated in later figures showing start transients in which starts at constant inlet pressure were attempted. As soon as the flow began, the inlet pressure dropped significantly. In future tests operating so close to the vapor pressure, better control over suction pressure and flow should be sought.

Test Instrumentation

Table 11 lists the instrumentation requirements and Table 12 presents the redline parameters used during the tests. Figures 48 and 49 are closeup photographs of the installed pump with instrumentation indicated.

TABLE 11. OXYGEN PUMP INSTRUMENTATION REQUIREMENTS

Parameter	Range	Precision	Type Instrument	Recorder
I LOW FREQUENCY				
A. PRESSURE				
1. Run Tank, P_o, N/M^2 (psig)	0 to 344,738 (0 to 50)	±1/2%	Strain Gage	DIGR, Mag Tape
2. Suction, P_{s1}, N/m^2 (psig)	0 to 344,738 (0 to 50)	±1/2%	Strain Gage	DIGR, Mag Tape
P_{s2}, N/m^2 (psig)	0 to 344,738 (0 to 50)	±1/2%	Strain Gage	DIGR
P_{s3}, N/m^2 (psig)	0 to 344,738 (0 to 50)	±1/2%	Strain Gage	DIGR
P_{s4}, N/m^2 (psig)	0 to 344,738 (0 to 50	±1/2%	Strain Gage	DIGR
3. Discharge, P_{d1}, N/m^2 (psig)	0 to 689,476 (0 to 100)	±1/2%	Strain Gage	DIGR, Mag Tape
P_{d2}, N/m^2 (psig)	0 to 689,476 (0 to 100)	±1/2%	Strain Gage	DIGR, Mag Tape
4. Pump Delta, P_{d1}-P_{s3}, N/m^2 (psid)	0 to 344,738 (0 to 50)	±1/2%	Strain Gage	DIGR, Mag Tape
5. Inducer Exit, P_{s5}	0 to 344,738 (0 to 50)	±1/2%	Strain Gage	DIGR, Mag Tape
B. TEMPERATURE				
1. Suction, T_{s1}, K (F)	88.7 to 116.5 (-300 to -250)	±1/2%	Resistance Bulb	DIGR, Mag Tape
T_{s2}, K (F)	88.7 to 116.5 (-300 to -250)	±1/2%	Resistance Bulb	DIGR
T_{s3}, K (F)	88.7 to 116.5 (-300 to -250)	±1/2%	Resistance Bulb	DIGR
T_{s4}, K (F)	88.7 to 116.5 (-300 to -250)	±1/2%	Resistance Bulb	DIGR
2. Inducer Exit, T_{s5}, K (F)	88.7 to 116.5 (-300 to -250)	±1/2%	Resistance Bulb	DIGR
3. Discharge, T_{d1}, K (F)	88.7 to 116.5 (-300 to -250)	±1/2%	Resistance Bulb	DIGR
T_{d2}, K (F)	88.7 to 116.5 (-300 to -250)	±1/2%	Resistance Bulb	DIGR
4. Inlet Skin, T_1, K (F)	88.7 to 338.7 (-300 to 150)	±5%	Thermocouple	DIGR
5. Pump Skin, T_2, K (F)	88.7 to 338.7 (-300 to 150)	±5%	Thermocouple	DIGR
6. Motor Skin, T_3, K (F)	88.7 to 338.7 (-300 to 150)	±5%	Thermocouple	DIGR
7. Disch. Skin, T_4, K (F)	88.7 to 338.7 (-300 to 150)	±5%	Thermocouple	DIGR
II CYCLIC				
1. Inlet Flow, Q, m^3/s (gpm)	0 to 0.01892 (0 to 300)	±1%	Turbine	DIGR, Mag Tape
2. Pump Speed, N, Rad/s (rpm)	0 to 418.9 (0 to 4000)	±1/2%	Magnetic Pickup	DIGR, Mag Tape
III DYNAMIC				
1. Pump Inlet, P_1, N/m^2 (psig)	0 to 344,738 (0 to 50)	±1%	Data Sensor	Mag Tape
P_2, N/m^2 (psig)	0 to 344,738 (0 to 50)	±1%	Data Sensor	Mag Tape
2. Pump Disch, P_3, N/m^2 (psig)	0 to 689,476 (0 to 100)	±1%	Data Sensor	Mag Tape
3. Inlet Axial, A_1, m/s^2 (g's rms)	*6.096 (20)	--	Accelerometer	Oscill, Scope
	**60.96 (200)	---	Accelerometer	Mag Tape
4. Disch. Axial, A_2, m/s^2 (g's rms)	*6.096 (20)	---	Accelerometer	Oscill, Scope
	**60.96 (200)	---	Accelerometer	Mag Tape
5. Disch. Radial, R, m/s^2 (g's rms)	*6.096 (20)	---	Accelerometer	Oscill, Scope
	**60.96 (200)	---		Mag Tape
IV ELECTRIC				
1. Frequency/Phase, F_1, F_2, F_3	0 to 150 Hz	±2%	Frequency Meter	DIGR, Oscill
2. Ampere/Phase, A_{p1}, A_{p2}, A_{p3}	0 to 50	±2%	Ammeter	DIGR, Oscill
3. Volt/Phase, V_1, V_2, V_3	0 to 250 (L-N)	±2%	Voltmeter	DIGR, Oscill
4. Throttle Valve Position	0 to 100%	---	Voltmeter	DIGR

*0.8K-Hz Low Pass

**10K-Hz Wide Band

FOLDOUT FRAME

TABLE 12. OXYGEN PUMP REDLINE PARAMETERS

Key Numbers	Parameter	Maximum Value
P_o	Run Tank Pressure, N/m^2 (psig)	344,738 (50)
$P_{s1}, P_{s2}, P_{s3}, P_{s4}$	Suction Pressures, N/m^2 (psig)	344,738 (50)
P_{d1}, P_{d2}	Discharge Pressures, N/m^2 (psig)	689,476 (100)
$P_{d1}-P_{s3}$	Pump Delta Pressure N/m^2 (psid)	275,790 (40)
A_{p1}	Maximum Amperes/Phase at Steady State Operation	20
N_{min}	Minimum Pump Speed at Steady State Operation, rad/s (rpm)	261.8 (2500)
N_{max}	Maximum Pump Speed, rad/s (rpm)	418.9 (4000)
A_1	Inlet Axial Accelerometer, m/s^2 (g's rms)	3.048 (10)
A_2	Discharge Axial Accelerometer, m/s^2 (g's rms)	3.048 (10)
R_1	Discharge Radial Accelerometer, m/s^2 (g's rms)	3.048 (10)
T_{s1}	Pump Inlet Temperature, F	-285

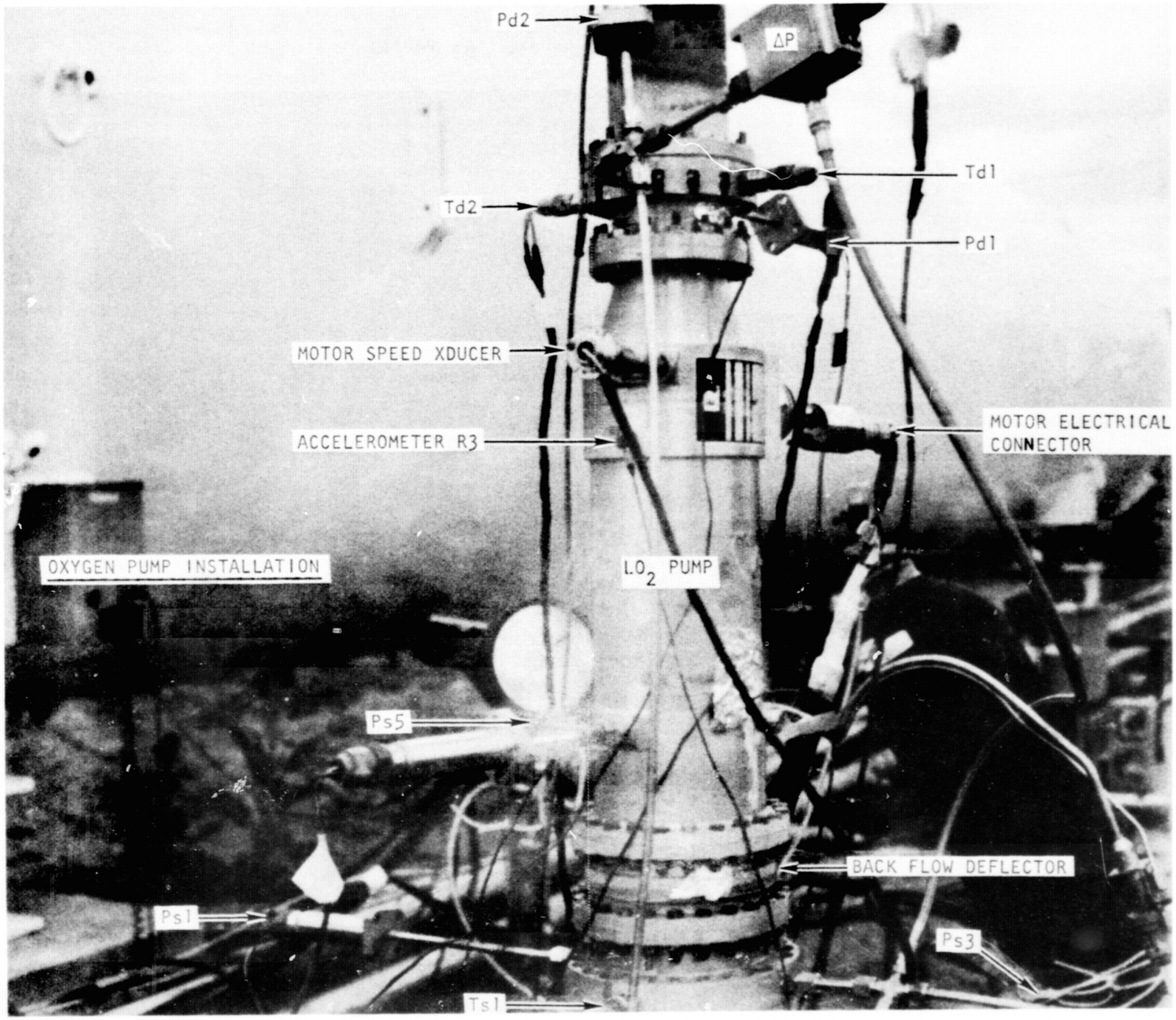

Figure 48. Oxygen Pump Installation

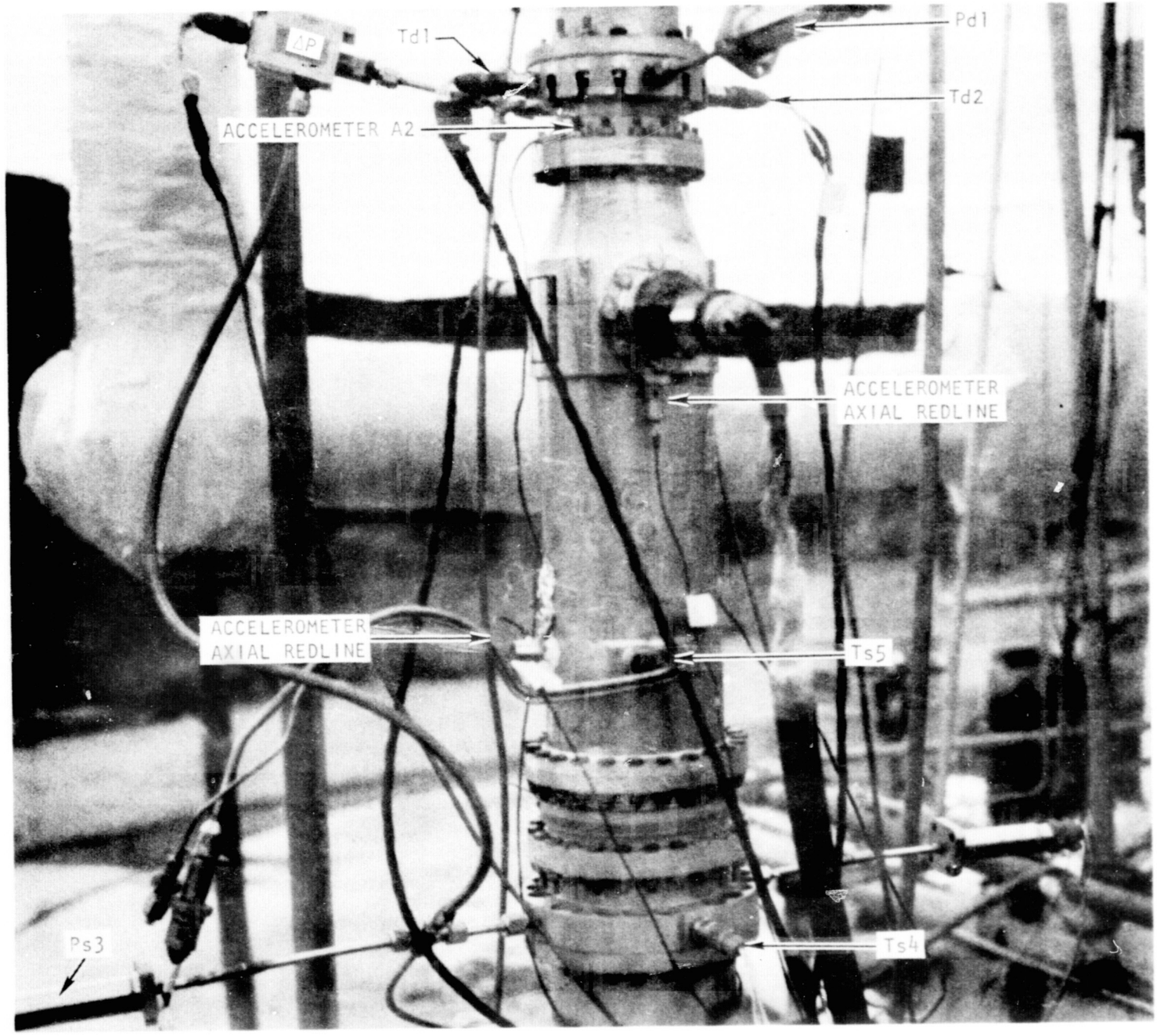

Figure 49. Oxygen Pump Instrumentation

Figure 50 shows the location of the instruments relative to the pump assembly. Most of the instrumentation is located immediately upstream or downstream of the pump. The major exceptions are P_{s_5} and T_{s_5} which are located at the inducer exit (upstream of the stator vanes). All of the pressures are static pressure taps and no total pressure measurements were made. The static taps are adequate at the upstream and downstream positions of the pump for velocities are low and are designed to be axial only so they can be calculated from the flowrate. However, at the inducer exit, velocities are not necessarily low (relative to the static pressures) so that establishing an inducer discharge total pressure is subject to significant inaccuracies. As a result, pump overall performance is discussed in detail but not inducer or stator performance as subcomponents.

The DIGR recordings were actually on-site strip charts used only to check out the instrumentation during the test periods. The accuracy of these data recordings was not controlled as carefully as the magnetic tape data and, therefore, the latter data were reduced to establish the pump performance.

The pressure measurements used to establish the low-frequency performance were not close-coupled to the line. This can be seen in Fig. 48 and 49 where the pressure gages are located at the end of a line segment. With such an arrangement, the frequency response is bad, and with two-phase flow and trapped gas in the instrument lines, the resonant frequency of the line can drop so low that the data could indicate oscillations that do not actually occur in the flow. Such a phenomenon is believed to have occurred at times. For example, Fig. 51 shows data from the transducer downstream of the inducer exit (P_{s_5}) with an indication of a ringing due to the instrumentation line for, if the instrument line resonant frequency were not very low, the data should show significant higher frequency content as well. For example, at a pump speed of 3000 rpm and with a four-bladed inducer, the frequencies of 50 and 200 Hz should always be discernible at the rotor exit. However, the data show no frequency content above the very low frequency indicating this to be a line resonance. Although close-coupled data sensors were initially planned to be used in the test program, they were not included so that no high-frequency, pressure-oscillation performance data were obtained.

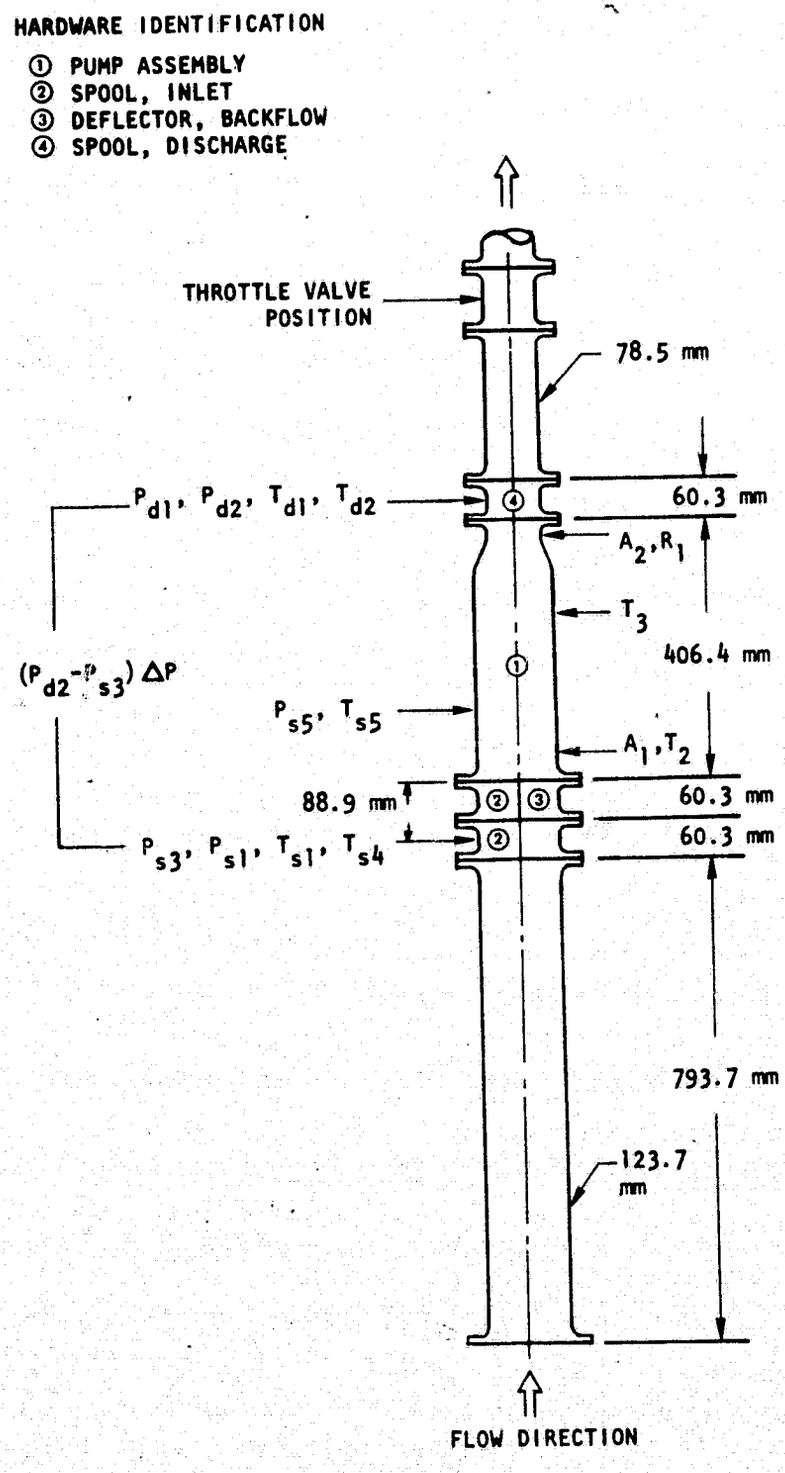

Figure 50. Oxygen Pump Instrumentation and Assembly Schematic

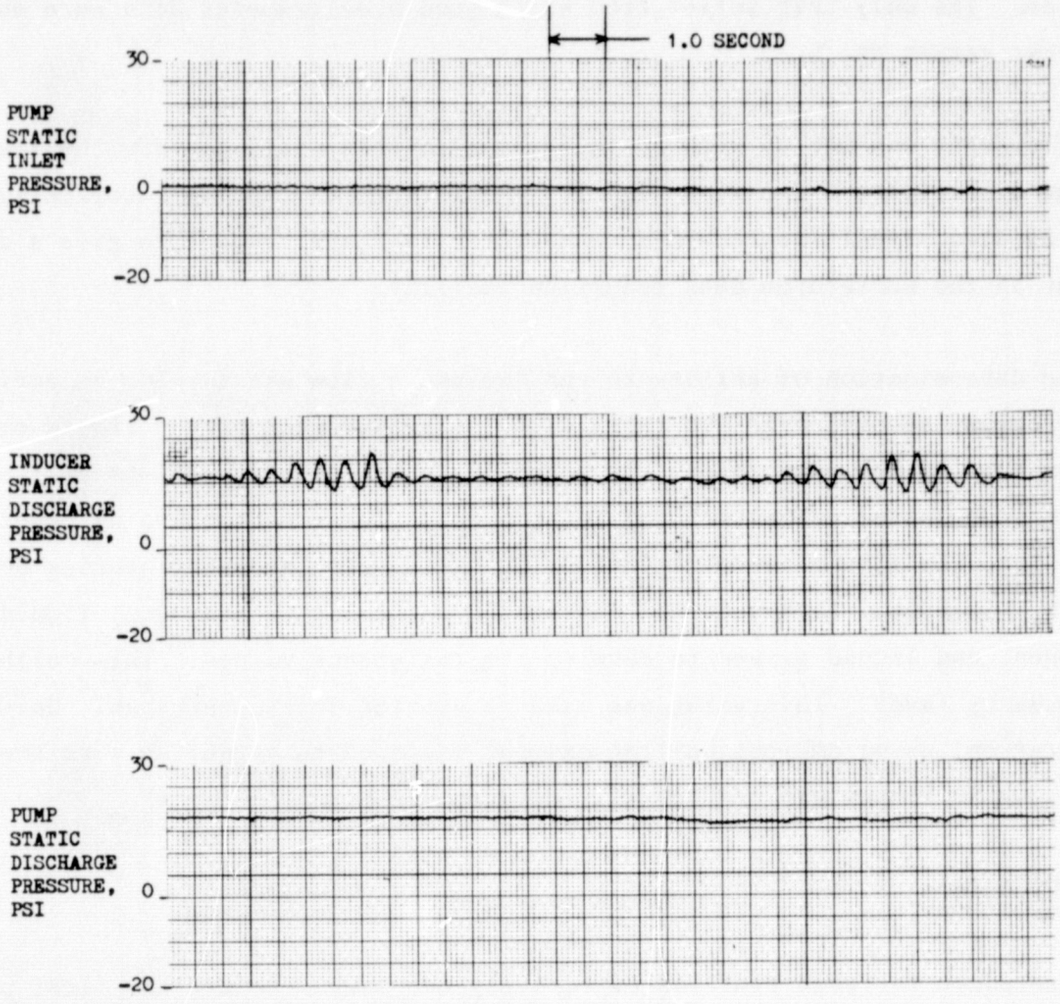

Figure 51. Data Slice From Test Series 5d

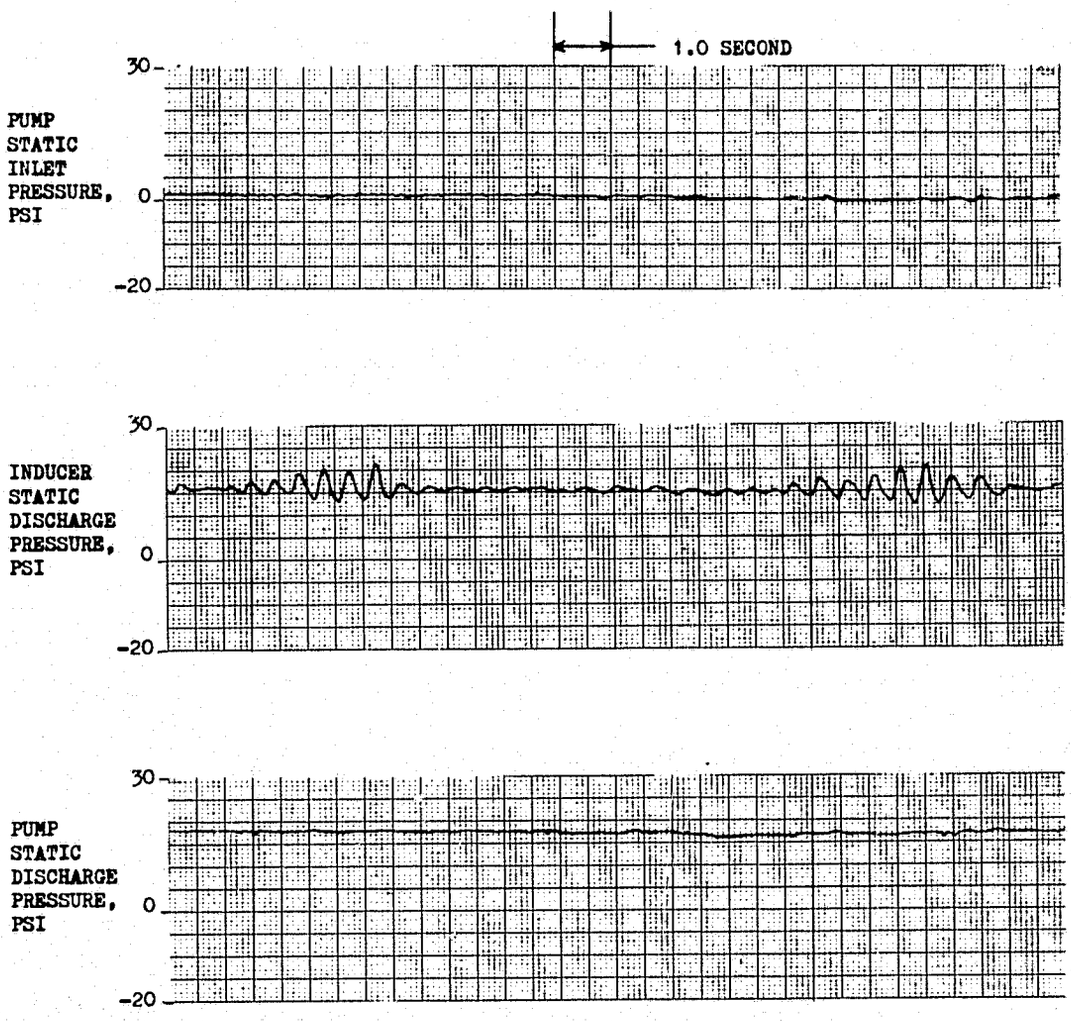

Figure 51. Data Slice From Test Series 5d

Accelerometers were also used on the tests, but problems were experienced with them. The problem was never clearly defined; insulation of the mounting blocks from the ducts was eventually used to eliminate the problem. This indicated either a problem due to the low temperatures or an instrumentation grounding problem. The only test series from which good accelerometer data were obtained was test series No. 5.

The flowmeter was set up with an Anadex system that would convert the frequency output directly to a d-c flow signal. This system did not work correctly, but the raw data signal was recorded on magnetic tape and reduced to give a d-c flow output in the Rocketdyne data reduction facility.

As the determination of ability to run two-phase flow was a prime objective of the program, special care was taken with the measurement of the liquid oxygen temperature at the pump inlet. As noted in Table 11, two resistance-type transducers were installed in the pump inlet spool. These units have an injection depth into the flow of about 1 inch. The units were Tayco Engineering devices, Part No. 50-2916. Each unit was calibrated using liquid hydrogen, liquid nitrogen, and liquid oxygen to develop its resistance values. This calibration was made by Tayco. This value was used to set the instrument span. On-site calibration, using ambient boiling oxygen, was used to establish a reference point. A 50 F span was used on all measurements.

Test Procedure

The procedure for each test was effectively the same. Before the first pump start, the inlet valve was opened and liquid oxygen was allowed to seek its own level in the flow circuit. As the system chilled down, the oxygen level was near the inducer inlet hub. The run tank was then pressurized and oxygen was caused to flow through the discharge system and into the vented 13,000-gallon storage tank. When the pump inlet temperature would indicate approximately liquid temperature, the pump was started.

Transient start tests were made with decreasing suction pressures from test-to-test. However, the lack of capability in holding a fairly uniform inlet pressure during these tests complicated the interpretation of the results. Also, the tests were generally run as quickly as possible to keep from heating up the LOX too soon, but later tests did indicate the presence of vapor bubbles in the stream and eventually the point was reached where the pump would not start.

The head-capacity tests were made while attempting to hold constant inlet pressure and manually controlling the throttle valve. However, the run tank pressure had to be manually adjusted to maintain the constant inlet pressure and, as a result, the pressure did vary some during the tests. The cavitation tests were made with a constant throttle valve position while allowing inlet pressure to slowly decay until the flow stopped. This reduction in inlet pressure was affected by blow down of the run tank ullage.

Test Matrix

The test matrix actually run is shown in Table 13. In the following sections the objectives of each test and the results are discussed.

ELECTRICAL PERFORMANCE

The drive system for the oxygen pump is a four-pole, three-phase induction motor. Primary power was supplied by a variable frequency inverter unit manufactured by the General Electric Company, Model No. 6V25B5045. This unit is a standard production model that included the high-frequency option. Photographs of the unit are presented in Fig. 52 and 53.

The output wave form of the inverter is a three-phase square wave generated through a series of solid-state switching devices operating against an internal full wave rectifier set at 310 vdc. The motor unit is a wye connection requiring 115 volts line to neutral. The output of the inverter is a nominal 3-phase 230 volts rms balanced system. A transformer was installed between the

TABLE 13. SUMMARY OF OXYGEN INDUCER TESTING

Test Series No.	Number of Pump Starts	Average Length of Run, seconds	Total Time Accumulated, seconds	Remarks
1	10	10	100	Instrumentation Checkout
2a	1	240	240	Initial H/Q Mapping
2b	1	255	255	Mapping
3a	7	10	70	2.5 Second Ramp
3b	1	180	180	Performance
3c	19	7	133	Start Transients
3d	1	270	270	Performance
4a	1	250	250	Performance
4b	27	10	270	Start Transient
4c	1	45	45	Performance
4d	1	280	280	Performance
5a	19	10	190	Installed Backflow Deflector Tests for Start Transients and Suction Performance
5b	2	60	120	
5c	6	40	240	
5d	1	250	250	
Totals	98		2893	

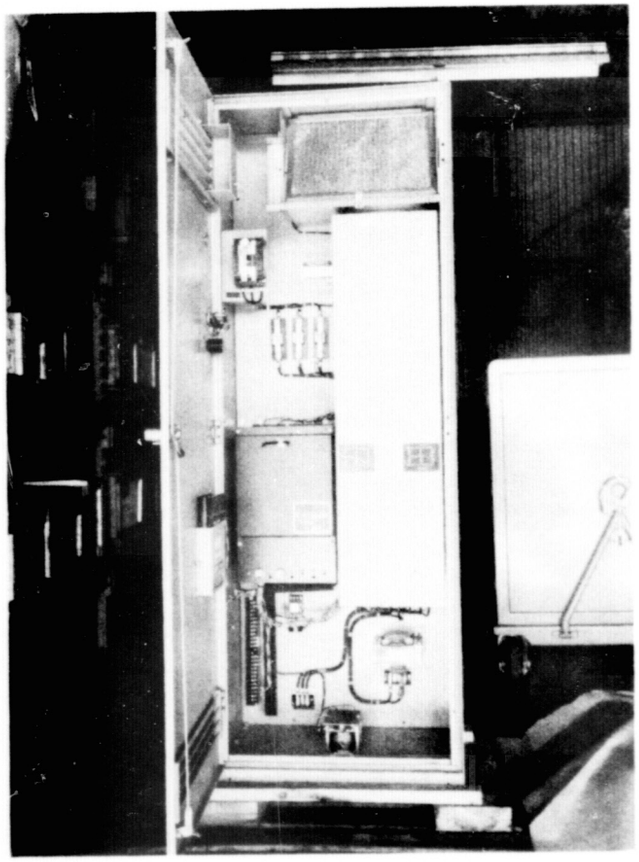

4MA91-4/2/74-C1A

Figure 52. Variable-Frequency Inverter Unit

4MA91-4/2/74-C1B

Figure 53. Variable-Frequency Inverter Unit

inverter and the motor to effect the correct voltage and line match. The neutral was carried on the motor side only. The inverter is capable of being set to any frequency, and an adjustment is also available to set the correct voltage at that frequency. Internal voltage regulation maintains the setting.

For these tests, the frequency was set with a frequency meter and the voltage adjusted under load. The voltage for all tests was held between 112 and 115 volts rms line to neutral. This measurement was made using a standard 20,000 ohms/ voltmeter. This technique was recommended by General Electric for the frequency range being used. The motor input wave form is complex and this type of instrument has a better "rms" reading than other devices.

The ramp-up rate, the time from switch-on to full speed, is also controlled by the inverter. This rate is set by using a varying series of "chopped" pulses, the number of "chops" decreasing as the operating frequency is approached. This method is used to provide the proper frequency/rms voltage values to prevent excessive current during the ramp-up time. The two ramp-up rates used for these tests were 2.5 and 7 seconds.

Sundstrand predicted a slip of 9.75 percent at the motor design operating point (Table 4). Using data from one series of tests (Fig.54), this estimate by Sundstrand appears to be approximately correct.

The input currents were noted continuously during all tests and varied between 10 and 12 amps at a line voltage of 112 to 115. This value is also close to the Sundstrand predictions. For estimates of motor pump performance, the Sundstrand provided characteristics were used.

Once the small connectors were replaced by units capable of carrying the required current, the electric motor ran smoothly, could be accurately ramped and regulated, and seemed ideal for this type of application.

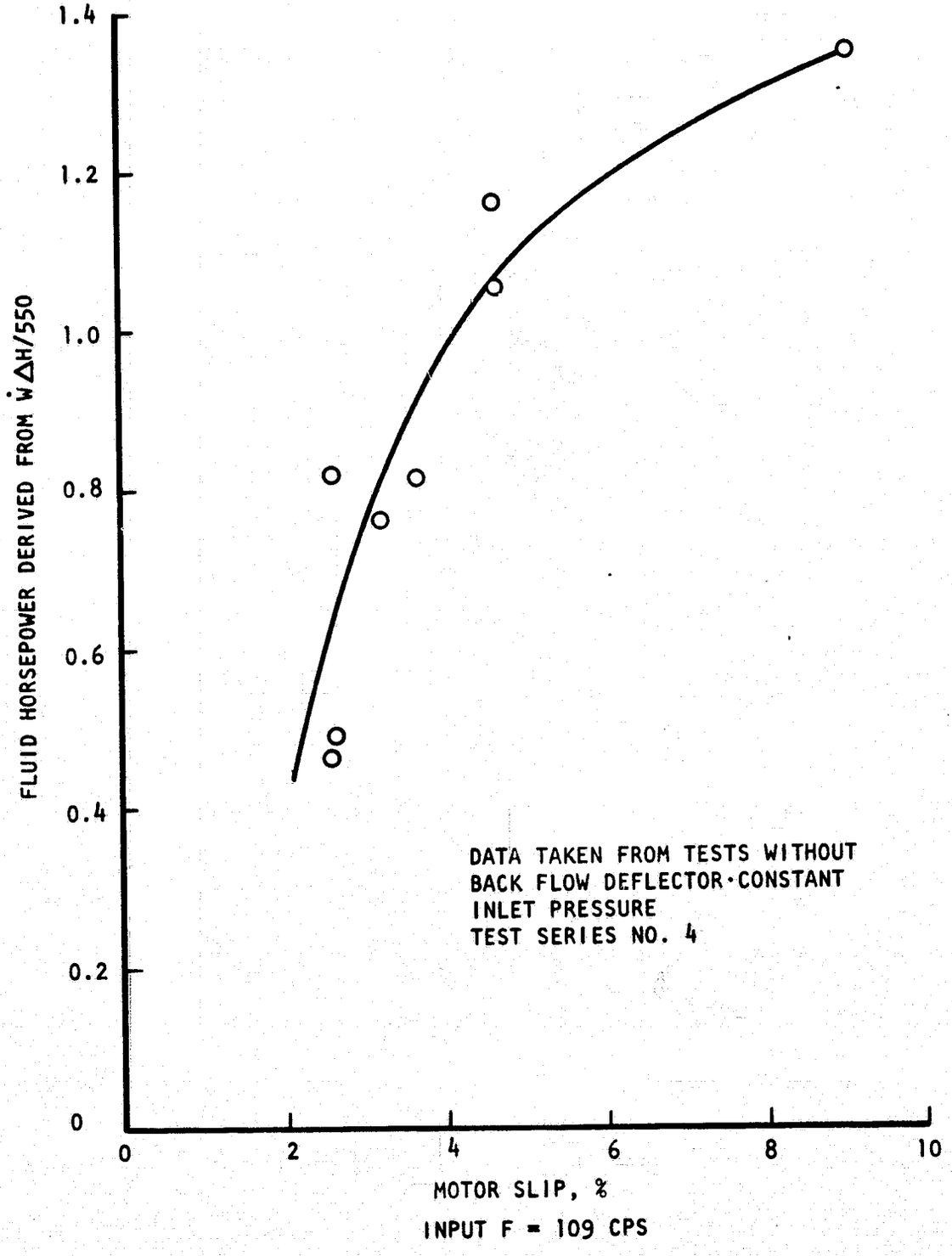

Figure 54. Motor Slip vs Fluid Horsepower

TEST RESULTS

The test series are presented below and discussed in the order of testing.

Test Series 1 was conducted to obtain a checkout of the instrumentation and to indicate the proper throttle valve settings required for obtaining the desired flow range. Ten test starts were made with a total accumulated run time of approximately 100 seconds. The initial throttle valve settings were giving too high a flow, most of the data being well above the design flow and the pump head was down. The high flow and low head generation led to a lot of vapor in the lines. As the throttle valve position was changed to get a lower flow, some good data points were achieved indicating an overall pump head in agreement with the prediction. The suction pressure parameters did not get recorded on these tests due to a facility malfunction. No further data reduction of these tests was needed.

Test Series 2 was designed to establish the head-flow relationship of the pump primarily at higher suction pressure values. The attempt was made to hold constant tank pressure and vary the throttle valve setting to change flowrate, recording steady-state values at different settings. The initial tests (No. 2a) were attempted using 5 psi as the run tank pressure. However, this value was low enough so that with the variations experienced in line presssure due to flow changes, significant variations were occurring in the flow presumably due to the gas in the inlet line. Thus, the tank pressure was raised to 12 psi, and the tests repeated (Series No. 2b). These tests also experienced some flow variations, and suction and tank pressures were varying during the run. However, enough good data were obtained to establish the head-flow relationship of the pump. Figure 55 shows a typical slice of data obtained from this run. Note that all parameters are relatively smooth with the exception of flow.

Data obtained from tests series No. 2b are plotted in Fig. 56. The data have been corrected to 3008 rpm, the design operating speed, and are compared to a curve indicating the predicted performance and the design point (as indicated

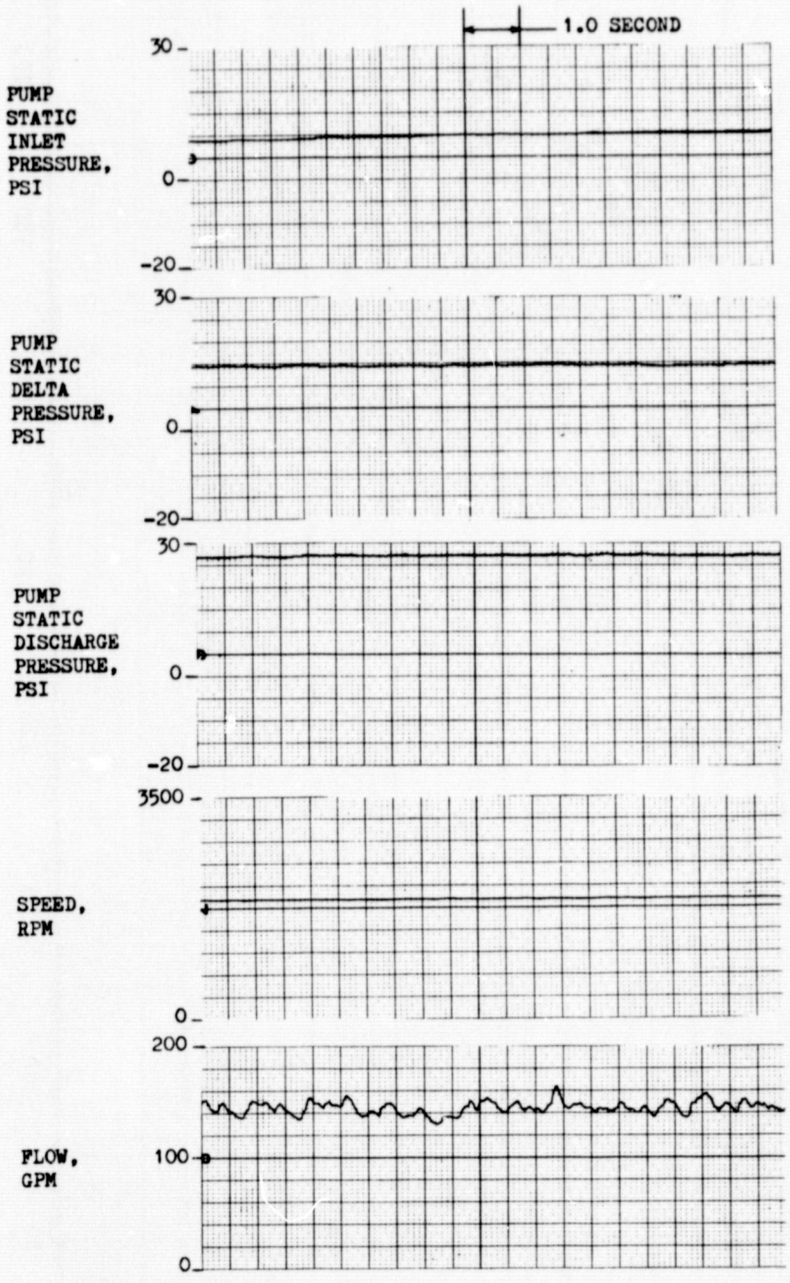

Figure 55. Data Slice From Test Series 2b

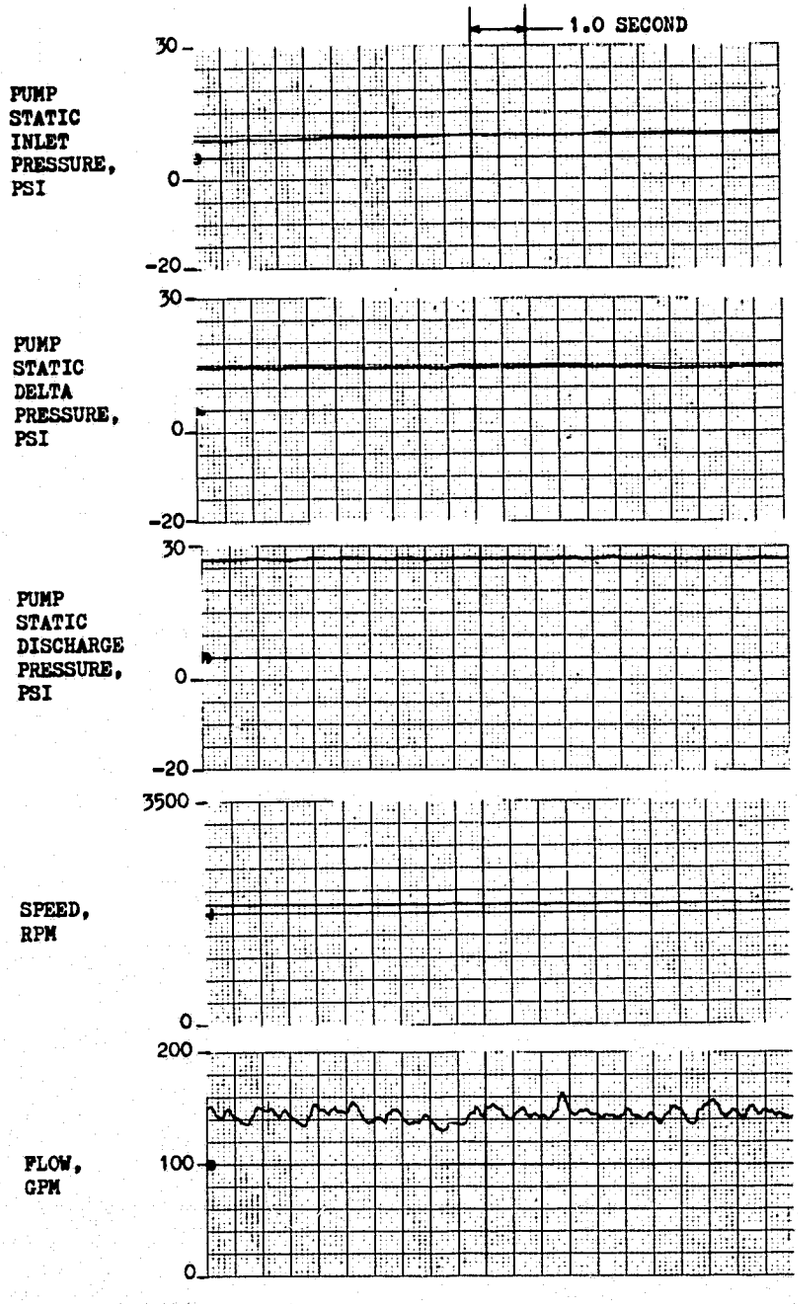

Figure 55. Data Slice From Test Series 2b

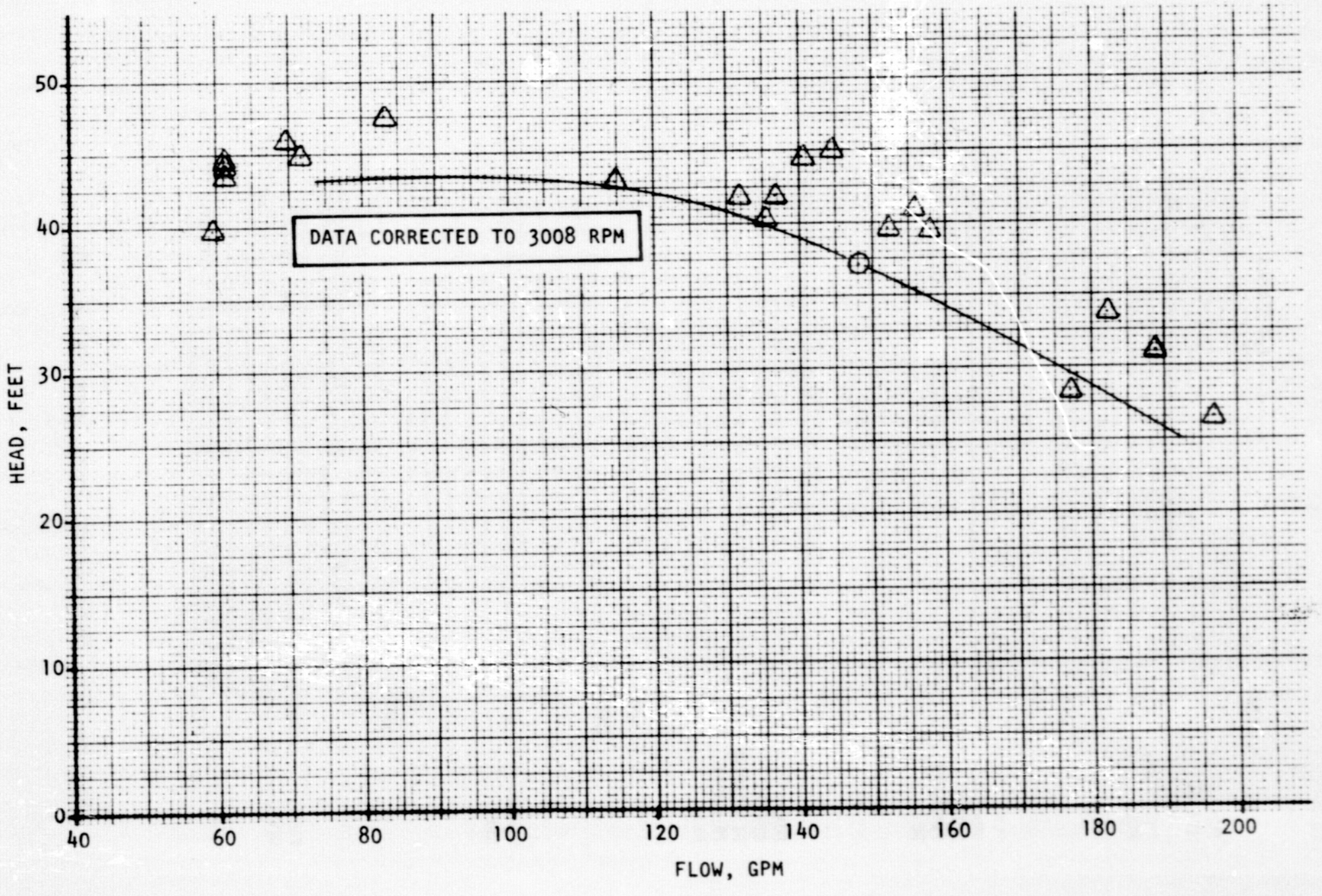

Figure 56. Performance of the No. 1 Oxygen Unit

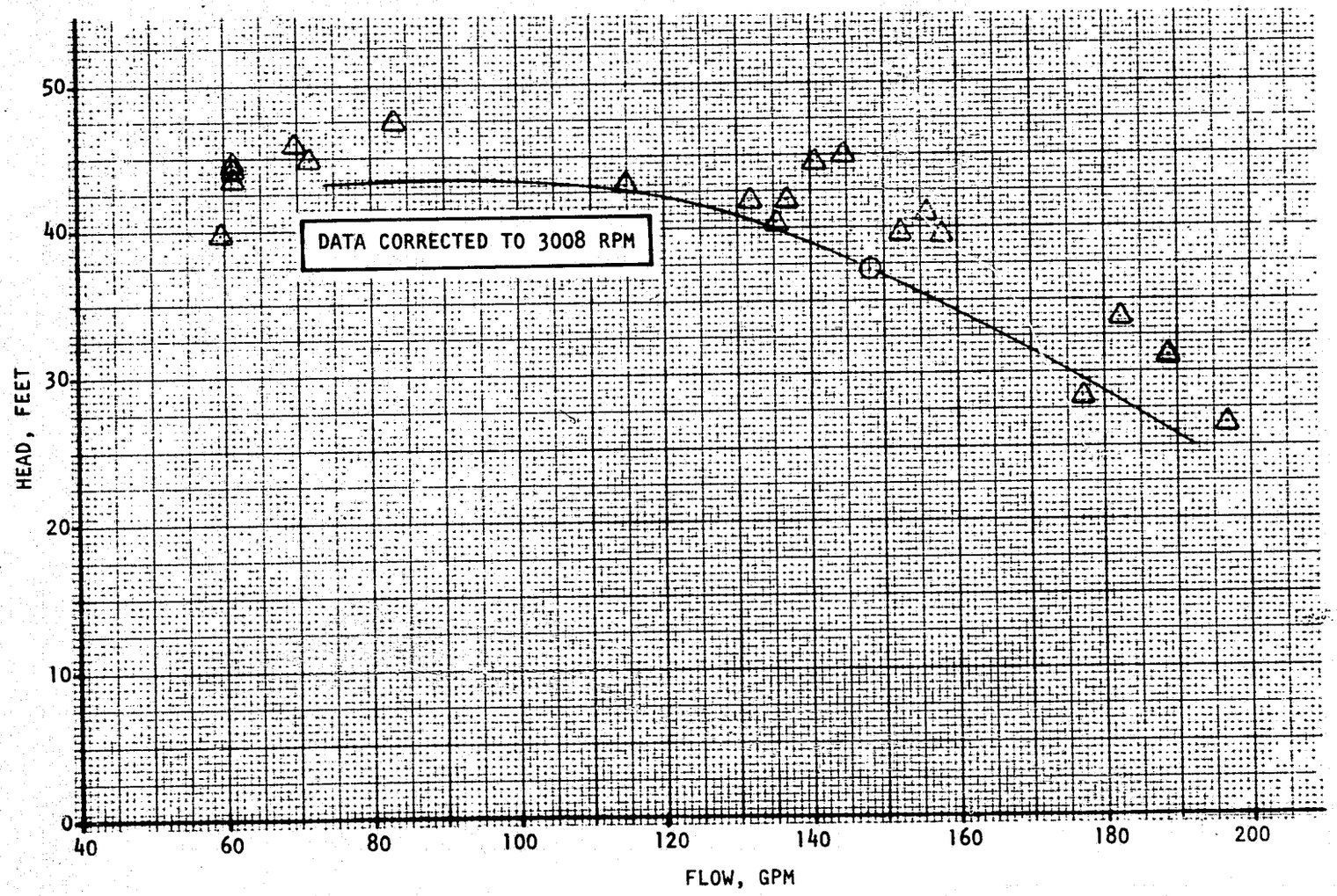

Figure 56. Performance of the No. 1 Oxygen Unit

by the circle). The agreement with the prediction is very good and even indicates slightly more head then predicted.

An attempt was made to use the static pressure behind the inducer and an analytical prediction of the velocity triangles at the inducer exit to predict a rotor head, which could also be used to derive the stator and passage losses for comparison with the analytical predictions. However, the results were so inconsistent that they could not be relied on as an accurate representation of the flow conditions. Some of the data indicated losses approximately in the range predicted, but most of the data indicated a significantly higher rotor head and higher stator losses than predicted. The difficulty with this type of calculation comes from using a local static pressure as measured without knowing the specific local velocity associated with that pressure (both being needed to get a total pressure). Even if a single total pressure reading were available, there is no guarantee that the local value is a true representation of the average condition across the radial height of the passage.

An attempt was also made to establish a pump overall efficiency using the site measured data and the motor performance data as supplied by the vendor (Table 4). For the same data points plotted in Fig. 56, the calculated pump efficiency varied from 11 to 38 percent. The analytical prediction of pump efficiency in the same flow range and for the same speed varied from 47 to 67 percent. This difference is so large that it indicates some discrepancy either in the data, the motor performance prediction, or the failure to account for some other horsepower loss not yet recognized. Rocketdyne has attempted to pursue this discrepancy but without any success. The data consistently yield the same results. One hypothesis that could be offered is that the inducer head is indeed very much higher than the prediction and that the stator-diffuser passage losses are much higher than predicted. However, to raise the efficiencies enough to get a better agreement would require inducer heads of at least 1.5 times, and sometimes up to 3.0 times, as much as predicted. None of the data indicated rotor heads approaching these limits (nor could the head possibly be as high as required by some of these data points). Of course, a pump similar to the one tested here is not expected to get a high efficiency, but it is doubtful if its efficiency is as low as indicated by the tests comparison.

Two starts were made during test Series No. 2, with an additional accumulated time of 495 seconds duration running.

Test Series No. 3 consisted of both start transient tests and longer-duration runs to establish performance. Series No. 3a was an attempt to run start transients at relatively low suction pressures and low flows adjusting the throttle valve and the tank pressure from run to run. However, the flow was very erratic, and the data were not reduced, suspecting that too much vapor was present in the lines to achieve a representative start condition for the pump. Test Series No. 3b followed, which was allowed to run for longer duration to attempt to chill down the lines and eliminate some of the vapor. This test seemed to accomplish this purpose so that start transients could be made.

Test series No. 3c consisted of 19 start transients using a ramp rate of approximately 3.0 seconds. Figures 57 through 59 show actual traces of the data for six different start ramps. As can be readily seen, the flow data are very erratic, yet the pump did start successfully. The starts were all of rather short duration to attempt to accomplish as many as possible before the fluid would tend to vaporize in the lines. However, as the inlet pressure was further reduced, the flow became more and more erratic and eventually the pump would not start. The last set of data presented in Fig. 59 shows the pump starting with approximately 1-psi static inlet pressure. Note also from the data that the flow buildup tended to lag somewhat behind the speed buildup, and the pump developed head is not following the H-Q curve in most of these tests. It appears that the pump needs more time to establish its design head before dropping to the lower pressures. In other words, the pump may be able to run at lower pressures after a successful start than it can during a start condition.

Test series No. 3d consisted of a single test for long-duration run with decreasing suction pressure to establish a cavitation performance capability.

The data were not as consistent as tests performed in series No. 5 and were not reduced as extensively. The initial data were following the H-Q map until the suction pressure dropped too low.

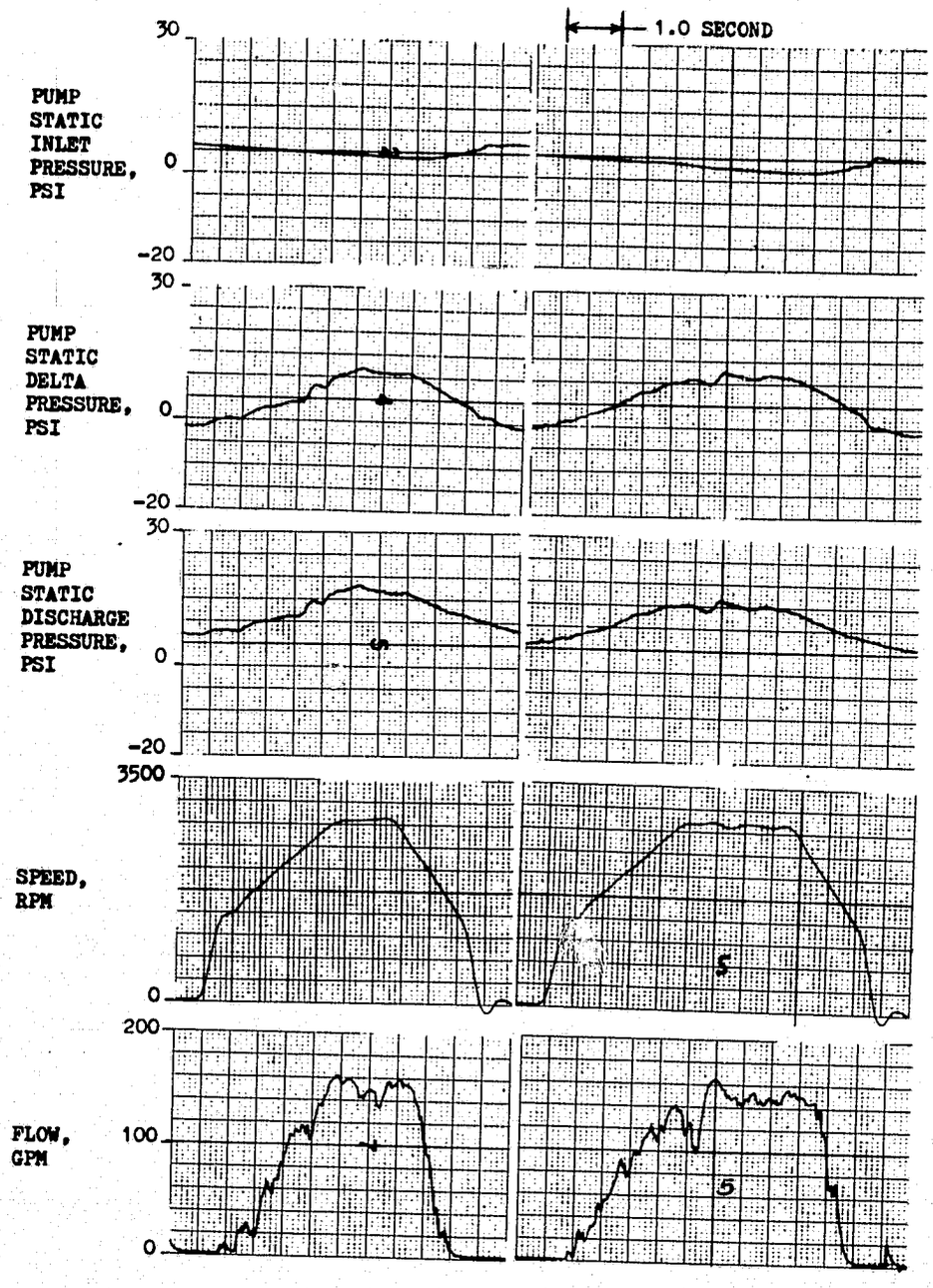

Figure 57. Data Slice From Test Series 3c

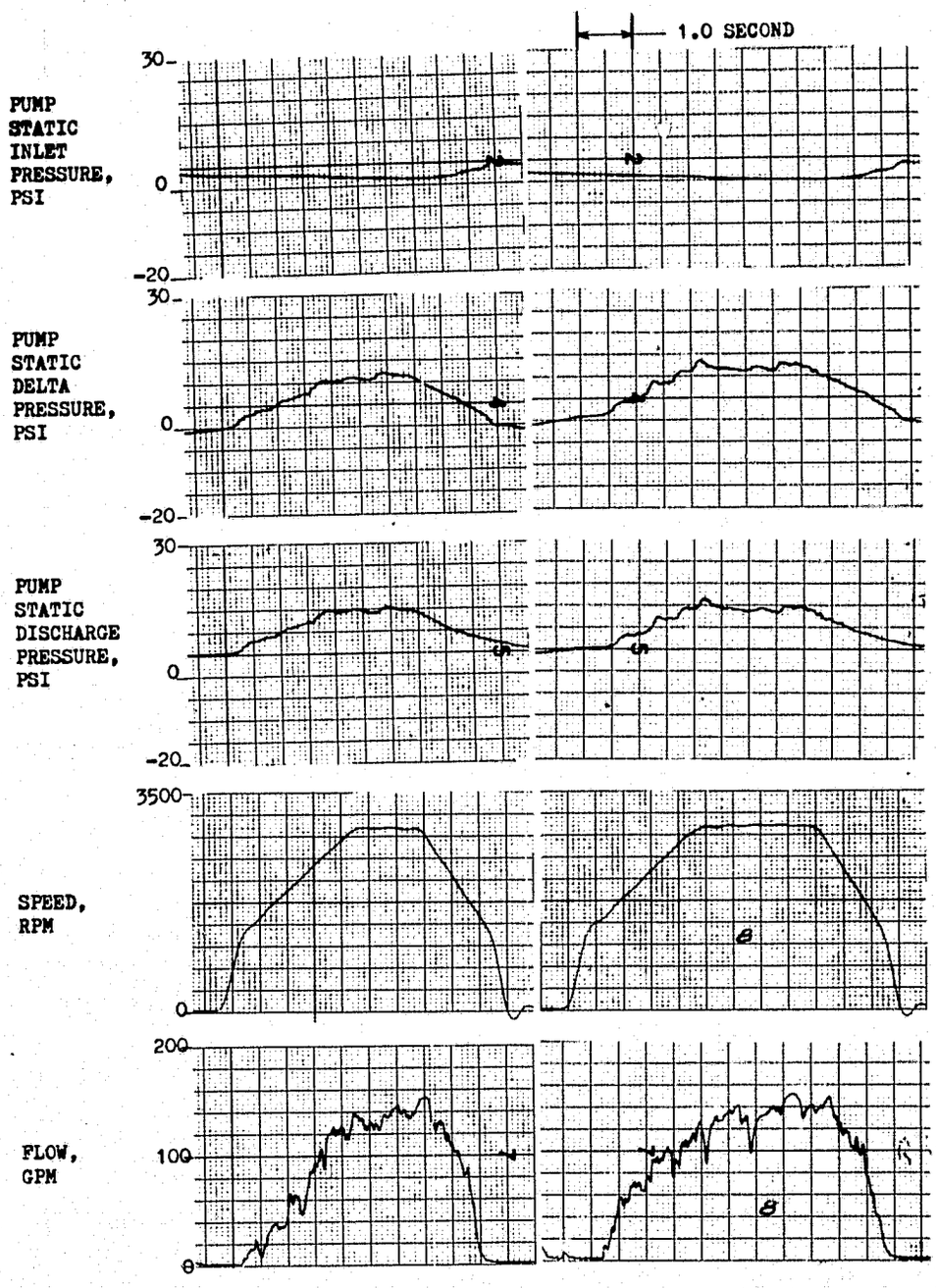

Figure 58. Data Slice From Test Series 3c

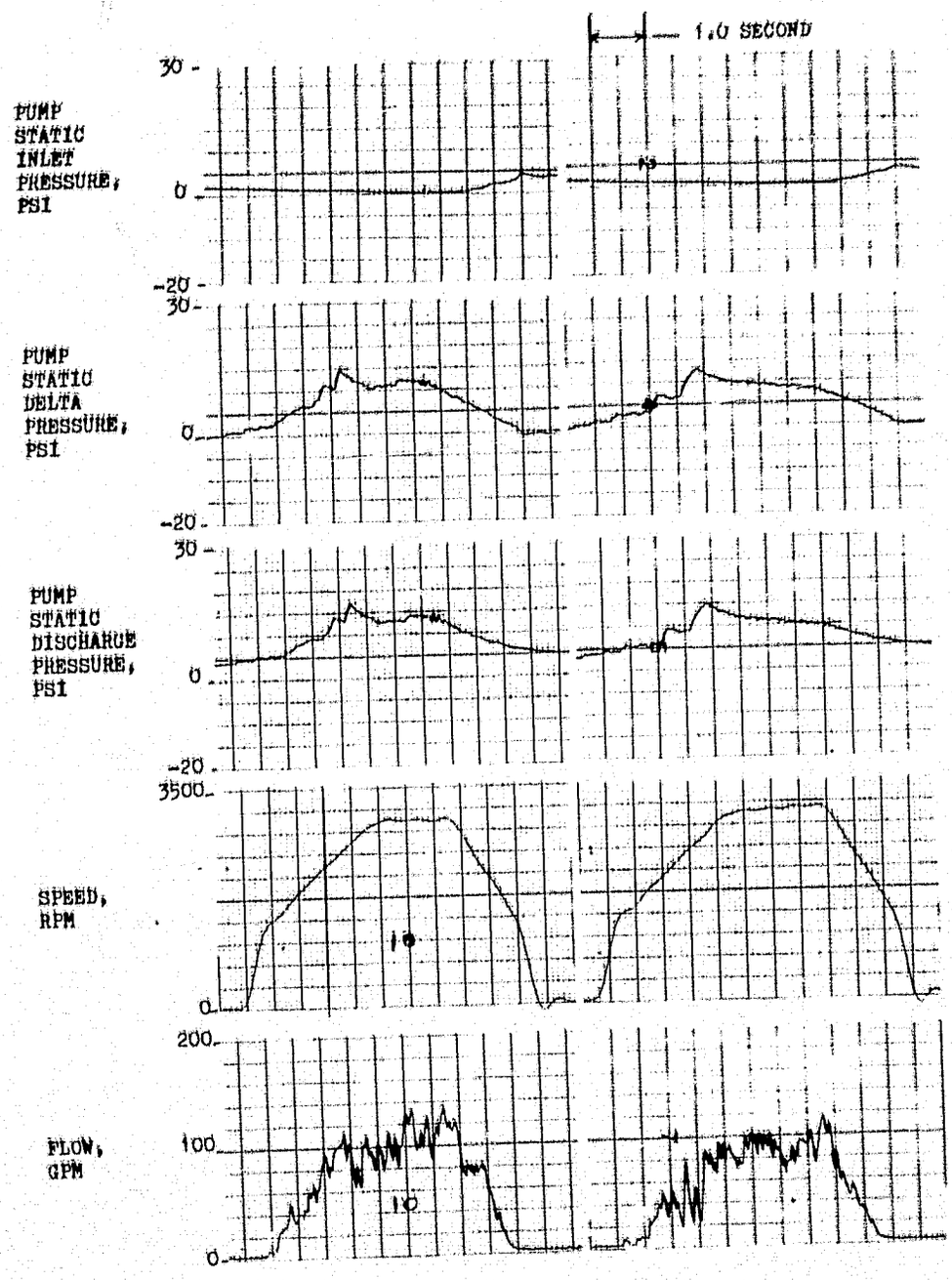

Figure 59. Data Slice From Test Series 3c

The complete test series No. 3 added an additional 28 starts and 467 accumulated seconds of run time.

Test series No. 4 consisted of tests run to add duration on the pump and tests to start with a longer start ramp (5 to 7 seconds). Test series No. 4a was a long-duration run but both flow and speed were varying significantly during the test. As with test No. 3c, the first test in the series appeared to have too much vapor in the lines. Reduction of some of the data points where speed and flow appeared to be more stable indicated pump heads that were well below the predicted H-Q performance as verified on earlier tests. This also would indicate that too much vapor was in the line to achieve a successful test.

The start transients in test series No. 4b were generally successful; representative data slices are shown in Fig. 60 and 61. The longer start ramp does give a better appearance of a smooth start than did the shorter start ramps. However, this appearance could be strongly affected by the amount of vapor in the lines from test series to test series that cannot be established. There were no indications that the starts could be achieved at a lower inlet pressure using the longer start ramp. The presence of the oscillations in the pump discharge pressure during these tests may be real. They indicate some high-frequency content (as indicated by the wave shape). Note, however, that the delta pressure across the pump shows no such oscillations. Without close-coupled dynamic pressure measurements, the oscillation performance cannot be established.

Test series No. 4c and 4d were longer-duration runs to put more time on the pump and to get more cavitation data, letting suction pressure vary during the tests. The data were so erratic that it was decided to use data from test series No. 5 to establish cavitation performance. It was noticed during test series No. 4d that each time the suction pressure dropped to low values (1 to 2 psi), one of the pump discharge pressures began to oscillate with a characteristic indicating higher frequency data (implying more accurate oscillation data). This is illustrated in Fig. 62. If the suction pressure were subsequently raised then lowered again, the oscillations would go away then return at the low values.

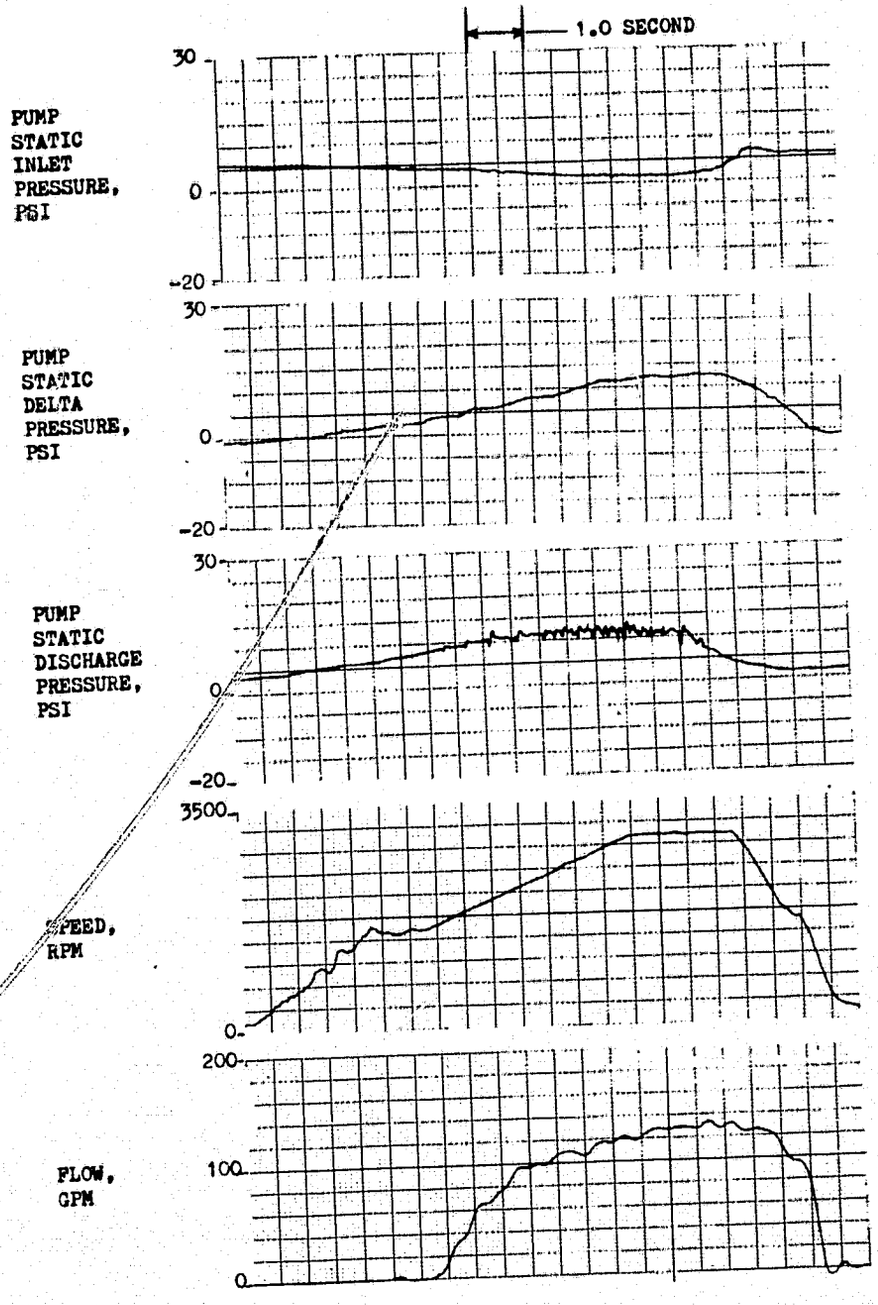

Figure 60. Data Slice From Test Series 4b

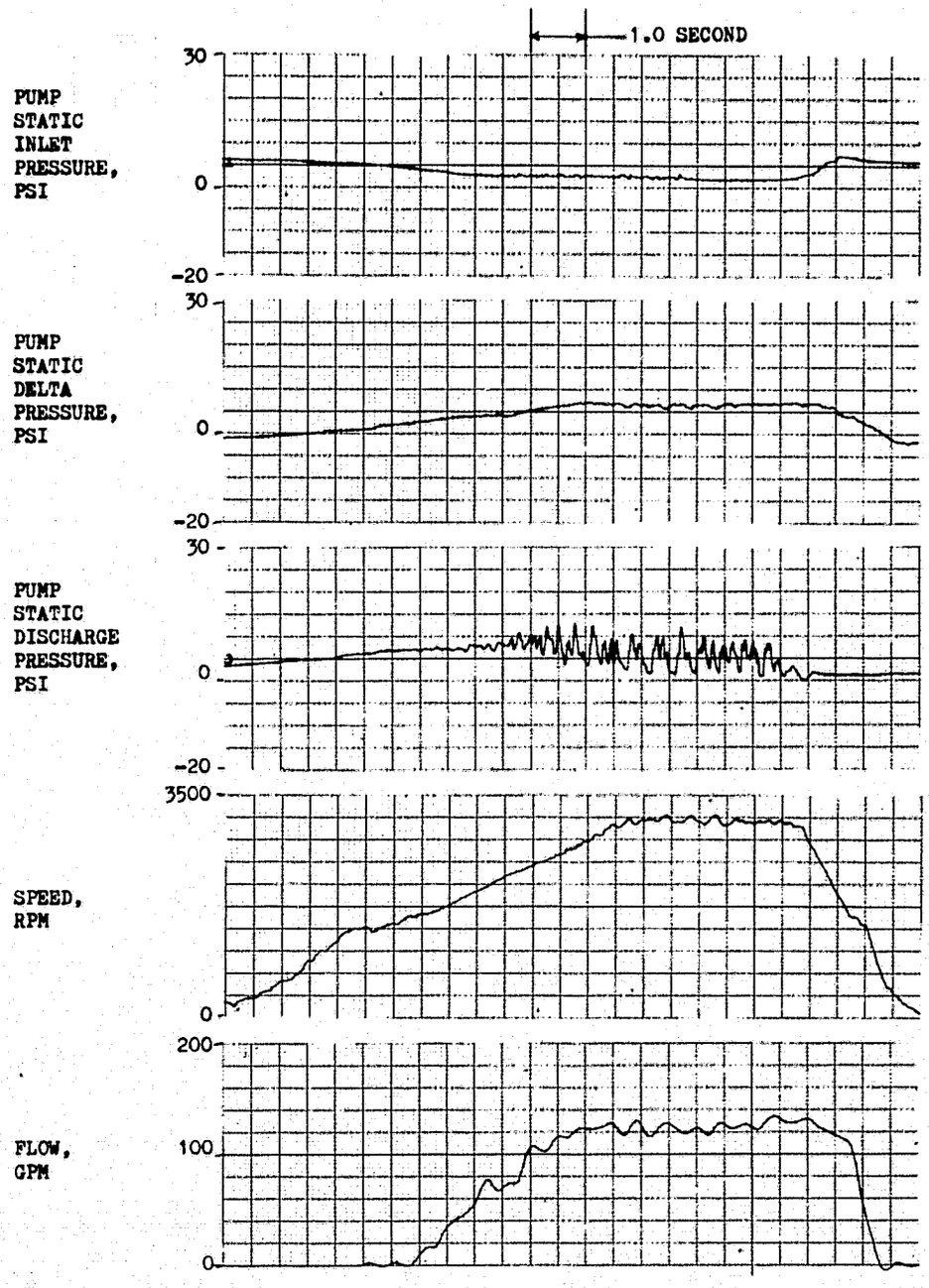

Figure 61. Data Slice From Test Series 4b

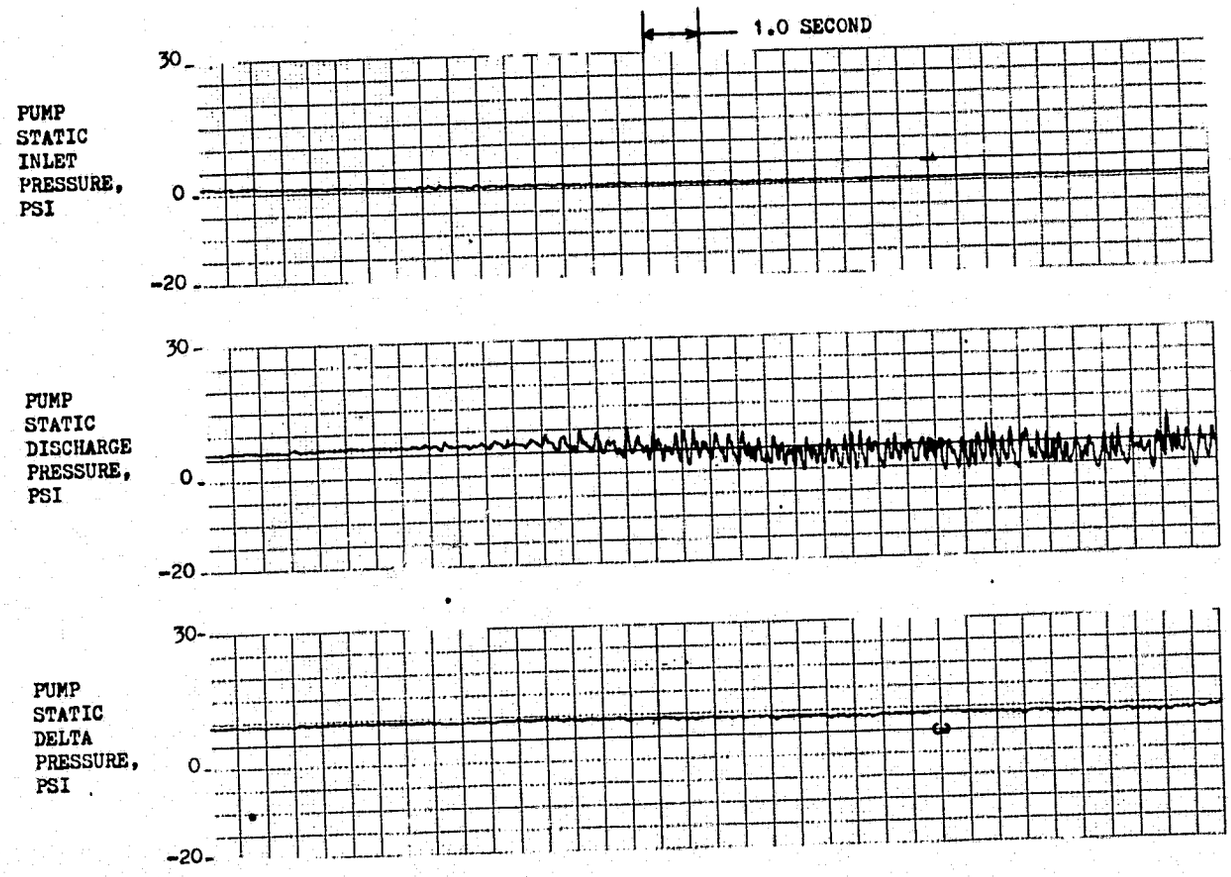

Figure 62. Data Slice From Test Series 4d

This indicates a potential oscillation problem, although it was not obvious in most of the tests nor in the other parameters of this test. It calls for use of high-frequency instrumentation in any future tests.

During test series No. 4, an additional 30 starts were made and 585 seconds more time was accumulated.

For test series No. 5, the backflow deflector was installed and both start transients and suction performance tests run. The data with the backflow deflector were generally comparable to the data without including both H-Q performance and the start transients. Some of the long-duration suction performance tests yielded the best data and were analyzed to establish the vapor pumping capability of the pump.

Three two-phase transients were analyzed and are identified as runs A, B, and C in Table 14. As shown in the table, the first run was at a higher vapor pressure of 19.2 psia and the other two were at a vapor pressure of 15.4 psia, which is close to ambient. For the first and third runs, the inlet static pressure was decreased until the head and flow dropped and, for the second run, the inlet static pressure was dropped into the two-phase flow regime and was then increased back into the liquid flow regime before the head and flow dropped.

The flow and speed transients for run A are shown in Fig. 63. As shown, the rotational speed was cut shortly after the flowrate and the static pressure rise (Fig. 64) dropped. Also shown in Fig. 64 is that the measured vapor pressure at the pump inlet varied throughout the run. In reality, the vapor pressure should remain constant until two-phase flow occurs and then should coincide with the inlet static pressure as long as operation in the two-phase flow regime is maintained. It is believed that prior to the initiation of the transient, the propellant in the inlet line warmed up and, during the transient, the propellant cavitated as it passed over the temperature measuring device. Under these conditions, the only time when the measured pump inlet vapor pressure would be accurate would be just after the run was terminated. There would be no vapor because the propellant would be fresh from the tank at a static pressure greater

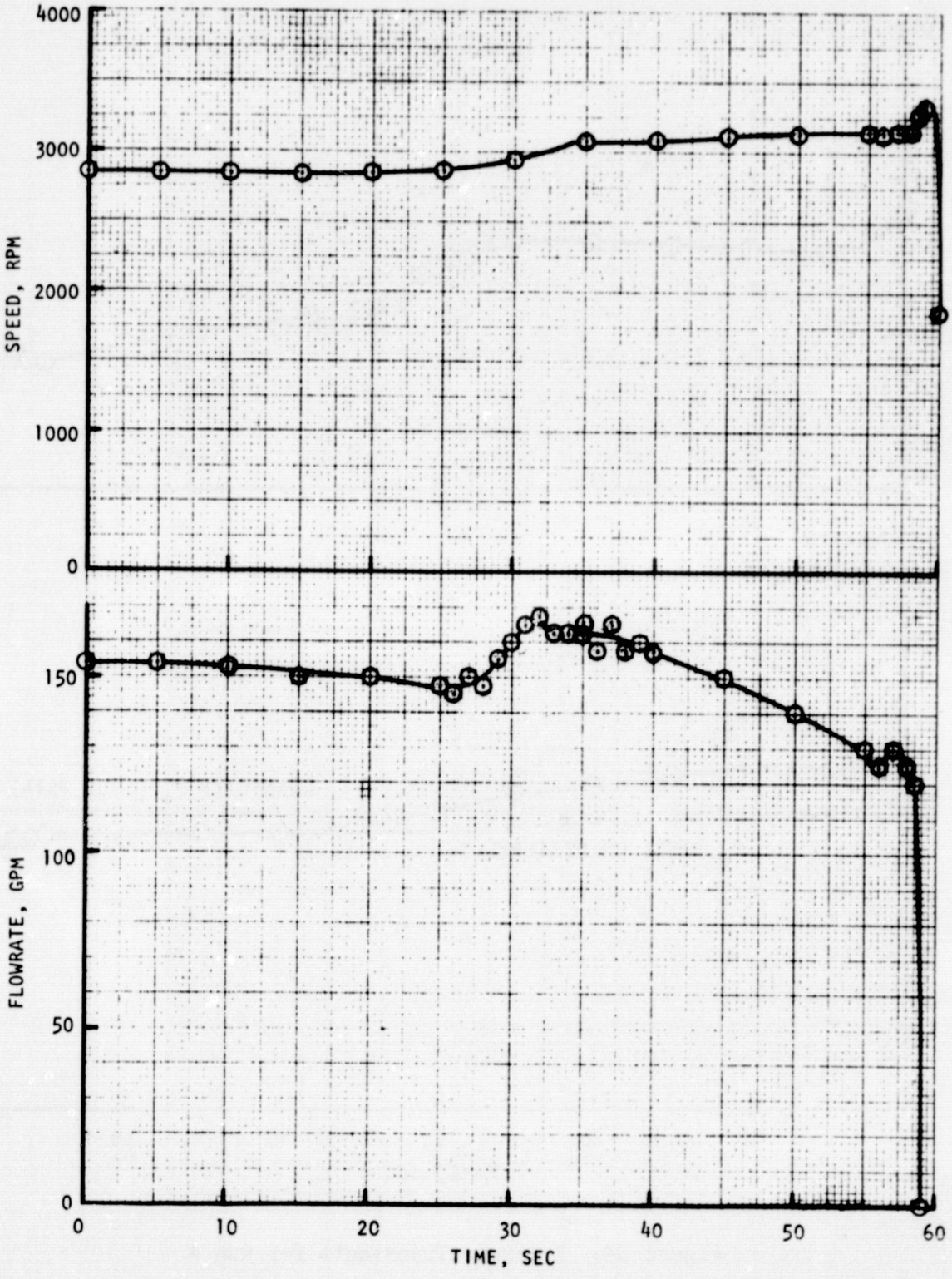

Figure 63. Flow and Speed Transients for Run A

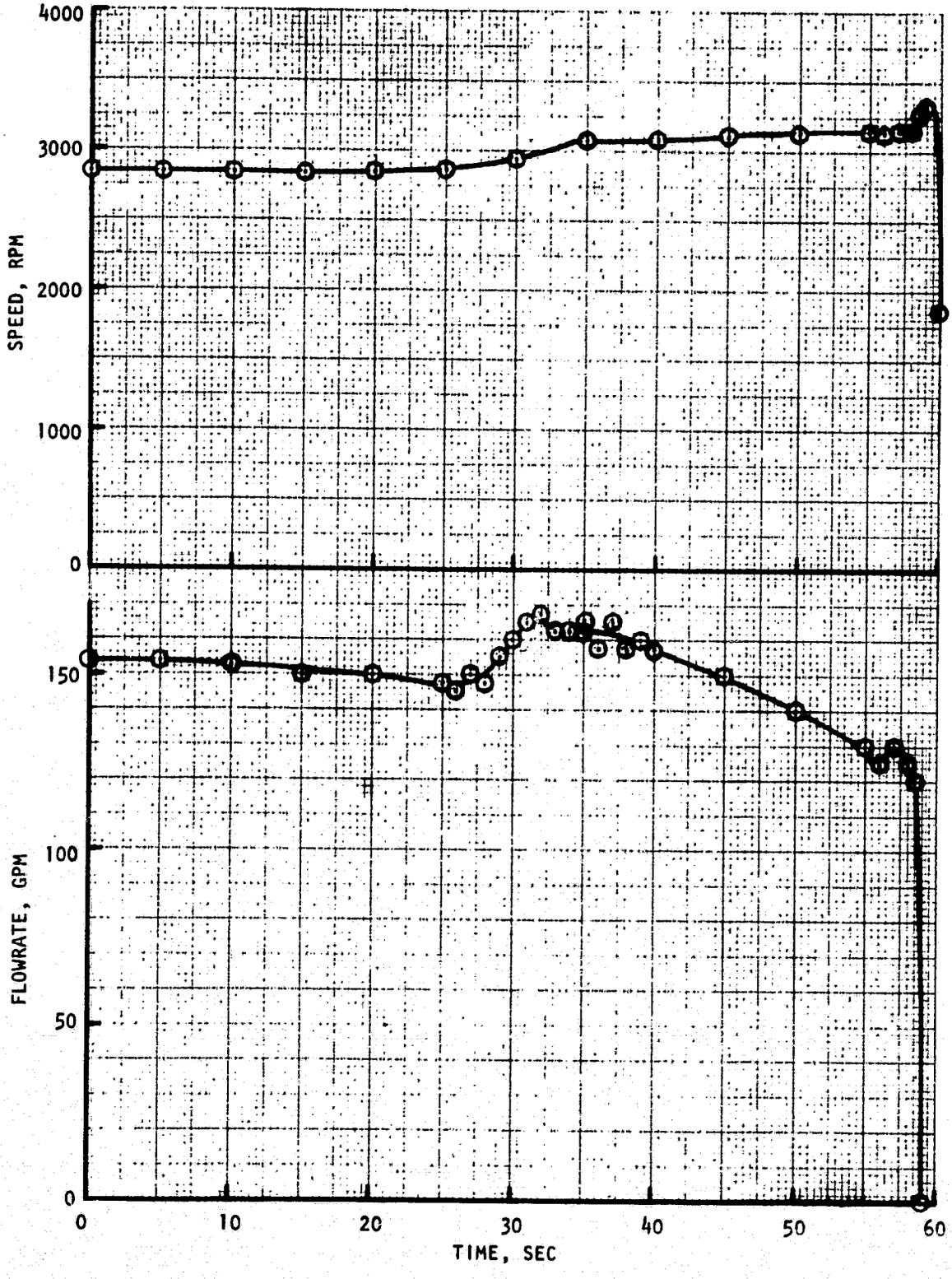

Figure 63. Flow and Speed Transients for Run A

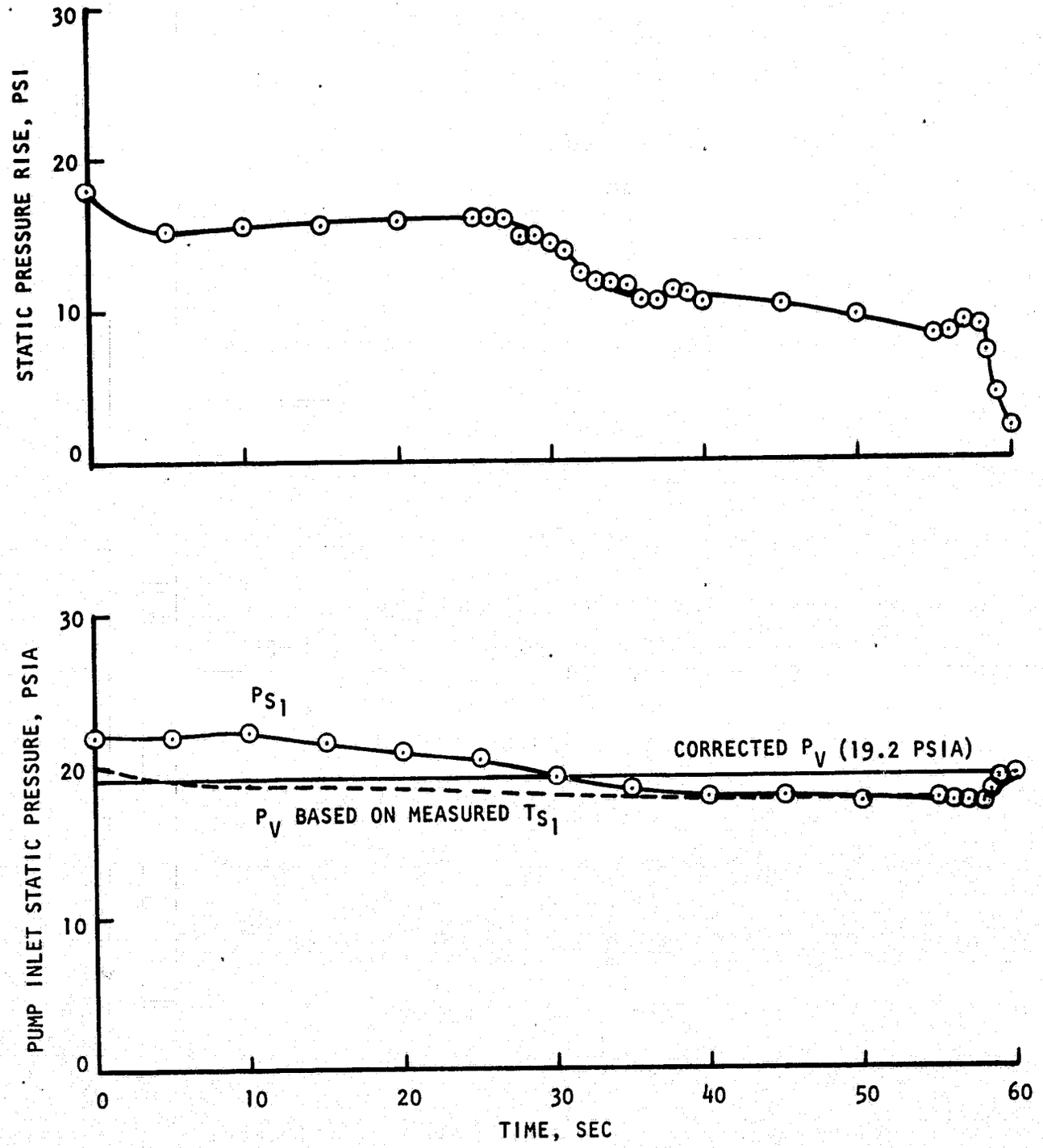

Figure 64. Pressure Transients for Run A

TABLE 14. CASES ANALYZED

Test Series	Run	Liquid Temperature, F	Liquid Vapor Pressure psia	Type of Run
5b	A	-292.7	19.2	Inlet static pressure was decreased until head fell, then the run was terminated.
5c	B	-296.5	15.4	Inlet static pressure was decreased until two-phase flow occurred, was held constant for 20 seconds, and was then increased back into the liquid flow regime.
5c	C	-296.5	15.4	Inlet static pressure was decreased until tank was empty, then the run was terminated.

than the vapor pressure and, due to the low flowrate, under noncavitating conditions. This corrected vapor pressure is also shown in Fig. 64 . It is interesting to note that oscillations in the pump discharge pressure trace occurred during the time period from 30 seconds to the end of the run. As shown in Fig. 64 , the inlet static pressure was below the corrected vapor pressure (which indicates two-phase flow) during the same time period. Therefore, the oscillations were probably due to the presence of two-phase flow.

The vapor volume fraction was determined from the amount that the inlet static pressure fell below the corrected vapor pressure (Fig. 64). This was done by assuming an isentropic expansion from the liquid condition at the corrected vapor pressure to the two-phase condition at the inlet static pressure. This correlation is based on data from an oxygen temperature entropy chart (Ref. 4). The results are shown in Fig. 65 for an initial liquid vapor pressure of 19.2 psia (T_{sat} = -292.7 F). Equation 1 was used to predict the vapor volume fraction from the quality and density correlations.

$$\alpha = \frac{1}{1 + \left(\frac{1-X}{X}\right)\frac{\rho V}{\rho_L}} \qquad (1)$$

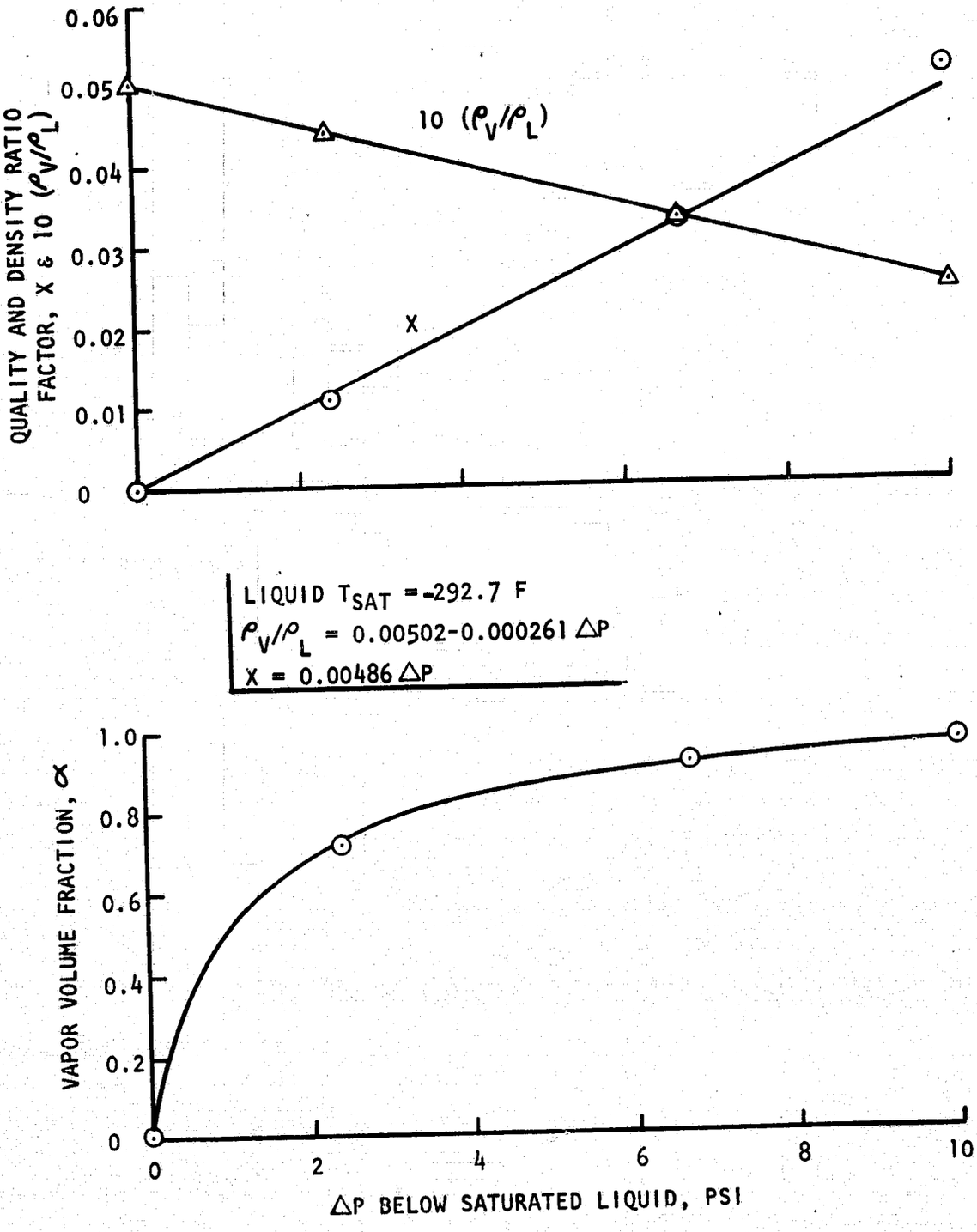

Figure 65. Isentropic Expansions from Saturated LO_2 at -292.7 F

In addition, the vapor pumping capacity of the pump was estimated using the simplified theory from Ref. 5 and 2 and the inducer blade leading edge geometry (Fig. 66) which was taken from the inducer drawing. For this inducer, Eq. 2 calculates the vapor pumping capability:

$$\alpha_{max} = 1 - \frac{\phi L}{\phi_{max}} = 1 - \frac{\phi L}{\tan\left(\beta_{suction} - 1.5\right)} \qquad (2)$$

Equation 3 was used to obtain the liquid flow coefficient ϕ_L from the flow and speed transients shown in Fig. 63. A boundary layer blockage of 0.07 was used

$$\phi_L = \frac{93.6\ Q}{N D_T^3\ (1-\lambda^2)(1-BLKG)} \qquad (3)$$

The resulting vapor fraction predictions are shown in Fig. 67 . The estimated vapor fraction did not exceed the predicted capability during the run and the pump static pressure rise decreased with increasing vapor fraction. The maximum quantity of vapor pumped was estimated to be 65 percent by volume.

The corresponding results for Runs B and C are shown in Fig. 68 through 71 and 72 through 74, respectively. As with Run A, the pump discharge pressure trace oscillated over the regions of indicated two-phase flow and did not oscillate over the regions of indicated liquid flow. The maximum amount of vapor pumped was 81 percent in Run C (Fig. 74). However, the tank was close to empty and, therefore, the flow was relatively unstable. Figures 67 , 71, and 73 show that this pump was able to pump with vapor volume fractions in excess of 60 percent and that the simplified method for predicting vapor volume fraction capacity appears to be reasonably accurate because the predicted limit was not significantly exceeded during any of the runs.

The total number of accumulated starts in test series No. 5 was 28 with an additional test duration of 360 seconds. This yields a total of 98 starts on the pump and 2893 seconds of total run duration, which was in excess of the requirement for 2500 seconds. The mechanical and hydrodynamic integrity of the pump was verified with no indication of mechanical problems.

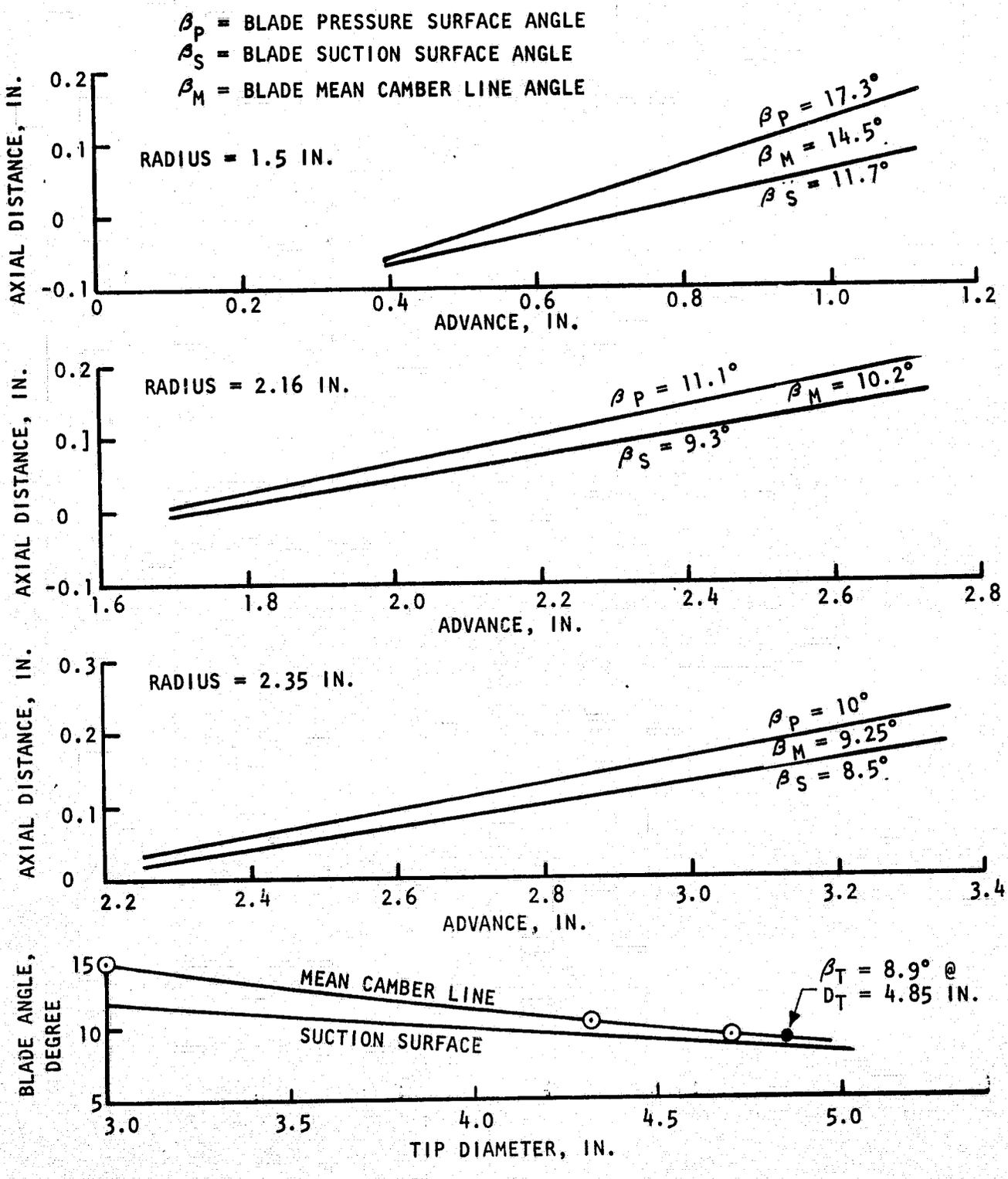

Figure 66. Inducer Geometry - LO_2 Unit

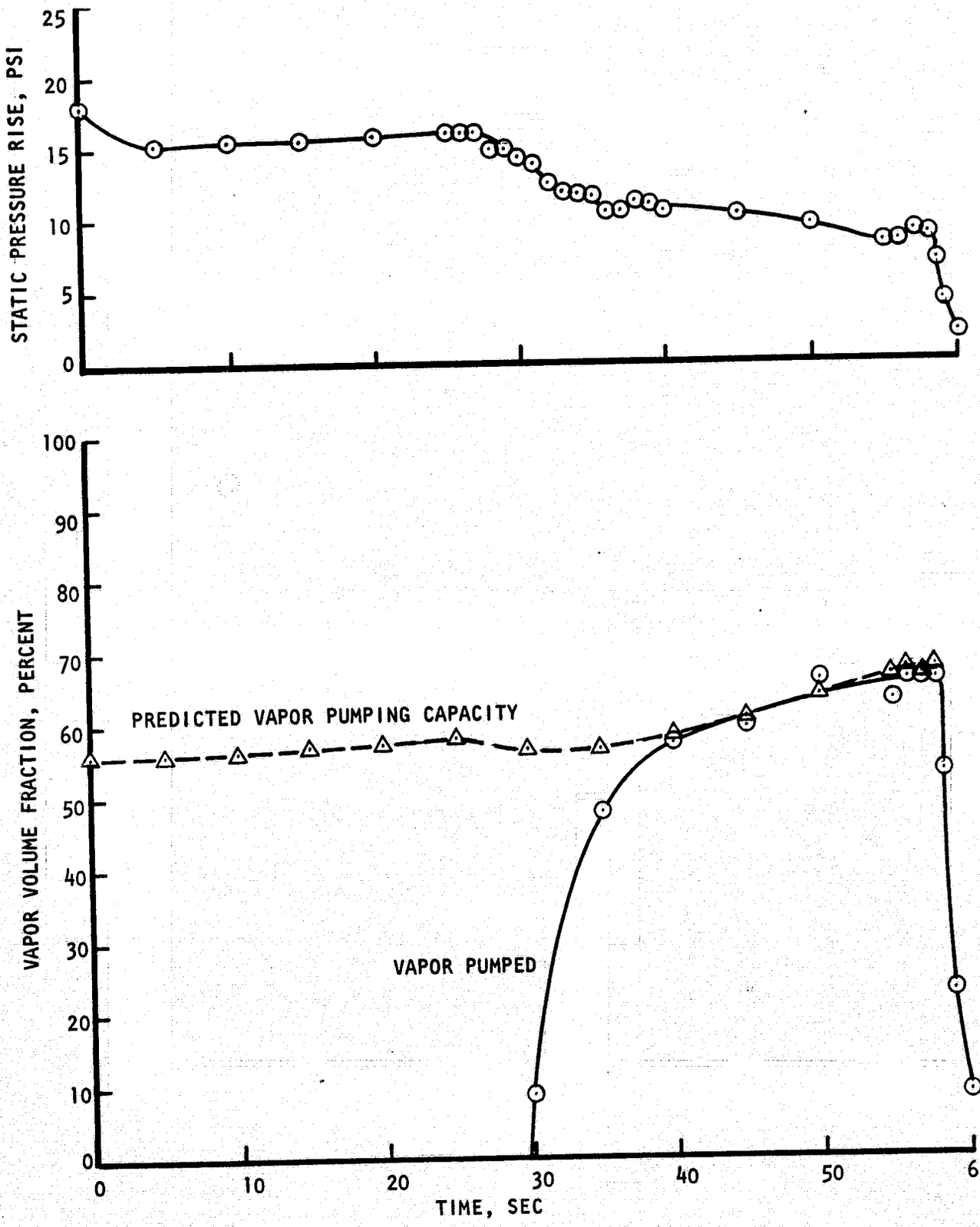

Figure 67. Vapor Volume Fraction Transfer for Run A

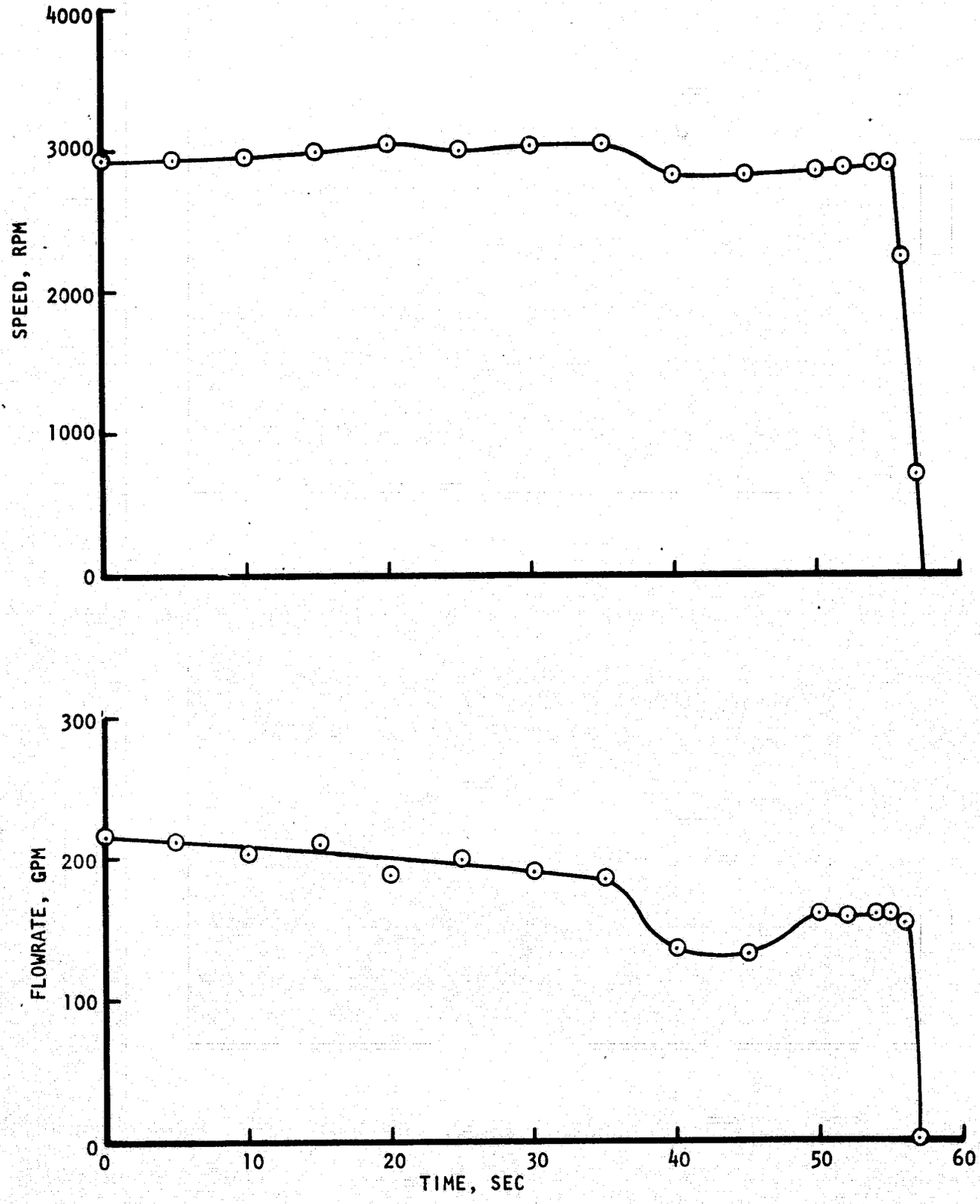

Figure 68. Flow and Speed Transients for Run B

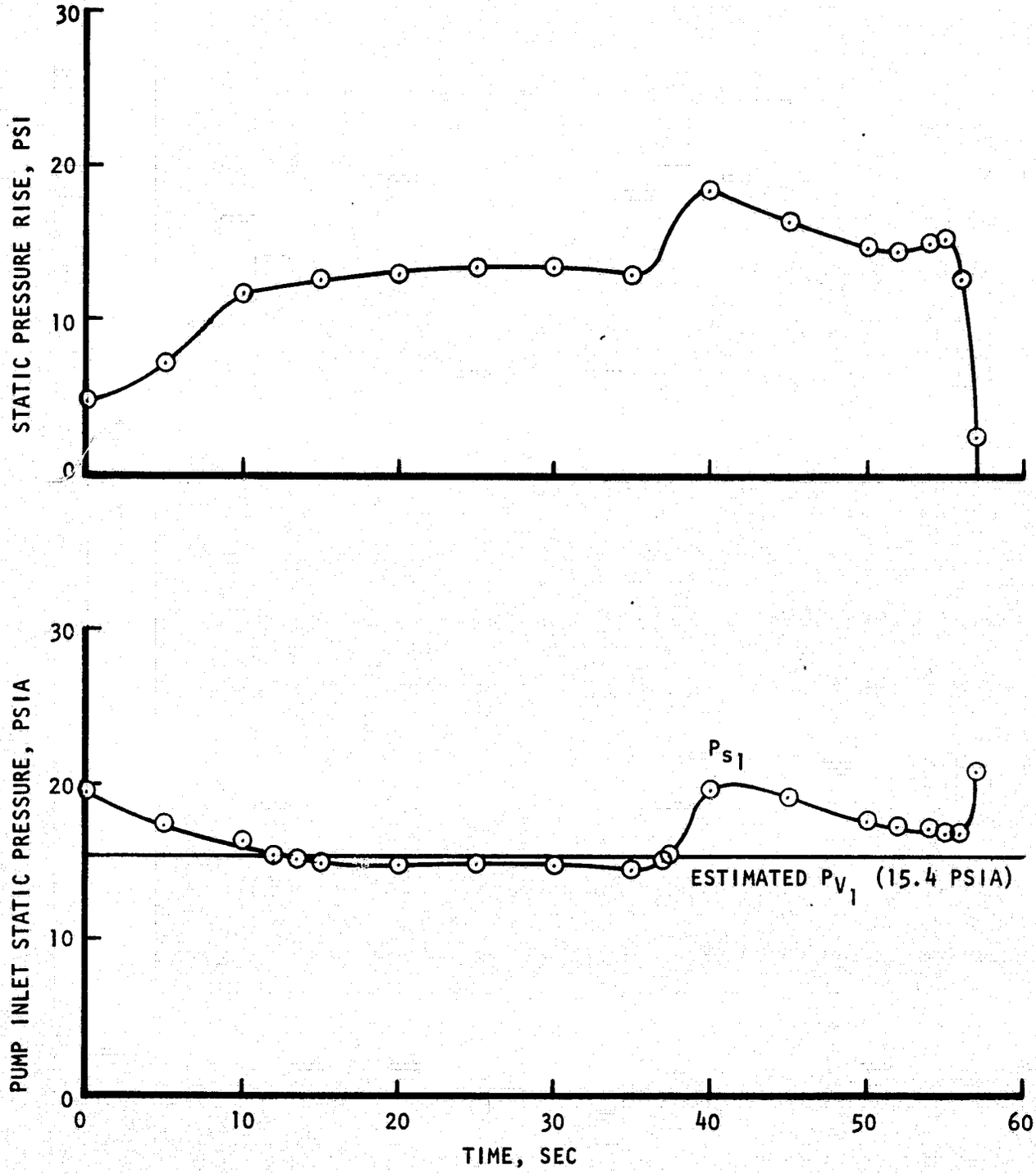

Figure 69. Pressure Transients for Run B

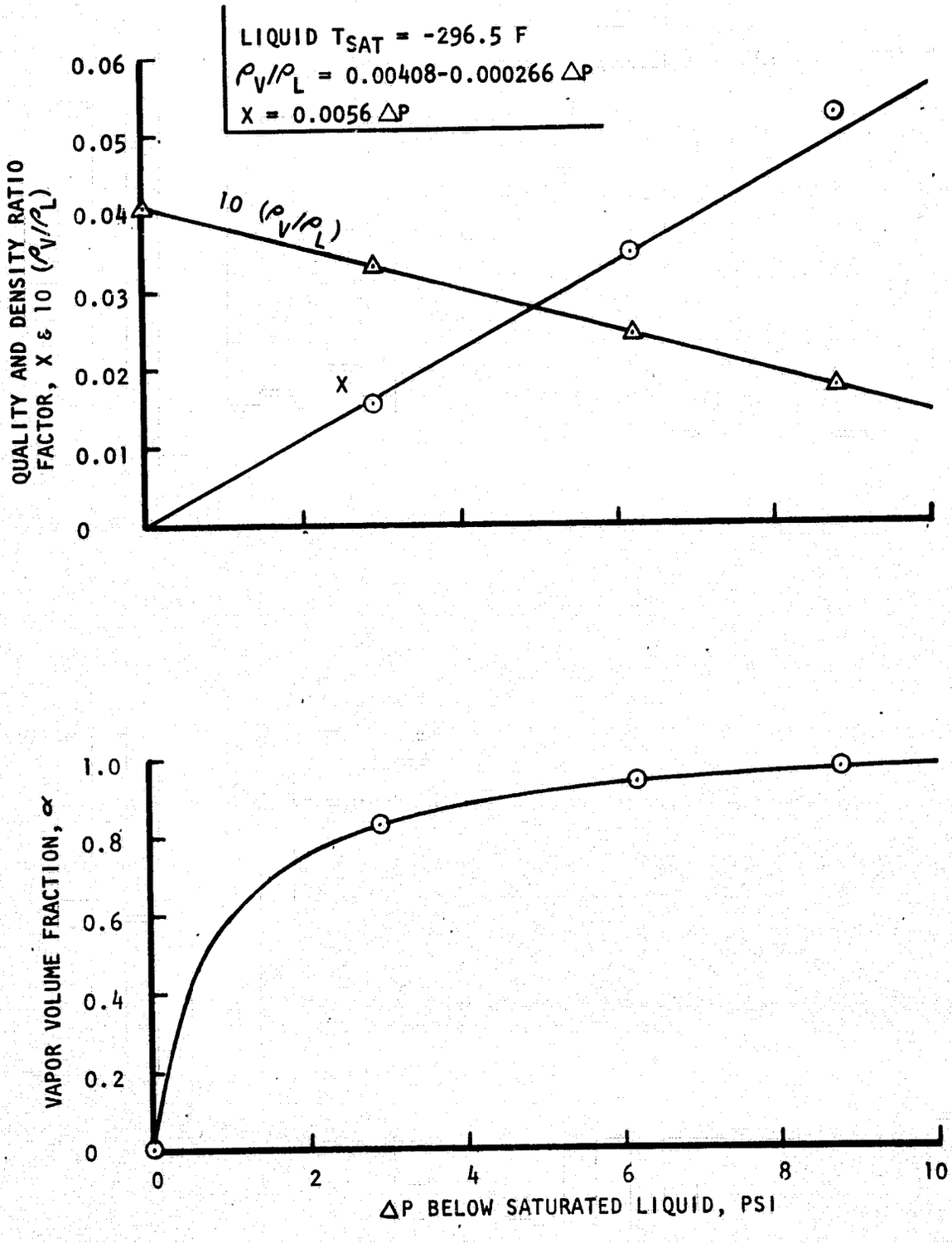

Figure 70. Isentropic Expansions from Saturated LO_2 at -296.5 F

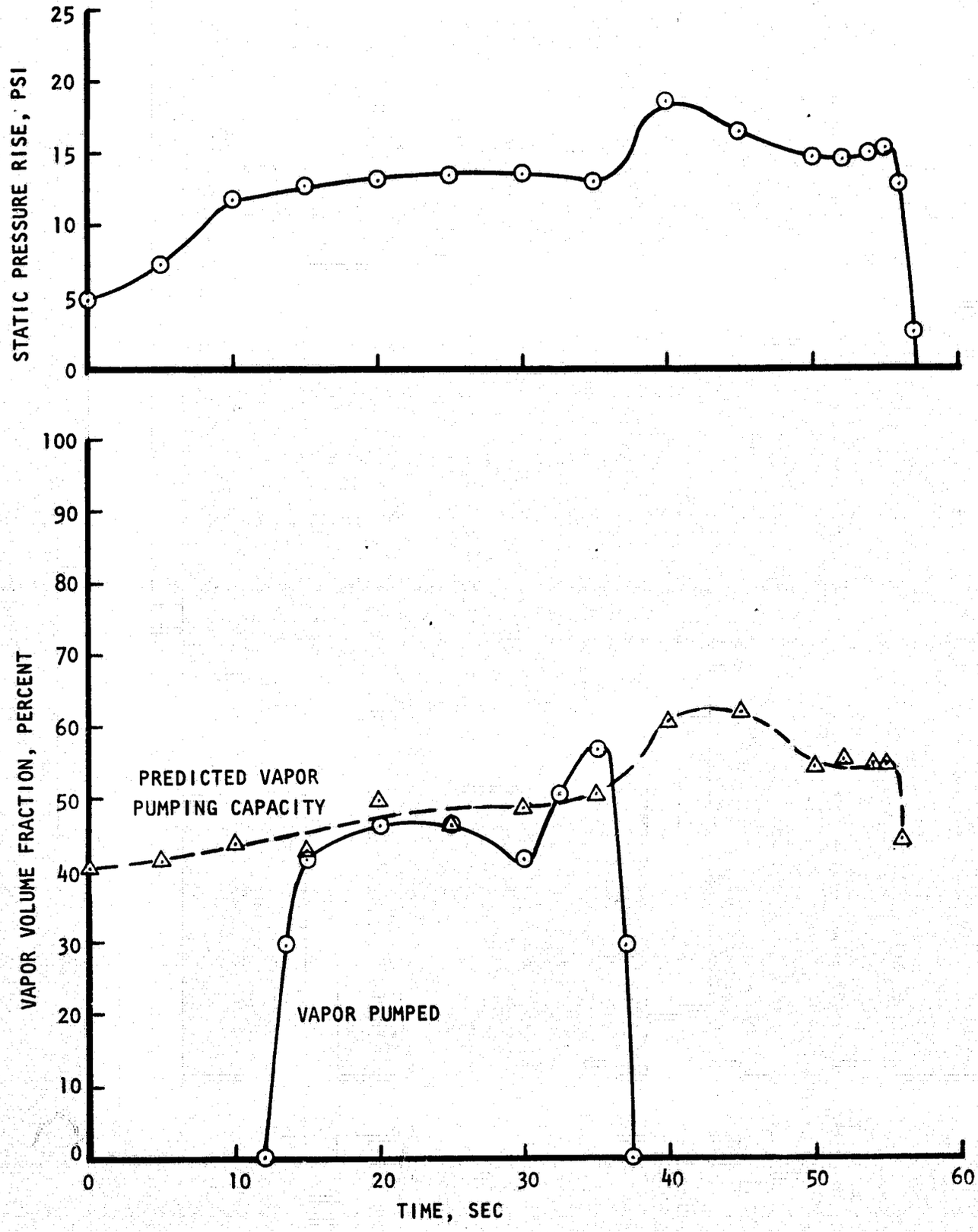

Figure 71. Vapor Volume Fraction Transients for Run B

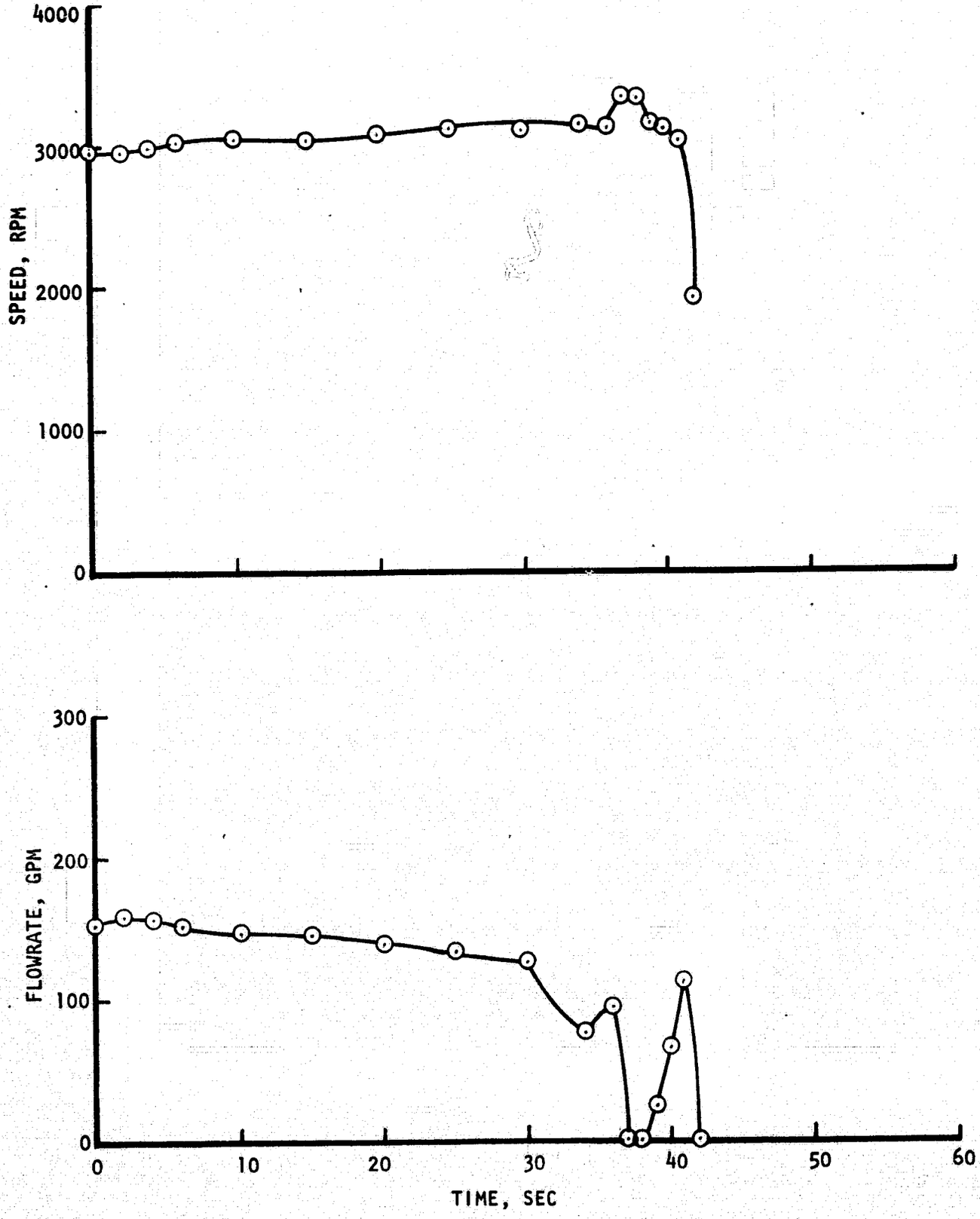

Figure 72. Flow and Speed Transients for Run C

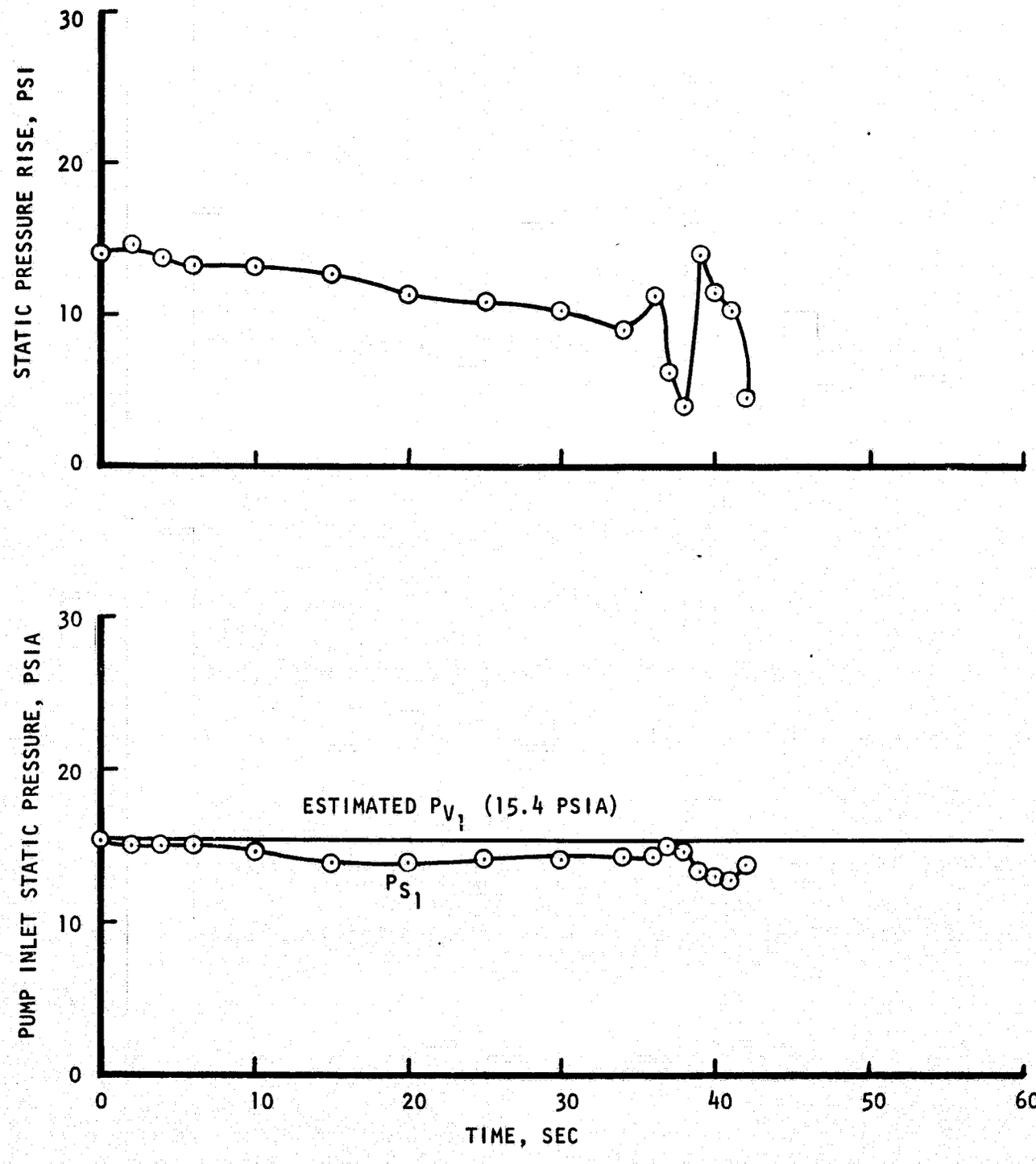

Figure 73. Pressure Transients for Run C

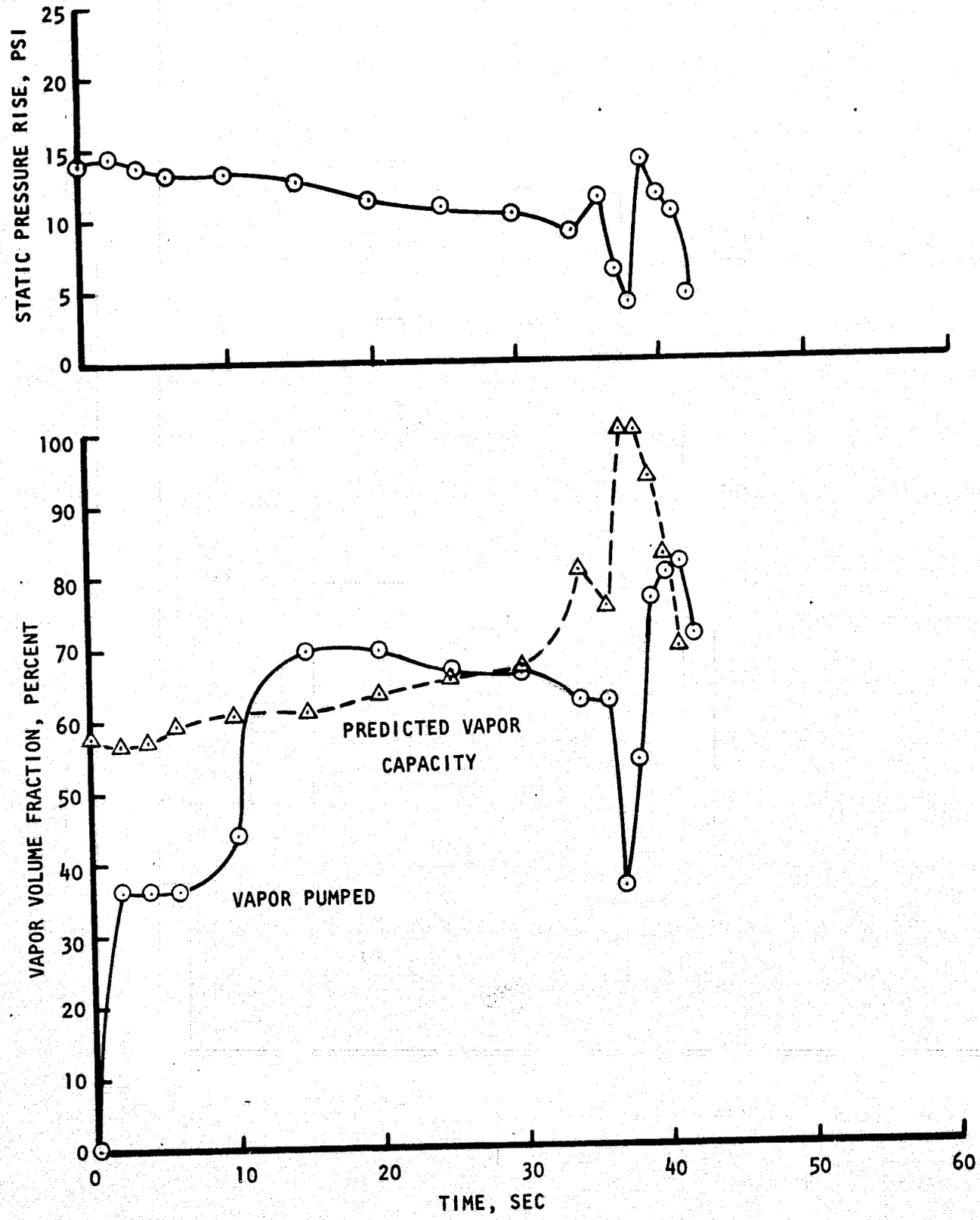

Figure 74. Vapor Volume Fraction Transients for Run C

The pump was shown to have the capability of starting with low inlet pressures and even with indications of some vapor in the inlet lines during starts. The electric motor performance was good, providing repeatable and well-regulated speed transients. The pump was shown to have the capability of pumping two-phase flow with vapor volume fractions in excess of 60 percent. Some difficulty was obtained in achieving good chilldown performance but the facility was not well insulated and this problem also contributed significantly to the questionable value of much of the data. Future testing must be careful to include adequate line insulation, adequate instrumentation, and better control of the two independent variables (inlet pressure and flowrate) to provide more useful data for establishing the two-phase pumping technology.

REFERENCES

1. King, J. A.: Design of Inducers for Two-Phase Operation - Final Report, Rocketdyne Report R-8283, Contract NAS8-25069, Rocketdyne, a Division of Rockwell International, Canoga Park, California 91304, July 1970.

2. King, J. A.: Design of Inducers for Two-Phase Oxygen - Final Report, Rocketdyne Report R-8832, Contract NAS8-26645, Rocketdyne, a Division of Rockwell International, Canoga Park, California 91304, January 1972.

3. King, J. A. and E. C. Farrel: The Transient Performance of a Hydraulic-Turbine-Driver Inducer: Computer Predictions and Test Verification, Rocketdyne a Division of Rockwell International, Canoga Park, California 91304, February 1969.

4. Moses, R. A.: Physical and Thermodynamic Properties for Heat Transfer Analysis, Pub. 575-A-5, Rocketdyne a Division of Rockwell International, Canoga Park, California 91304, 1966.

5. Bissell, W. R., G. S. Wong, and T. W. Winstead: "Analysis of Two-Phase Flow in LH_2 Pumps for O_2/H_2 Rocket Engines," AIAA, Journal of Spacecraft and Rockets, June 1970.

APPENDIX A

NOMENCLATURE

A	=	area, sq ft
BLKG	=	boundary layer blockage fraction
C_m	=	axial velocity, ft/sec
D_h	=	hub diameter, inches
D_i	=	rotor entrance (eye) diameter, inches
D_t	=	tip diameter inches
D_w	=	wall diameter, inches
g	=	gravitational constant taken as 32.174
H	=	(or ΔH) head rise, feet
hp	=	horsepower
i	=	incidence angle, $i = \beta_b - \beta_f$, degrees
L	=	inertia, sec^2/in^2
N	=	rotational speed, rpm
N_S	=	specific speed, $N\sqrt{Q}/H^{0.75}$
p	=	(or Δp) pressure, psi
Q	=	flowrate, qpm
R	=	resistance, sec^2/in^5
T	=	temperature, R
t	=	time (as in dw/dt) seconds
U	=	tip speed, ft/sec
U_i	=	rotor entrance tip speed, ft/sec
$\dot{w}$	=	flow lb/sec
α	=	vapor volume fraction
α_{max}	=	vapor volume fraction capacity
β_b	=	blade angle with the tangent at the inducer tip, degrees
β_f	=	fluid angle with the tangent at the inducer tip, degrees
$\beta_{suction}$	=	angle at blade tip leading edge suction surface with tangential direction, degrees

λ	=	inducer inlet hub to tip diameter ratio
ξ	=	D_h/D_t
ρ	=	density, lb/cu ft or lb/cu in.
ρ_L	=	liquid density, lb/ft^3
ρ_V	=	vapor density, lb/ft^3
ϕ	=	flow coefficient, cm/U_i
ϕ_L	=	flow coefficient based on liquid flow
ϕ_{max}	=	flow coefficient at predicted two-phase pumping limit
X	=	vapor fraction by weight
Ψ	=	head coefficient, $G\,\Delta H/U^2$